SEISMIC RESPONSE OF STRUCTURES WITH FLEXIBLE FLOOR SLABS BY A DYNAMIC CONDENSATION APPROACH

by

MARIO A. RIVERA

Dissertation submitted to the Faculty of the
Virginia Polytechnic Institute and State University
in partial fulfillment of the requirements for the degree of

Doctor of Philosophy
in
Engineering Mechanics

APPROVED:

M. P. Singh, Chairman
M. S. Cramer
R. A. Heller
S. M. Holzer
D. T. Mook

April, 1997
Blacksburg, Virginia

Keywords: Dynamic Condensation, Seismic Response, Flexible Floors,
Vertical Ground Excitation

Seismic Response of Structures with Flexible Floor Slabs

by a Dynamic Condensation Approach

by

Mario A. Rivera

Mahendra P. Singh, Chairman

Engineering Mechanics

(ABSTRACT)

The flexibility of the floor slabs is quite often ignored in the seismic analysis of structures. In general, the rigid behavior assumption is appropriate to describe the in-plane response of floors. For seismic excitations with vertical components, however, the flexibility of the floor slabs in the out-of-plane direction may play a significant role and it can result in an increase in the seismic response. The simplified procedures used in the current practice to include the floor flexibility can lead to highly conservative estimates of the slab and supported equipment response. To include floor flexibility, a detailed finite element model of the structure can be constructed, but this procedure leads to a system with large degrees of freedom the solution of which can be time consuming and impractical.

In this study, a new dynamic condensation approach is developed and proposed to reduce the size of the problem and to calculate the seismic response of structures with flexible floor slabs. Unlike other currently available dynamic condensation techniques, this approach is applicable to classically as well as nonclassically damped structures. The approach is also applicable to structures divided into substructures. The approach can be used to calculate as many lower eigenproperties as one desires. The remaining higher

modal properties can also be obtained, if desired, by solving a complementary eigenvalue problem associated with the higher modes. The accuracy of the calculated eigenproperties can be increased to any desired level by iteratively solving a condensed and improved eigenvalue problem. Almost exact eigenproperties can be obtained in just a few iterative cycles. Numerical examples demonstrating the effectiveness of the proposed approach for calculating eigenproperties are presented.

To calculate the seismic response, first the proposed dynamic condensation approach is utilized to calculate the eigenproperties of the structure accurately. These eigenproperties are then used to calculate the seismic response for random inputs such as a spectral density function or inputs defined in terms of design response spectra. Herein, this method is used to investigate the influence of the out-of-plane flexibility of the floor slabs on the response of primary and secondary systems subjected to vertical ground motions. The calculated results clearly show that inclusion of the floor flexibility in the analytical model increases the design response significantly, especially when computing acceleration floor response spectra. This has special relevance for secondary systems and equipment the design of which are based on the floor response spectra.

The accuracy of the results predicted by two of the most popular methods used in practice to consider the floor flexibility effects, namely the cascade approach and the modified lumped mass method, is also investigated. The numerical results show that the cascade approach overestimates the seismic response, whereas the modified lumped mass method underestimates the response. Both methods can introduce significant errors in the response especially when computing accelerations and floor response spectra. For seismic design of secondary systems supported on flexible slabs, the use of the proposed condensation approach is thus advocated.

DEDICATION

To Gise,

A capable wife who can find?

Her value is far more than that of corals.

In her the heart of her owner has put trust,

and there is no gain lacking.

She has rewarded him with good, and not bad,

all the days of her life.

. . .

There are many daughters that have shown capableness,

but you - you have ascended above them all.

Charm may be false, and prettiness may be vain;

but the woman that fears JEHOVAH

is the one that procures praise for herself.

. . .

Proverbs 31:10-31

and to Alfredo, Camille, Kathia and Marah.

Looks! Sons are an inheritance from JEHOVAH;

The fruitage of the belly is a reward.

Like arrows in the hands of a mighty man,

So are the sons of youth.

Happy is the able-bodied man that has filled his quiver with them.

Psalms 127:3-5

ACKNOWLEDGMENTS

I would like to thank my advisor, Dr. Mahedra P. Singh, for his advice, patience, support and encouragement throughout my graduate studies. I would like to extend my gratitude to Professors Mark S. Cramer, Robert A. Heller, Dean T. Mook, and Siegfried M. Holzer for serving as members of my committee as well as Professor Pap. I will never forget the help offered by the secretary of the Department of Engineering Science and Mechanics, Cindy Hopkins.

I must thank the University of Puerto Rico-Mayagüez Campus for giving me the opportunity of pursuing graduate studies and for the economical support during it. I want to thank my colleagues from the Department of General Engineering of the University of Puerto Rico but specially to Professors Luis E. Suarez, Gustavo O. Maldonado, Héctor M. Rodríguez and Frederick Just, former VPI graduate students. Their help and support will ever be appreciated.

The partial support received through Grant No. BCS-8719078 with Dr. M. P. Singh as its Principal Investigator and Dr. S. C. Liu as the NSF Program Director is gratefully acknowledge.

I want to extend my gratitude to all my special friends from the Blacksburg Congregation of Jehovah's Witnesses. My heart will always be with you.

Furthermore I want to express my love to my parents, Ida and Arturo for their continuous support during these years. To my brothers and sisters, Turi, Bibi, Piri, Rafi and Angie for their trust. I want to thank my in-laws, Elpidio and Millín, for their unconditional support for me and my family.

I want to dedicate this achievement to my wife, Gisela, and to my son and daughters, Alfredo, Camille, Kathia and Marah.

Last of all but not least I want to thank JEHOVAH God.

TABLE OF CONTENTS

LIST OF FIGURES

LIST OF TABLES

CHAPTER I

INTRODUCTION

1.1 GENERAL REMARKS

In the seismic analysis of structures, the flexibility of the floor slabs is quite often ignored. However, the dynamic characteristics of the structure may change when the floor flexibility is included in the analytical model. The natural frequencies, mode shapes and participation factors can be significantly different. Obviously this will affect the response and distribution of inertia forces acting on the structure.

Another factor that is frequently ignored in the seismic analysis of structures is the effect of the vertical component of the ground acceleration. It is argued that the dynamic amplification of the vertical acceleration is relatively small primarily because the vertical rigidities of columns and walls are relatively very high compared to their lateral rigidities, and a structure designed for other load can accommodate the effect of vertical accelerations safely. But in some past earthquakes, damage patterns have also been attributed to the vertical component of the ground acceleration [16,21,27,56,77]. The vertical ground acceleration affects a structure in two ways. It plays the role of a parametric excitation to the structure which tends to increase the peak response level due to the horizontal ground acceleration [5,30,43] and it may give rise to instability of the columns [1,12,78]. In addition, it can amplify the vertical responses of long span horizontal members such as girders and flexible floor slabs.

Examining the appropriateness of assuming a floor slab rigid in its own plane has been of continued research interest in earthquake engineering research community. Although this assumption may be justified for many structures, there are some types of structures where it is necessary to include the in-plane shear deformation of the floor slabs in the calculation of seismic responses. Such types of structures include, among others, long narrow floor plan structures [46], structures with several wings [10] and crosswall structures [73]. It is also known that the in-plane floor flexibility mainly affects the distribution of horizontal forces in the primary load carrying members [70]. Some of the analytical procedures developed to incorporate the in-plane floor flexibility are described in references 25, 31, 34, 49, and 72.

Lately, the consideration of the out-of-plane flexibility of floor slabs in the seismic analysis of structures has also been of interest because of its significance to supported secondary systems such as equipment and piping, especially in nuclear plant facilities. When a structure is subjected to a vertical seismic excitation, the floor slabs may oscillate relative to its supports. The excitation is amplified first by the supporting structure and then by the floor slabs. This affects the forces in the primary support members through dynamic interaction effects and also affects the response of the secondary systems placed on the floors due to the additional response amplification produced by the slabs. Thus, it is of practical interest to study this topic for a proper structural design of primary as well as supported secondary systems.

One approach to include the floor flexibility in the analysis is to prepare a detailed analytical model of the structure including the slabs by a suitable finite element discretization scheme. In this way, the geometry and properties of the floor slabs are incorporated in the model in conjunction with the rest of the structure. However, the main problem with this brute-force method is that the number of degrees of freedom involved as well as the computational cost can become quite large.

To avoid the preparation of detailed analytical models which include the out-of-plane flexibility, some simplified procedures have evolved in practice, especially in the nuclear power plant design industry. The most simplified procedure is the cascade approach [39]. In this approach the floor slabs are assumed to be completely rigid. The masses of the structure are concentrated at each floor elevation and the columns and walls are represented by flexible vertical load-carrying elements. Then a vertical seismic analysis is performed and the response at the desired floor elevation is obtained. This response is then used as input to the flexible slab model to obtain its response. Although the additional response amplification produced by the floor flexibility is included in this approach, the effect of dynamic interaction between the supporting structure and the slabs is completely ignored. This may, however, lead to a very conservative estimate of the slab response.

To include the dynamic interaction effect and to reduce the conservatism associated with the decoupled analysis of floor slabs, some slightly improved analytical procedures have been proposed. A review of some of these improved procedures is given by Lee and Chen [39] and La Framboise et al. [38]. In these procedures each floor slab is represented by an equivalent single degree of freedom beam element, in which its mass and stiffness are calculated from the frequency and mode shape of the dominant mode of the flexible slab model. From this coupled model, the response of the floor slab can be obtained directly or by a cascading approach. Perumalswami and Dalal [55] utilized this analytical procedure in their study to evaluate the importance of including the floor flexibility in the calculation of seismic response. In other procedures, Chin et al. [13] developed the equations of motion of a column-slab system utilizing the Lagrange's energy formulation by considering only the first mode deformation pattern of the slab. Shiau [65] has proposed a procedure to analyze a combined slab-girder-column system, modeled as a continuous beam supported on girders which are in turn simply supported on columns. With this simplified model, each element is represented by more than one generalized degree of freedom.

The aforementioned procedures can approximately include the floor slab flexibility, but because of some simplifying assumptions made in their development, they may not provide accurate estimates of the response of structure. It is, therefore, necessary to develop methods that are rational, can provide accurate values of seismic response, and can incorporate the effect of floor flexibility without a full finite element modeling of the complete structure. Herein, new dynamic condensation approaches have been developed to reduce the size of the dynamic model of a generic structure to be analyzed. These approaches are used to calculate accurate values of the structural eigenproperties (frequencies, modal damping rations, participation factors and eigenvectors) which are essential quantities required for seismic response spectrum analyses of structural systems that are designed to respond linearly such as nuclear power plant facilities. Since it is usually a first few eigenproperties that are required for seismic analysis of structures, the condensation approaches developed here are efficient and ideally suited for such analyses as one finally deals with a reduced, but accurate, model of a structure with correspondingly reduced size eigenvalue problem.

1.2 BACKGROUND ON DYNAMIC CONDENSATION TECHNIQUES

The mode superposition approach [14] is commonly used for the dynamic response analysis of structural systems and especially for the response spectrum analysis of linearly behaving structures subjected to earthquake induced ground motions. To obtain dynamic characteristics such as mode shapes, natural frequencies and participation factors required in the mode superposition approach, the eigenvalue analysis of the structure is performed. In a modal analysis, it is a common practice to use only a first few modes in the calculation of the structural response because the contribution of the high modes to the response is usually small. Quite often, therefore, one needs to calculate only a first few modes by eigenvalue analysis. To obtain a first few modes, it is not necessary to solve the full eigenvalue problem. Therefore several techniques have been proposed to reduce the size of the eigenvalue problem.

Some type of schemes used to reduce the size of the problem are call condensation techniques. They primarily reduce the order of the system by condensing the number of coordinates. Since certain assumptions are made in effecting the condensation process, only approximate values of the lower eigenproperties can be obtained by these approaches. A review of condensation methods can be found in Reference 51.

In the dynamic condensation methods a small portion of the predecided coordinates of the structure, known as 'masters', are kept and the remaining coordinates, known as 'slaves', are eliminated by relating them to the retained coordinates. An arbitrary selection of the master coordinates, however, can lead to misleading results as some of the lower frequencies may be completely lost from the reduced spectrum [28]. Some qualitative guidelines [2,17,57] and analytical procedures [8,50,54,64] have been proposed in the literature for the selection of the appropriate degrees of freedom for an accurate representation of the lower modes. One of the popular analytical procedures computes the ratio of the diagonal coefficients of the stiffness to mass matrices, K_{ii}/M_{ii}, and then retains the degrees of freedom with the smallest ratios as the master coordinates. As will be indicated later by the example problems, this is not the best approach for selecting the master coordinates.

The first condensation approach for dynamic analysis of structures was proposed by Guyan [26]. However, because the relationship between the master and slave coordinates in this approach is based only on static considerations, this approach is also known as the static condensation method. Shortly after Guyan's paper, Irons [29] proposed an equivalent algorithm in which each slave coordinate is condensed at a time. Ramsden and Stoker [58] presented another method, known as the mass condensation method, which used the flexibility matrix to generate the reduced inertia matrix. Ojalvo and Newman [48] and Appa et al. [4] used the Lanczos' iteration procedure to condense the eigenvalue problem to a reduced rank tridiagonal form.

As the Guyan's approach ignores the masses at the slave degrees of freedom, some authors have studied the errors introduced by this omission of mass and have proposed some modifications to improve it. Geradin [24], Fox [22] and Thomas [71] developed formulas to estimate error bounds for the computed frequencies by expanding in series the exact relationship between the master and slave coordinates and neglecting terms containing powers greater than quadratic. Vysloukh et al. [74] have studied the convergence of this series. A study to determine the magnitude of error involved in reducing a two degree-of-freedom model was presented by Wolff et al. [76]. Kidder [35] and Miller [45], following the series expansion approach, proposed a back-transformation that included inertia terms to improve the mode shapes. But, as pointed out by Flax [19], these transformations may even introduce larger errors than the original Guyan transformation. Based on perturbation theory, Chen and Pan [11] estimated the error and developed an iterative technique to improve the accuracy of the Guyan reduction scheme.

More advanced dynamic condensation techniques have been presented in an effort to minimize the error introduced in the reduction process. Leung's condensation schemes [40-42] can provide exact reduced eigenproperties but the condensed eigenvalue problem is nonlinear which, however, can be solved by the techniques proposed by Wittrick and Williams [75]. Sotiropoulos [68] proposed another condensation process that is similar to Leung's method. It also leads to a nonlinear transcendental eigenvalue problem. Anderson and Hallauer [3] have used the Riccatti iteration algorithm to compute the exact condensation matrix and then obtained the exact lowest eigenproperties of the structure. The procedure presented by Johnson et al. [32] leads to a reduced eigenvalue problem in quadratic form the results of which can be improved by iterative techniques. Paz [52,53] proposed a method that used the Gauss-Jordan elimination process to compute the transformation matrix. Accurate estimates of the eigenproperties can be obtained by solving repetitively the reduced eigenvalue problem.

O'Callaghan [47] proposed a method which he called the Improved Reduced System (IRS) method. In his approach an extra term is added to the Guyan reduction to make some allowance for the inertia forces. Iterative versions of the IRS method have been proposed by Blair et al. [6], and Friswell et al. [23]. Other iterative dynamic condensation schemes to improve the accuracy of the calculated eigenproperties have been proposed by Suarez and Singh [69], Sauer [63], Razzaque [59], and Kim [36]. Rothe and Voss [61] use the Rayleigh functional of the nonlinear eigenvalue problem to improve the eigenvalue approximations. Bouhaddi and Fillod present a linearized dynamic condensation method that is applicable to substructures [7,9].

The application of the dynamic condensation techniques to nonclassically damped systems, however, has not received much attention. Reddy and Sharan [60] applied the Guyan reduction method to the analysis of machine tools. Rouch and Kao [62] used a method similar to the one proposed by Irons to calculate the complex eigenproperties of rotor bearing systems. Other methods, such as Leung's [42] and Paz's [53], are not applicable, in their current form, to this kind of systems. Furthermore, their application could be impractical for this case since the condensed matrices, which are defined in terms of a selected frequency, are complex. Finally, Flippen [20] has developed a new dynamic condensation model reduction theory which utilizes projection vectors that is applicable to structural systems with unsymmetrical matrices [18].

The condensation schemes can be effectively used to reduce the size of a frame and flexible slabs system. However, since these systems in general can be nonclassically damped, where undamped modes of the system cannot be used to uncouple the equations of motions, it is desirable to have a condensation approach which can be applied to damped systems to calculate their eigenproperties accurately. In this work, a generalization and extension of the condensation approach proposed by Suarez and Singh [69] for undamped systems is developed. In particular, a general condensation approach applicable to nonclassically damped systems is developed. Methods are also developed to use this condensation approach with a newly developed substructuring approach, herein called as the condensed substructure superposition approach, as well as with a modal synthesis approach, both applicable to nonclassically damped structures. Several sets of numerical results showing the effectiveness of the proposed condensation approach, condensed substructure superposition approach, and modal synthesis approach with condensation are presented. The application of the condensation approaches to structures with flexible floor slab structures is also demonstrated. Numerical results showing the importance of the out-of-plane flexibility of floor slabs on the displacement, acceleration, shear force, axial force, bending moment, and secondary system responses are also presented.

1.3 DISSERTATION ORGANIZATION

In Chapter 2, an approach called the condensed substructure superposition approach is developed. As mentioned before, approaches have been proposed to include the effect of the slab flexibility in dynamic analyses by representing the slab as one or more oscillators representing its modes. These approaches have lacked analytical rationale and dynamic compatibility. Here, an attempt has been made to include the effect of several modes of the supported slab in a dynamically consistent manner in the analysis of the supporting structure to incorporate the dynamic interaction between the two substructures. It is, however, observed that this approach does not provide very accurate values of the combined system modes until a large number of modes of the slab are included in the formulation. To improve this situation as well as to extend its applicability to damped systems, a generalized condensation approach applicable to nonclassically damped system is developed. Its formulation and numerical examples demonstrating its applicability are presented in Chapter 3.

In Chapter 4, the condensation approach of Chapter 3 is combined with the condensed substructure superposition approach of Chapter 2 to improve the accuracy of the later approach without solving a large eigenvalue problem. The combination of the condensation approach of Chapter 3 with the mode synthesis approach is also presented in this chapter. In this latter approach, the structure is divided into substructures which are defined by their eigenproperties. The combined structure synthesized from these substructure eigenproperties is then solved by the condensation approach of Chapter 3. The advantage of using the modal synthesis approach with condensation approach is that it offers a convenient and efficient way of defining the coordinates one should select for their condensation.

In Chapter 5, the combined approaches presented in Chapter 4 are specialized for classically damped systems. It is shown that this specialization can be simply effected by a proper replacement of the substructure matrices. Several sets of numerical results are presented for classically damped systems in this chapter.

In Chapter 6, we investigate three aspects of the seismic response of structures with flexible floors. First, we demonstrate the applicability of the dynamic condensation approach to this type of structures. Second, the influence of the out-of-plane flexibility of the floor slabs on the response of primary and secondary systems subjected to vertical ground motions is investigated. Finally, we evaluate the accuracy of the results obtained with some approximate approaches that have been used in nuclear power plant design industry for inclusion of the floor flexibility in the seismic analysis of secondary systems.

The summary and concluding remarks are given in Chapter 7.

CHAPTER I I

CONDENSED SUBSTRUCTURE SUPERPOSITION APPROACH

2.1 INTRODUCTION

As mentioned in the previous chapter, equivalent single degrees of freedom oscillators have been used to include the flexibility of the floor slab, and the dynamic interaction effect, in the seismic analysis of structures [39]. The mass and stiffness properties of an equivalent single degree of freedom oscillator are usually computed using the dominant mode of the flexible slab model. In this chapter, an analytical procedure is presented whereby several modes of a supported slab can be utilized to describe the equivalent system for the slab. To define the parameters of an equivalent system, the eigenproperties of the slab are used with a dynamic condensation scheme to reduce the degrees of freedom. A scheme to synthesize the condensed equivalent system with the supporting structure is proposed. Numerical results are presented to evaluate the applicability of the proposed approach.

2.2 ANALYTICAL FORMULATION

The equations of motion of an N degrees-of-freedom structural system subjected to a ground excitation $\ddot{X}(t)$, can be written as

$$[M]\ \ddot{\underset{\sim}{x}} + [C]\ \dot{\underset{\sim}{x}} + [K]\ \underset{\sim}{x} = -\ [M]\ \underset{\sim}{r}\ \ddot{X}(t) \tag{2.1}$$

in which $[M]$, $[C]$ and $[K]$ are the mass, damping and stiffness matrices respectively; $\underset{\sim}{r}$ is the excitation influence vector, and $\underset{\sim}{x}$ is the relative displacement vector. The dot over a quantity represents its derivative with respect to time.

Eq. (2.1) can be solved by the modal analysis approach. We will consider the case when the damping matrix $[C]$ is classical. Thus the solution is written in terms of the normal modes of the structural system. These modes are obtained from the solution of the following eigenvalue problem

$$[M]\ [\Phi]\ [\Lambda] = [K]\ [\Phi] \tag{2.2}$$

in which $[\Lambda]$ is a diagonal matrix containing the N eigenvalues and $[\Phi]$ is the eigenvector matrix.

We are interested in reducing the size of the eigenvalue problem of Eq. (2.2) and in obtaining only the first few modes of the structure. To accomplish this, first we divide the structure into substructures. For simplicity in the presentation, the formulation will be given in terms of two substructures, although it is applicable to any number of them.

Consider that the structure has been divided into two substructures which are identified as the α and β substructures. Let n and m be the number of the degrees of freedom of the α and β substructures, respectively, with their interface coordinates free. Also let n_b be the degrees of freedom at which the two substructures are connected. The total degrees of freedom of the combined structure is $N = n + m - n_b$.

The displacement vector of both substructures with their interface coordinates free can be partitioned as follows,

$$\underset{\sim}{x}^j = \begin{Bmatrix} \underset{\sim}{x}_b^j \\ \underset{\sim}{x}_i^j \end{Bmatrix} \quad \mathrm{j} = \alpha, \beta \tag{2.3}$$

in which $\underset{\sim}{x}_b^j$ is a (n_b x 1) vector that contains the degrees of freedom associated with the interfaces or boundaries of both substructures and $\underset{\sim}{x}_i^j$ is a vector containing the degrees of freedom associated with the interior of the substructures or those not shared by them. It has a dimension (n_i^α x 1) for the α substructure and (n_i^β x 1) for the β substructure. It is noted that the number of interior degrees of freedom for the α substructure is $n_i^\alpha = n - n_b$ and for the β substructure is $n_i^\beta = m - n_b$. A corresponding partitioning of the mass and stiffness matrices of both substructures is also affected as:

$$[\mathrm{M}^j] = \begin{bmatrix} \mathrm{M}_{bb}^j & \mathrm{M}_{bi}^j \\ \mathrm{M}_{ib}^j & \mathrm{M}_{ii}^j \end{bmatrix} \qquad [\mathrm{K}^j] = \begin{bmatrix} \mathrm{K}_{bb}^j & \mathrm{K}_{bi}^j \\ \mathrm{K}_{ib}^j & \mathrm{K}_{ii}^j \end{bmatrix} \qquad \mathrm{j} = \alpha, \beta \tag{2.4}$$

The displacement vector of the combined structure, written according to Eq. (2.3), is

$$\underset{\sim}{x} = \begin{Bmatrix} \underset{\sim}{x}_b \\ \underset{\sim}{x}_i^\alpha \\ \underset{\sim}{x}_i^\beta \end{Bmatrix} \tag{2.5}$$

where $\underset{\sim}{x}_b^\alpha = \underset{\sim}{x}_b^\beta = \underset{\sim}{x}_b$ to satisfy the compatibility conditions at the boundaries. In terms of the elements of the partitioned matrices in Eq. (2.4), the combined mass and stiffness matrices can be defined as:

$$[\mathrm{M}] = \begin{bmatrix} \mathrm{M}_{bb} & \mathrm{M}_{bi} \\ \mathrm{M}_{ib} & \mathrm{M}_{ii} \end{bmatrix} = \begin{bmatrix} \mathrm{M}_{bb}^{\alpha} + \mathrm{M}_{bb}^{\beta} & \mathrm{M}_{bi}^{\alpha} & \mathrm{M}_{bi}^{\beta} \\ \mathrm{M}_{ib}^{\alpha} & \mathrm{M}_{ii}^{\alpha} & 0 \\ \mathrm{M}_{ib}^{\beta} & 0 & \mathrm{M}_{ii}^{\beta} \end{bmatrix} \tag{2.6}$$

$$[\mathrm{K}] = \begin{bmatrix} \mathrm{K}_{bb} & \mathrm{K}_{bi} \\ \mathrm{K}_{ib} & \mathrm{K}_{ii} \end{bmatrix} = \begin{bmatrix} \mathrm{K}_{bb}^{\alpha} + \mathrm{K}_{bb}^{\beta} & \mathrm{K}_{bi}^{\alpha} & \mathrm{K}_{bi}^{\beta} \\ \mathrm{K}_{ib}^{\alpha} & \mathrm{K}_{ii}^{\alpha} & 0 \\ \mathrm{K}_{ib}^{\beta} & 0 & \mathrm{K}_{ii}^{\beta} \end{bmatrix} \tag{2.7}$$

We will assume that the eigenproperties of the α substructure, or at least a reduced set of them corresponding to the lower frequencies, are available. These eigenvalues, $[\Lambda_\alpha]$, and eigenvectors, $[\phi_\alpha]$, are obtained from the solution of the eigenvalue problem,

$$[\mathrm{M}^{\alpha}]\ [\phi_\alpha]\ [\Lambda_\alpha] = [\mathrm{K}^{\alpha}]\ [\phi_\alpha] \tag{2.8}$$

We plan to choose some modes of the α substructure to define its equivalent system. The number of modes to be kept from the reduced spectrum is arbitrary and any mode can be selected. Assuming that we use n_k modes, where n_k is less than n, we partition the modal matrix $[\phi_\alpha]$ as follows,

$$[\phi_\alpha] = [\phi_k^{\alpha} \quad \phi_r^{\alpha}] = \begin{bmatrix} \phi_{bk}^{\alpha} & \phi_{br}^{\alpha} \\ \phi_{ik}^{\alpha} & \phi_{ir}^{\alpha} \end{bmatrix} \tag{2.9}$$

where $[\phi_k^{\alpha}]$ is a (n x n_k) matrix that contains the eigenvectors to be kept and $[\phi_r^{\alpha}]$ is (n x n_r) matrix that contains the rest of the eigenvectors. Matrix $[\phi_{bk}^{\alpha}]$ contains the n_b rows of the modal matrix corresponding to the boundary degrees of freedom and matrix $[\phi_{ik}^{\alpha}]$ contains the remaining n_i^{α} rows associated to the interior degrees of freedom of the α

substructure. In general, both matrices will be rectangular. Now Eq. (2.8) can be written in terms of the n_k selected modal vectors of matrix $[\,\phi_\alpha\,]$ as

$$[\mathrm{M}^\alpha]\ [\,\phi_k^\alpha\,]\ [\,\Lambda_k^\alpha\,]\ =\ [\mathrm{K}^\alpha]\ [\,\phi_k^\alpha\,] \tag{2.10}$$

where $[\,\Lambda_k^\alpha\,]$ is a diagonal matrix of the n_k eigenvalues corresponding to the selected modes.

Matrix $[\phi_{ik}^\alpha]$ can be expressed in terms of matrix $[\phi_{bk}^\alpha]$ as follows,

$$[\,\phi_{ik}^\alpha\,]\ =\ \left[\hat{\mathrm{R}}\right]\ [\phi_{bk}^\alpha] \tag{2.11}$$

where the condensation matrix $\left[\hat{\mathrm{R}}\right]$ has a (n_i^α x n_b) dimension and is defined as,

$$\left[\hat{\mathrm{R}}\right]\ =\ [\,\phi_{ik}^\alpha\,]\ [\phi_{bk}^\alpha]^{-1} \tag{2.12}$$

Matrix $[\phi_{bk}^\alpha]$ may be singular and then the condensation matrix can not be computed. This will happen if some of its rows or columns are linearly dependent. Solution routines able to recognize linearly dependent equations should be used to avoid this problem. From the above equation we should expect that the number of kept modes, n_k, and the number of boundary degrees of freedom, n_b, must be the same, otherwise the inverse of matrix $[\phi_{bk}^\alpha]$ and matrix multiplication could not be computed. However, we can still define it using the Moore-Penrose generalized inverse [33] and get the following expression

$$\left[\hat{\mathrm{R}}\right] = [\,\phi_{ik}^\alpha\,]\ \left[\ \phi_{bk}^{\alpha\ \mathrm{T}}\ \phi_{bk}^\alpha\ \right]^{-1} [\phi_{bk}^\alpha]^{\mathrm{T}} \tag{2.13}$$

in which $\left[\ \phi_{bk}^{\alpha\ \mathrm{T}}\ \phi_{bk}^{\alpha}\ \right]$ is a square matrix with dimension n_k.

Now the reduced modal matrix $[\ \phi_k^{\alpha}\ ]$ can be written as

$$[\ \phi_k^{\alpha}\ ] = \begin{bmatrix} \mathrm{I} \\ \hat{\mathrm{R}} \end{bmatrix} \ [\phi_{bk}^{\alpha}\ ] = [\ \mathrm{S}\ ]\ \ [\phi_{bk}^{\alpha}\ ] \tag{2.14}$$

Substituting Eq. (2.14) into Eq. (2.10) and pre-multiplying by $[\ \mathrm{S}\ ]^{\mathrm{T}}$, we obtain the following condensed eigenvalue problem,

$$\left[\hat{\mathrm{M}}_{bb}^{\alpha}\right]\ \left[\phi_{bk}^{\alpha}\right]\ \left[\Lambda_k^{\alpha}\right]\ =\ \left[\hat{\mathrm{K}}_{bb}^{\alpha}\right]\ \left[\phi_{bk}^{\alpha}\right] \tag{2.15}$$

in which the condensed mass and stiffness matrices, $\left[\hat{\mathrm{M}}_{bb}^{\alpha}\right]$ and $\left[\hat{\mathrm{K}}_{bb}^{\alpha}\right]$, are symmetric ($n_b$ x n_b) matrices and are given by

$$\left[\hat{\mathrm{M}}_{bb}^{\alpha}\right] = [\mathrm{M}_{bb}^{\alpha}] + \left[\hat{\mathrm{R}}\right]^{\mathrm{T}}[\mathrm{M}_{ib}^{\alpha}] + [\mathrm{M}_{ib}^{\alpha}]^{\mathrm{T}}\left[\hat{\mathrm{R}}\right] + \left[\hat{\mathrm{R}}\right]^{\mathrm{T}}[\mathrm{M}_{ii}^{\alpha}]\ \left[\hat{\mathrm{R}}\right] \tag{2.16a}$$

$$\left[\hat{\mathrm{K}}_{bb}^{\alpha}\right] = [\mathrm{K}_{bb}^{\alpha}] + \left[\hat{\mathrm{R}}\right]^{\mathrm{T}}[\mathrm{K}_{ib}^{\alpha}] + [\mathrm{K}_{ib}^{\alpha}]^{\mathrm{T}}\left[\hat{\mathrm{R}}\right] + \left[\hat{\mathrm{R}}\right]^{\mathrm{T}}[\mathrm{K}_{ii}^{\alpha}]\ \left[\hat{\mathrm{R}}\right] \tag{2.16b}$$

The condensed matrices in Eq. (2.15) contain information about the n_k kept modes of the α substructure. They can be considered to represents a smaller dimensional structure which is equivalent to the α substructure. These matrices can be used to replace the stiffness and mass matrices of the α substructure in the eigenvalue problem of the combined structure, Eq. (2.2). This equation, now incorporating the effect of the α substructure through a reduced size equivalent structure, can be written as,

$$\left[\hat{M}\right] \left[\Phi_\beta\right] \left[\hat{\Lambda}\right] = \left[\hat{K}\right] \left[\Phi_\beta\right] \tag{2.17}$$

where the combined mass and stiffness matrices are given by

$$\left[\hat{M}\right] = \begin{bmatrix} \hat{M}_{bb} & \hat{M}_{bi} \\ \hat{M}_{ib} & \hat{M}_{ii} \end{bmatrix} = \begin{bmatrix} \hat{M}^{\alpha}_{bb} + M^{\beta}_{bb} & M^{\beta}_{bi} \\ M^{\beta}_{ib} & M^{\beta}_{ii} \end{bmatrix} \tag{2.18}$$

$$\left[\hat{K}\right] = \begin{bmatrix} \hat{K}_{bb} & \hat{K}_{bi} \\ \hat{K}_{ib} & \hat{K}_{ii} \end{bmatrix} = \begin{bmatrix} \hat{K}^{\alpha}_{bb} + K^{\beta}_{bb} & K^{\beta}_{bi} \\ K^{\beta}_{ib} & K^{\beta}_{ii} \end{bmatrix} \tag{2.19}$$

In Eq. (2.17) the effect of dynamic interaction between the two substructures has been properly included in the analytical model by means of the condensed matrices $\left[\hat{M}^{\alpha}_{bb}\right]$ and $\left[\hat{K}^{\alpha}_{bb}\right]$.

The size of the eigenvalue problem, Eq. (2.2), has now been reduced from *N* to *m*, the number of degrees of freedom of the β substructure with its boundary degrees of freedom free. It is expected that the solution of this reduced size eigenvalue problem will provided approximations of m eigenvalues, $\left[\hat{\Lambda}\right]$, and corresponding eigenvectors, $\left[\Phi_\beta\right]$, of the combined structures. Of course, the elements of the modal matrix are those associated only with the degrees of freedom of the β substructure. To obtain the elements of the eigenvectors corresponding to the interior degrees of freedom of the α substructure, we need to partition the modal matrix $\left[\Phi_\beta\right]$ into boundary and interior degrees of freedom as follow,

$$\left[\Phi_\beta\right] = \begin{bmatrix} \Phi^{\beta}_{b} \\ \Phi^{\beta}_{i} \end{bmatrix} \tag{2.20}$$

Since the boundary degrees of freedom are common to both substructures, $[\,\Phi_b\,] = \left[\,\Phi_b^{\beta}\,\right]$, we can relate them to the interior degrees of freedom of the α substructure using Eq. (2.11) as follows,

$$[\,\Phi_i^{\alpha}\,] = \left[\,\hat{R}\,\right]\ [\,\Phi_b\,] \tag{2.21}$$

Thus, the complete *m* eigenvectors of the combined structure arranged according to Eq. (2.5) are

$$\left[\,\hat{\Phi}\,\right] = \begin{bmatrix} \Phi_b \\ \Phi_i^{\alpha} \\ \Phi_i^{\beta} \end{bmatrix} \tag{2.22}$$

It is noted that the dimension of matrix $\left[\,\hat{R}\,\right]$ is (n_i x n_b) and consequently the size of the reduced eigenvalue problem (2.17) is independent of the number of the kept modes of the α substructure in the condensation process. We will have more information from the α substructure in the reduced analytical model as more modes are used. But the computational effort involved to compute $\left[\,\hat{R}\,\right]$ will increase as more modes are considered since it requires the inversion of a (n_k x n_k) matrix. Rather than increase the number of modes to be kept in the condensation process to improve the accuracy of the eigenproperties of the combined structure, we should include more degrees of freedom of the α substructure. Some of its interior degrees of freedom can then be considered as boundary degrees of freedom. Of course, this will increase the dimension of the condensed matrices $\left[\,\hat{M}_{bb}^{\alpha}\,\right]$ and $\left[\,\hat{K}_{bb}^{\alpha}\,\right]$ and consequently the order of the eigenvalue problem, Eq. (2.17). This will lead to an increased computational effort because of a bigger eigenvalue problem, but the accuracy of the results will be improved.

The solution of the eigenvalue problem, Eq. (2.17), provides the modal information required in the response calculation of the combined structure. In addition to the eigenproperties, the participation factors are also needed. They are defined as,

$$\underset{\sim}{\Gamma} = [\Phi]^{\mathrm{T}} [\mathrm{M}] \underset{\sim}{r} \tag{2.23}$$

where $\underset{\sim}{r}$ is the influence vector, $[\mathrm{M}]$ is the mass matrix of the combined structure and $[\Phi]$ is the modal matrix defined in Eq. (2.22). It is assumed that $[\Phi]$ has been normalized with respect to the mass matrix $[\mathrm{M}]$.

The participation factors can be computed considering the contribution of each substructure separately as

$$\underset{\sim}{\Gamma} = \underset{\sim}{\Gamma}^{\alpha} + \underset{\sim}{\Gamma}^{\beta} \tag{2.24}$$

where

$$\underset{\sim}{\Gamma}^{j} = \left[\Phi_b^{\mathrm{T}} \quad \Phi_i^{j\,\mathrm{T}} \right] \; [\mathrm{M}^j] \; \begin{Bmatrix} \underset{\sim}{r}_b \\ \underset{\sim}{r}_i^j \end{Bmatrix} \qquad \mathrm{j} = \alpha, \beta \tag{2.25}$$

in which the influence vector $\underset{\sim}{r}$ has been partitioned according to Eq. (2.5). Now we will define the participation factors in terms of the eigenvectors calculated from Eq. (2.17) and not the complete eigenvectors of the α substructure.

The contribution of the α substructure from Eq. (2.25) can be written as,

$$\underset{\sim}{\Gamma}^{\alpha} = [\Phi_b]^{\mathrm{T}} [\mathrm{M}_{bb}^{\alpha} \; \underset{\sim}{r}_b \; + \; \mathrm{M}_{bi}^{\alpha} \; \underset{\sim}{r}_i^{\alpha}] + [\Phi_i^{\alpha}]^{\mathrm{T}} [\mathrm{M}_{ib}^{\alpha} \; \underset{\sim}{r}_b \; + \; \mathrm{M}_{ii}^{\alpha} \; \underset{\sim}{r}_i^{\alpha}] \tag{2.26}$$

Substituting for $[\,\Phi_i^{\alpha}\,]$ from Eq. (2.21) in the above equation and after reordering terms we obtain,

$$\underset{\sim}{\Gamma}^{\alpha} = [\,\Phi_b\,]^{\mathrm{T}}\ \underset{\sim}{Z} \tag{2.27}$$

where

$$\underset{\sim}{Z} = \left[(\,\mathrm{M}_{bb}^{\alpha} + \hat{\mathrm{R}}^{\mathrm{T}}\ \mathrm{M}_{ib}^{\alpha}\,)\, \underset{\sim}{r}_b + (\,\mathrm{M}_{bi}^{\alpha} + \hat{\mathrm{R}}^{\mathrm{T}}\ \mathrm{M}_{ii}^{\alpha}\,)\, \underset{\sim}{r}_i \right] \tag{2.28}$$

Substituting Eq. (2.25) for the β substructure and Eq. (2.27) for the α substructure in Eq. (2.24), we get the expression for the participation factors of combined structure as follows,

$$\underset{\sim}{\Gamma} = \left[\,\Phi_b^{\mathrm{T}} \quad \Phi_i^{\beta\,\mathrm{T}}\,\right] \left[\begin{Bmatrix} \underset{\sim}{Z} \\ \underset{\sim}{0} \end{Bmatrix} + [\mathrm{M}^{\beta}] \begin{Bmatrix} \underset{\sim}{r}_b \\ \underset{\sim}{r}_i^{\beta} \end{Bmatrix} \right] \tag{2.29}$$

Knowing the eigenproperties, participation factors and the input excitation, any response quantity of the combined structure can be calculated by an appropriate modal analysis technique.

For the seismic analysis of a structure with several flexible floor slabs, the supporting structure should be identified as the β substructure with one α substructure for each slab in the structure. The condensed matrices of the slabs are then computed from Eqs. (2.16a) and (2.16b), and included in the eigenvalue problem of the supporting structure. The elements of the mode shapes associated to the interior degrees of freedom for each slab are then computed by using Eq. (2.21). After computing the modal properties of the combined structure any response quantity can be calculated.

2.3 NUMERICAL RESULTS

The procedure presented above was used to obtain the eigenproperties and responses of the structure shown in Figure 2.1. The structure was modeled using 21 beam elements and 24 nodes with 6 degrees of freedom per node. It has a total of 102 degrees of freedom. Properties of the structure and first 24 exact natural frequencies, obtained considering all degrees of freedom, are given in Table 2.1 and Table 2.2 respectively. The combined structure is divided into two substructures, Figure 2.2. The 3-Dimensional frame has 72 degrees of freedom and is considered as the α substructure. The cross structure has 54 degrees of freedom and is considered as the β substructure. There are 24 degrees of freedom at the substructures' interface. In this example the cross structure has been used to represent a floor slab.

The first 24 modes of the α substructure were used to compute the condensation matrix $\left[\hat{R}\right]$, Eq. (2.12). Only the boundary degrees of freedom were kept. Thus, the solution of the eigenvalue problem (2.17) will provide an approximation of the first 54 modes of the combined structure. Table 2.3 shows the first 24 natural frequencies calculated by the proposed approach. Percent errors in the frequencies, calculated as

$$\% \text{ Error} = \left(\frac{\omega_{approx} - \omega_{exact}}{\omega_{exact}} \right) \text{ x } 100 \tag{2.30}$$

are also shown in the table. It is noted that eight of them have an error in excess of 5 percent and are in general unacceptable [53]. Higher frequencies have larger errors and are, of course, unacceptable.

Root mean square values for displacements, shear forces, and bending moments at different points of the structure were computed with these approximate eigenproperties.

The modal combination rule proposed by Singh and Chu [66] was used to compute the responses and a 5% damping in each mode was assumed. Ground excitation was defined by the Kanai-Tajimi spectral density function with parameters given in Table 2.4.

Responses were obtained for the following ground excitations: 1) horizontal excitation only, 2) vertical excitation only, and 3) horizontal and vertical excitations together. Since the excitations were assumed statistically uncorrelated, the responses under the combined input were computed as the square root of the sum of the squares of the responses due to each of the excitations. Tables 2.5 and 2.6 show the root mean square value of the responses obtained with the exact eigenproperties. Horizontal displacements were computed only for the horizontal excitation because under the vertical excitation these displacements are considerably small. The same was done with the vertical displacements for the horizontal excitation.

Tables 2.7 and 2.8 show the normalized root mean square responses computed with the approximate eigenproperties. Normalized responses are computed as

$$\mathrm{NR} = \frac{\mathrm{R}_{approx}}{\mathrm{R}_{exact}} \tag{2.31}$$

Therefore, the closer this value is to 1.00 the better the result. In the first case, with only horizontal input, excellent results were obtained for the displacements. However, the error in shear forces and bending moments are significantly large. In the second case, with only vertical input, the results are better than those obtained for the horizontal input, but the errors in some of the bending moments are still somewhat large. In the third case of the combined horizontal and vertical inputs, the errors in the shear forces are large. The results obtained for the three cases indicate that more degrees of freedom of the α

substructure should be used to compute the condensed matrices of Eqs. (2.16a) and (2.16b) if better eigenproperties are desired.

2.4 SUMMARY AND CONCLUSIONS

In this chapter an analytical procedure is developed to include the effect of vertical flexibility of horizontal components such as slabs in seismic analysis of structures. It is a mathematical formalization of an intuitive approach being used in the industry. The formulation is presented to include several modes of a slab. Although presented for a structure composed only of two substructures, it can also be applied to a structure with any number of substructures.

Numerical results are presented to evaluate the performance of the proposed method. Approximations of the lower modes of vibration of the combined structure were obtained from the solution of two eigenvalue problems of smaller size. However, for the examples considered here the size of their eigenvalue problems are still large. Furthermore, the accuracy of the response seems to depends upon the number of degrees of freedom and the number of modes used to define an equivalent condensed structure. To improve the accuracy of the results more degrees of freedom should be included to compute the condensation matrix. This will, however, increase the dimension of the eigenvalue problem associated with the combined structure. Further extensions and modifications to improve this approach are presented in the following chapters.

Table 2.1 Properties of the frame structure in Figure 2.1.

Length	60.0 in
Area	64.0 in^2
Area Moment of Inertia about X-axis	680.0 in^4
Area Moment of Inertia about Y-axis	340.0 in^4
Area Moment of Inertia about Z-axis	340.0 in^4
Modulus of Elasticity	3000.0 ksi
Modulus of Rigidity	1320.0 ksi
Density	2608.0 (10^{-6}) slugs/in^3

Table 2.2 First 24 exact frequencies (in rad/sec) of the frame structure in Figure 2.1.

Mode	Frequency
1	12.39
2	12.39
3	17.71
4	44.54
5	61.46
6	72.06
7	72.06
8	72.75
9	95.48
10	95.48
11	107.93
12	118.38
13	120.97
14	120.97
15	121.40
16	126.22
17	127.14
18	127.14
19	133.01
20	231.45
21	241.80
22	241.80
23	262.21
24	278.53

Table 2.3 Frequencies (in rad/sec) and percent errors of the frame in Figure 2.1 calculated with the condensed substructure superposition approach.

Mode	Frequency	Percent Error
1	12.51	0.93
2	12.51	0.93
3	17.71	0.04
4	45.15	1.36
5	67.77	10.37
6	72.75	0.96
7	73.60	2.13
8	73.60	1.17
9	102.13	6.96
10	102.13	6.96
11	118.47	9.77
12	118.94	0.47
13	121.11	0.12
14	121.11	0.12
15	122.82	1.17
16	129.21	2.37
17	133.98	5.38
18	133.98	5.38
19	188.46	41.73
20	232.50	0.45
21	244.18	0.98
22	244.18	0.98
23	262.26	0.02
24	419.89	50.84

Table 2.4 Parameters of the Kanai-Tajimi Spectral Density Function ($S_0 = 0.0015$),

$$\Phi_g(\omega) = S_0 \sum_{i=1}^{3} S_i \frac{\omega_i^4 + 4\zeta_i^2\omega_i^2\omega^2}{(\omega_i^2-\omega^2)^2 + 4\zeta_i^2\omega_i^2\omega^2}$$

i	S_i (ft^2-s / rad)	ω_i (rad/sec)	ζ_i
1	0.001500	13.5	0.3925
2	0.000495	23.5	0.3600
3	0.000375	39.0	0.3350

Table 2.5 Exact root mean square shear forces and bending moments of the frame in Figure 2.1.

a) Shear Forces (kips)

Node	Direction	Input		
		Horizontal	Vertical	Combined
11	Y	53.81	53.28	75.72
11	X	68.21	10.26	68.98
14	Y	48.41	22.76	53.50
18	Y	10.95	9.35	14.40

b) Bending Moments (kips-in)

Node	Direction	Input		
		Horizontal	Vertical	Combined
11	Z	3301.64	558.02	3348.48
11	Z	103.18	1001.35	1006.63
14	X	433.19	114.02	447.95
18	Z	542.05	584.80	797.38

Table 2.6 Exact root mean square displacements (inches x 10^{-2}) of the frame in Figure 2.1.

	Input	
Node	Horizontal	Vertical
7	0.4968	0.0030
11	1.1298	--------
14	--------	0.0907
21	1.1642	0.1927

Table 2.7 Normalized root mean square shear forces and bending moments of the frame in Figure 2.1. Eigenproperties obtained with the condensed substructure superposition approach.

a) Shear Forces

	Input		
Node	Horizontal	Vertical	Combined
11	1.9786	1.3412	1.6933
11	0.9280	1.0425	0.9307
14	0.9894	1.0183	0.9947
18	1.8742	0.9732	1.5603

b) Bending Moments

	Input		
Node	Horizontal	Vertical	Combined
11	1.0575	1.0486	1.0572
11	3.1155	1.0302	1.0734
14	0.4655	1.8370	0.4522
18	1.3400	0.8244	1.0937

Table 2.8 Normalized root mean square displacements of the frame in Figure 2.1. Eigenproperties obtained with the condensed substructure superposition approach.

Node	Input	
	Horizontal	Vertical
7	0.9941	1.3307
11	0.9881	--------
14	--------	1.0501
21	0.9825	0.9367

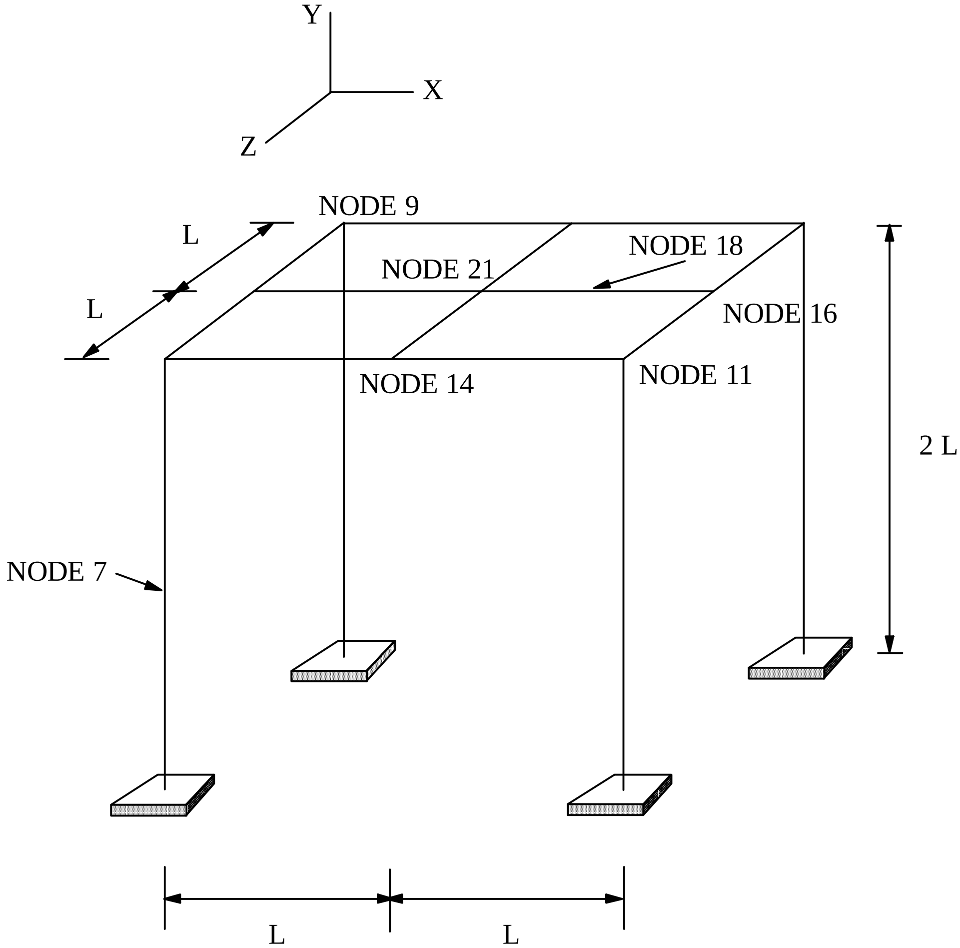

Figure 2.1 Structural configuration of the three dimensional frame of example problem.

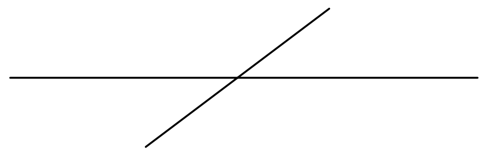

β substructure

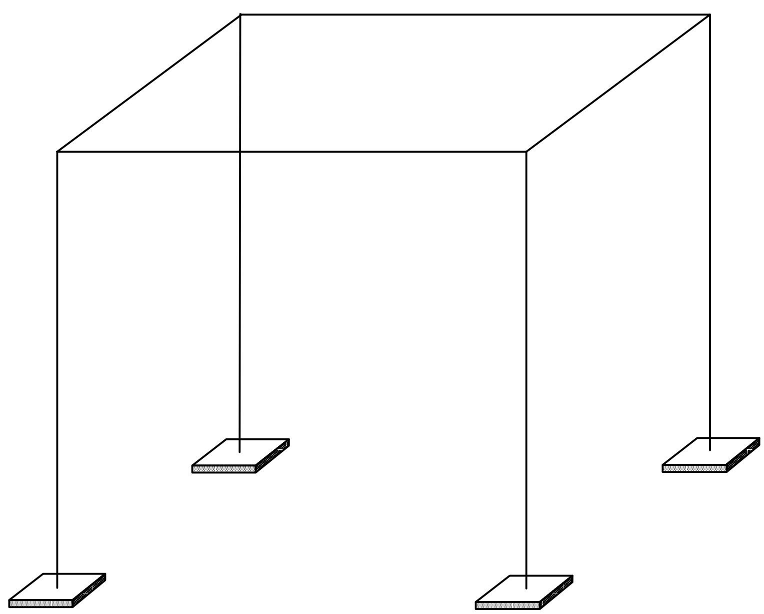

α substructure

Figure 2.2 Substructures of the frame in Figure 2.1.

CHAPTER III

DYNAMIC CONDENSATION APPROACH FOR NONCLASSICALLY DAMPED STRUCTURES

3.1 INTRODUCTION

As mentioned earlier, most dynamic condensation methods are restricted to the determination of vibration modes of structures with classical damping. However, there may be situations in which classical damping assumptions are invalid. Examples of such situations are structures made up of materials with different damping characteristics in different parts, structures with passive control systems or with concentrated dampers, and structures with rotating parts. In such cases, complex eigenproperties are required to incorporate the nonclassical damping effect in the dynamic analysis.

In this chapter, a dynamic condensation approach for nonclassically damped structures is developed. It is an important extension of the condensation approach proposed by Suarez and Singh [69] for undamped structures. The proposed method requires iterative solution of a reduced size eigenvalue problem. The eigenproperties obtained in an iteration step are used to improve the condensation matrix in the following iterative step. Accurate values can be obtained with a few iteration steps. The formulation is also developed to calculate the remaining eigenproperties from the solution of a complementary eigenvalue problem. Examples are presented to illustrate the effectiveness and convergence properties of the proposed approach. The effect of the selection of coordinates in the condensation process on the accuracy of the eigenproperties is also critically examined.

3.2 CONDENSED EIGENVALUE PROBLEMS

We will consider a general case of a structural system with equations of motion:

$$[M]\ \ddot{\underset{\sim}{x}} + [C]\ \dot{\underset{\sim}{x}} + [K]\ \underset{\sim}{x} = -[M]\ \underset{\sim}{r}\ \ddot{X}(t) \tag{3.1}$$

in which the damping matrix $[C]$ is not classical. This means that the normal modes of the undamped structural system cannot be used to uncoupled Eq. (3.1). The mathematical formulation that is commonly used for the modal analysis of such systems is the state vector approach. In this approach, Eq. (3.1) is transformed into an equivalent $2N$ dimension equations of the following form

$$[A]\ \dot{\underset{\sim}{y}} - [B]\ \underset{\sim}{y} = -[D]\ \bar{\underset{\sim}{r}}\ \ddot{X}(t) \tag{3.2}$$

in which $[A]$, $[B]$ and $[D]$ are ($2N$ x $2N$) real symmetric matrices defined as

$$[A] = \begin{bmatrix} [0] & [M] \\ [M] & [C] \end{bmatrix} \tag{3.3a}$$

$$[B] = \begin{bmatrix} [M] & [0] \\ [0] & -[K] \end{bmatrix} \tag{3.3b}$$

$$[D] = \begin{bmatrix} [0] & [0] \\ [0] & [M] \end{bmatrix} \tag{3.3c}$$

Vectors $\underset{\sim}{y}$ and $\bar{\underset{\sim}{r}}$, respectively, are the relative displacement and excitation influence state vectors of dimension (2*N* x 1). They are defined as

$$\underset{\sim}{y} = \begin{Bmatrix} \dot{\underset{\sim}{x}} \\ \underset{\sim}{x} \end{Bmatrix} \qquad\qquad \bar{\underset{\sim}{r}} = \begin{Bmatrix} \underset{\sim}{0} \\ \underset{\sim}{r} \end{Bmatrix} \tag{3.4}$$

The eigenproperties of the structural system that uncouple Eq. (3.2) can be obtained from the solution of its associated eigenvalue problem

$$[A]\ [\Psi]\ [\Omega] = [B]\ [\Psi] \tag{3.5}$$

in which $[\Omega]$ is a diagonal matrix containing the 2*N* eigenvalues and $[\Psi]$ is the (2*N* x 2*N*) eigenvector matrix. Eigenvalues and corresponding eigenvectors occur in complex conjugate pairs. Here the eigenvectors are assumed to have been normalized such that

$$[\Psi]^T [A]\ [\Psi] = [\ I\ ] \tag{3.6a}$$

$$[\Psi]^T [B]\ [\Psi] = [\Omega] \tag{3.6b}$$

where [I] is an (2*N* x 2*N*) unity matrix.

In general, the dimension of this eigenvalue problem can be large. Instead of solving it directly, we will solve two reduced size eigenvalue problems to obtain the complete set of eigenproperties. It is expedient to obtain the lowest modes from the solution of one of the eigenvalue problems and the higher modes from the solution of the other one. For this purpose, the displacement vector $\underset{\sim}{x}$ in Eq. (3.1) is partitioned as follow

$$\underset{\sim}{x} = \begin{Bmatrix} \underset{\sim}{x}_k \\ \underset{\sim}{x}_r \end{Bmatrix} \tag{3.7}$$

in which $\underset{\sim}{x}_k$ contains the degrees of freedom to be kept in the eigenvalue problem associated with the lower modes and $\underset{\sim}{x}_r$ contains the remaining degrees of freedom, those to be kept in the eigenvalue problem associated with the higher modes.

The partitioning of the displacement vector is, however, not arbitrary. Some guidelines have been proposed in the literature [2,8,17,28,44,50,54,57,64] for choosing the degrees of freedom for an accurate representation of the lower modes, which are usually the most important in the dynamic analysis. To decide about the degrees of freedom to be kept, associated with $\underset{\sim}{x}_k$, it is common to compute the ratio of the diagonal coefficients of the stiffness and mass matrices, K_{ii}/M_{ii}, and then select the first n_k degrees of freedom with the smallest ratios as the kept degrees of freedom. The remaining n_r degrees of freedom belong to the $\underset{\sim}{x}_r$. Of course, $N = n_k + n_r$.

Consistent with the partitioning of the displacement vector, the mass, damping and stiffness matrices are also partitioned as follows:

$$[M] = \begin{bmatrix} M_{kk} & M_{kr} \\ M_{rk} & M_{rr} \end{bmatrix} \tag{3.8a}$$

$$[C] = \begin{bmatrix} C_{kk} & C_{kr} \\ C_{rk} & C_{rr} \end{bmatrix} \tag{3.8b}$$

$$[K] = \begin{bmatrix} K_{kk} & K_{kr} \\ K_{rk} & K_{rr} \end{bmatrix} \tag{3.8b}$$

in which submatrices $[M_{ij}]$, $[C_{ij}]$ and $[K_{ij}]$ have dimensions (n_i x n_j).

A similar partitioning is also effected on the state vector and matrices of the state equation (3.2) as:

$$\underset{\sim}{y} = \begin{Bmatrix} \underset{\sim}{y}_k \\ \underset{\sim}{y}_r \end{Bmatrix} \tag{3.9a}$$

where

$$\underset{\sim}{y}_j = \begin{Bmatrix} \dot{\underset{\sim}{x}}_j \\ \underset{\sim}{x}_j \end{Bmatrix} \qquad j = k, r \tag{3.9b}$$

and,

$$[\mathrm{A}] = \begin{bmatrix} \mathrm{A}_{kk} & \mathrm{A}_{kr} \\ \mathrm{A}_{rk} & \mathrm{A}_{rr} \end{bmatrix} \tag{3.10a}$$

$$[\mathrm{B}] = \begin{bmatrix} \mathrm{B}_{kk} & \mathrm{B}_{kr} \\ \mathrm{B}_{rk} & \mathrm{B}_{rr} \end{bmatrix} \tag{3.10b}$$

in which submatrices $[\mathrm{A}_{ij}]$ and $[\mathrm{B}_{ij}]$ have dimensions ($2n_i$ x $2n_j$) and are defined as

$$[\mathrm{A}_{ij}] = \begin{bmatrix} 0_{ij} & \mathrm{M}_{ij} \\ \mathrm{M}_{ij} & \mathrm{C}_{ij} \end{bmatrix} \qquad i, j = k, r \tag{3.11a}$$

$$[\mathrm{B}_{ij}] = \begin{bmatrix} \mathrm{M}_{ij} & 0_{ij} \\ 0_{ij} & -\mathrm{K}_{ij} \end{bmatrix} \qquad i, j = k, r \tag{3.11b}$$

Modal matrices in Eq. (3.5) are also consistently partitioned as follows:

$$[\Omega] = \begin{bmatrix} \Omega_k & 0 \\ 0 & \Omega_r \end{bmatrix} \tag{3.12a}$$

$$[\Psi] = \begin{bmatrix} \Psi_{kk} & \Psi_{kr} \\ \Psi_{rk} & \Psi_{rr} \end{bmatrix} \tag{3.12b}$$

The submatrices $[\Omega_k]$, $[\Psi_{kk}]$ and $[\Psi_{rk}]$ contain the $2n_k$ eigenvalues and eigenvectors corresponding to the lower modes. Similarly, submatrices $[\Omega_r]$, $[\Psi_{kr}]$ and $[\Psi_{rr}]$ contain the $2n_r$ eigenvalues and eigenvectors of the higher modes. Both sets of modes occur in complex conjugate pairs and eigenvector submatrices $[\Psi_{ij}]$ are of size ($2n_i$ x $2n_j$) with $i,j = k,r$.

The eigenvalue problem corresponding to the $2n_k$ lower modes can be written as

$$\begin{bmatrix} A_{kk} & A_{kr} \\ A_{rk} & A_{rr} \end{bmatrix} \begin{bmatrix} \Psi_{kk} \\ \Psi_{rk} \end{bmatrix} [\Omega_k] = \begin{bmatrix} B_{kk} & B_{kr} \\ B_{rk} & B_{rr} \end{bmatrix} \begin{bmatrix} \Psi_{kk} \\ \Psi_{rk} \end{bmatrix} \tag{3.13}$$

In order to reduce the size of this eigenvalue problem, we will express matrix $[\Psi_{rk}]$ in terms of matrix $[\Psi_{kk}]$ as indicated Eq. (2.11),

$$[\Psi_{rk}] = \left[\hat{R}\right] [\Psi_{kk}] \tag{3.14}$$

in which the condensation matrix for the lower modes $\left[\hat{R}\right]$ is defined as

$$\left[\hat{R}\right] = [\Psi_{rk}] [\Psi_{kk}]^{-1} \tag{3.15}$$

Notice that here matrix $[\Psi_{kk}]$ is a square matrix, thus the number of degrees of freedom kept per mode and the number of modes are the same. Now the eigenvector matrix of the lower modes can be written in term of the condensation matrix $\left[\hat{R}\right]$ as

$$\begin{bmatrix} \Psi_{kk} \\ \Psi_{rk} \end{bmatrix} = \begin{bmatrix} I_k \\ \hat{R} \end{bmatrix} [\Psi_{kk}] = \left[\hat{S} \right] [\Psi_{kk}] \tag{3.16}$$

The condensed eigenvalue problem associated with the lower modes is then obtained by introducing Eq. (3.16) in Eq. (3.13) and pre-multiplying by $\left[\hat{S}\right]^T$. After simplifying, we obtain the following expression

$$\left[\hat{A}\right] [\Psi_{kk}] [\Omega_k] = \left[\hat{B}\right] [\Psi_{kk}] \tag{3.17}$$

where the condensed matrices $\left[\hat{A}\right]$ and $\left[\hat{B}\right]$ are

$$\left[\hat{A}\right] = [A_{kk}] + \left[\hat{R}\right]^T [A_{rk}] + [A_{kr}] \left[\hat{R}\right] + \left[\hat{R}\right]^T [A_{rr}] \left[\hat{R}\right] \tag{3.18a}$$

$$\left[\hat{B}\right] = [B_{kk}] + \left[\hat{R}\right]^T [B_{rk}] + [B_{kr}] \left[\hat{R}\right] + \left[\hat{R}\right]^T [B_{rr}] \left[\hat{R}\right] \tag{3.18b}$$

On the other hand, the eigenvalue problem corresponding to the $2n_r$ higher modes,

$$\begin{bmatrix} A_{kk} & A_{kr} \\ A_{rk} & A_{rr} \end{bmatrix} \begin{bmatrix} \Psi_{kr} \\ \Psi_{rr} \end{bmatrix} [\Omega_r] = \begin{bmatrix} B_{kk} & B_{kr} \\ B_{rk} & B_{rr} \end{bmatrix} \begin{bmatrix} \Psi_{kr} \\ \Psi_{rr} \end{bmatrix} \tag{3.19}$$

can be reduced to its condensed form, if we express matrix $[\Psi_{kr}]$ in terms of $[\Psi_{rr}]$ as follow

$$[\Psi_{kr}] = [\bar{R}] [\Psi_{rr}] \tag{3.20}$$

The condensation matrix for the higher modes $[\bar{R}]$ in Eq. (3.20) is defined as

$$[\bar{R}] = [\Psi_{kr}] \ [\Psi_{rr}]^{-1} \tag{3.21}$$

The eigenvector matrix of the higher modes in term of the condensation matrix $[\bar{R}]$ can be written as

$$\begin{bmatrix} \Psi_{kr} \\ \Psi_{rr} \end{bmatrix} = \begin{bmatrix} \bar{R} \\ I_r \end{bmatrix} [\Psi_{rr}] = [\bar{S}] \ [\Psi_{rr}] \tag{3.22}$$

By introducing Eq. (3.22) into Eq. (3.19) and pre-multiplying by $[\bar{S}]^T$, we obtain the condensed eigenvalue problem associated with the higher modes as

$$[\bar{A}] \ [\Psi_{rr}] \ [\Omega_r] = [\bar{B}] \ [\Psi_{rr}] \tag{3.23}$$

where the condensed matrices $[\bar{A}]$ and $[\bar{B}]$ are

$$[\bar{A}] = [A_{rr}] + [\bar{R}]^T [A_{kr}] + [A_{rk}] \ [\bar{R}] + [\bar{R}]^T [A_{kk}] \ [\bar{R}] \tag{3.24a}$$

$$[\bar{B}] = [B_{rr}] + [\bar{R}]^T [B_{kr}] + [B_{rk}] \ [\bar{R}] + [\bar{R}]^T [B_{kk}] \ [\bar{R}] \tag{3.24b}$$

From the solution of Eqs. (3.17) and (3.23) one can obtain the complete set of eigenproperties of the structural system. Once $[\Psi_{kk}]$ and $[\Psi_{rr}]$ are known, submatrices $[\Psi_{rk}]$ and $[\Psi_{kr}]$ can be computed from Eqs. (3.14) and (3.20) respectively. It can be shown that the complete set of eigenvectors computed from the reduced eigenvalue problems will automatically be normalized as indicated Eq. (3.6a) if the eigenvector submatrices $[\Psi_{kk}]$ and $[\Psi_{rr}]$ are normalized such that

$$[\Psi_{kk}]^T \left[\hat{A}\right] [\Psi_{kk}] = [I_k] \tag{3.25a}$$

$$[\Psi_{rr}]^T [\bar{A}] [\Psi_{rr}] = [I_r] \tag{3.25b}$$

The complete eigenvector matrix is then given as

$$[\Psi] = \begin{bmatrix} \Psi_{kk} & \Psi_{kr} \\ \Psi_{rk} & \Psi_{rr} \end{bmatrix} = \begin{bmatrix} \Psi_{kk} & \bar{R}\,\Psi_{rr} \\ \hat{R}\,\Psi_{kk} & \Psi_{rr} \end{bmatrix} \tag{3.26}$$

It is relevant to mention here that, although both condensation matrices, $\left[\hat{R}\right]$ and $[\bar{R}]$, are defined in terms of complex matrices, all their elements are real. Therefore, state matrices $[A]$ and $[B]$ in both condensed eigenvalue problems will also be real. This topic will be addressed in more details in the next section.

It is also of interest to derive the relationship between the two condensation matrices. For this we can use the orthogonality condition of the eigenvector matrix $[\Psi]$ Eq. (3.6a). This equation is equivalent to the following four matrix equations

$$[\Psi_{kk}]^T [A_{kk}\ \Psi_{kk} + A_{kr}\ \Psi_{rk}] + [\Psi_{rk}]^T [A_{rk}\ \Psi_{kk} + A_{rr}\ \Psi_{rk}] = [I_k] \tag{3.27a}$$

$$[\Psi_{kk}]^T [A_{kk}\ \Psi_{kr} + A_{kr}\ \Psi_{rr}] + [\Psi_{rk}]^T [A_{rk}\ \Psi_{kr} + A_{rr}\ \Psi_{rr}] = [\,0\,] \tag{3.27b}$$

$$[\Psi_{kr}]^T [A_{kk}\ \Psi_{kk} + A_{kr}\ \Psi_{rk}] + [\Psi_{rr}]^T [A_{rk}\ \Psi_{kk} + A_{rr}\ \Psi_{rk}] = [\,0\,] \tag{3.27c}$$

$$[\Psi_{kr}]^{\mathrm{T}}\,[\mathrm{A}_{kk}\;\Psi_{kr}\;+\;\mathrm{A}_{kr}\;\Psi_{rr}] + [\Psi_{rr}]^{\mathrm{T}}\,[\mathrm{A}_{rk}\;\Psi_{kr}\;+\;\mathrm{A}_{rr}\;\Psi_{rr}] = [\,\mathrm{I}_r\,] \tag{3.27d}$$

Substituting Eqs. (3.14) and (3.20) in Eq. (3.27b) and rearranging the terms, we obtain

$$[\Psi_{kk}]^{\mathrm{T}}\left[\mathrm{A}_{kk}\,\bar{\mathrm{R}}\;+\;\mathrm{A}_{kr} + \hat{\mathrm{R}}^{\mathrm{T}}\mathrm{A}_{rk}\,\bar{\mathrm{R}}\;+\;\hat{\mathrm{R}}^{\mathrm{T}}\,\mathrm{A}_{rr}\right]\;[\Psi_{rr}]\;=\;[\,0\,] \tag{3.28}$$

For Eq. (3.28) to be zero, the matrix in the middle must be a null matrix, hence

$$\left[\mathrm{A}_{kk}\,\bar{\mathrm{R}}\;+\;\mathrm{A}_{kr} + \hat{\mathrm{R}}^{\mathrm{T}}\,\mathrm{A}_{rk}\,\bar{\mathrm{R}}\;+\;\hat{\mathrm{R}}^{\mathrm{T}}\,\mathrm{A}_{rr}\right] = \;[\,0\,] \tag{3.29}$$

Solving for $[\,\bar{\mathrm{R}}\,]$ we obtain the desired relationship

$$[\,\bar{\mathrm{R}}\,] = \;-\;\left[\mathrm{A}_{kk} + \hat{\mathrm{R}}^{\mathrm{T}}\,\mathrm{A}_{rk}\right]^{-1}\left[\mathrm{A}_{kr}\;+\;\hat{\mathrm{R}}^{\mathrm{T}}\,\mathrm{A}_{rr}\right] \tag{3.30}$$

Thus, if one knows the condensation matrix $\left[\,\hat{\mathrm{R}}\,\right]$, then Eq. (3.30) can be used to compute $[\,\bar{\mathrm{R}}\,]$ as well. This is of help in defining the reduced eigenvalue problem for the higher modes if the eigenvalue problem of the lower modes is solved. An equation similar to Eq. (3.30) can be developed to calculate $\left[\,\hat{\mathrm{R}}\,\right]$ if one known $[\,\bar{\mathrm{R}}\,]$. For this purpose we use the orthogonality condition (5.6b). This provides

$$\left[\,\hat{\mathrm{R}}\,\right]^{\mathrm{T}} = \;-\;[\mathrm{B}_{kk}\,\bar{\mathrm{R}} + \mathrm{B}_{kr}\;]\;[\;\mathrm{B}_{rk}\,\bar{\mathrm{R}} + \mathrm{B}_{rr}\;]^{-1} \tag{3.31}$$

Thus, it is noted that to define the matrices of the condensed eigenvalue problems, we have to know at least one of the two condensation matrices $\left[\,\hat{\mathrm{R}}\,\right]$ or $[\,\bar{\mathrm{R}}\,]$ in advance.

Eqs. (3.15) and (3.21) cannot be used to compute these matrices since the eigenvectors are unknown. In the next sections we present an iterative procedure to compute the condensation matrices.

3.3 ITERATIVE CONDENSATION PROCESS WITH LOWER MODES

An initial approximation for the condensation matrix $\left[\hat{\mathrm{R}}\right]$ can be obtained from the eigenvalue problem, Eq. (3.13), associated with the lower modes. This equation is equivalent to the following matrix equations

$$[\mathrm{A}_{kk}\ \Psi_{kk} + \mathrm{A}_{kr}\ \Psi_{rk}]\ [\,\Omega_k\,] = [\mathrm{B}_{kk}\ \Psi_{kk} + \mathrm{B}_{kr}\ \Psi_{rk}] \tag{3.32a}$$

$$[\mathrm{A}_{rk}\ \Psi_{kk} + \mathrm{A}_{rr}\ \Psi_{rk}]\ [\,\Omega_k\,] = [\mathrm{B}_{rk}\ \Psi_{kk} + \mathrm{B}_{rr}\ \Psi_{rk}] \tag{3.32b}$$

To obtain an initial approximation of the condensation matrix assume that the left hand side of Eq. (3.32b) is equal to a null matrix. The equation is then reduced to

$$\left[\mathrm{B}_{rk}\ \Psi_{kk}^{(0)} + \mathrm{B}_{rr}\ \Psi_{rk}^{(0)}\right] = [\,0\,] \tag{3.33}$$

where the superscript (0) indicates that the quantities are associated with the initial estimate. Solving Eq. (3.33) one obtains

$$\left[\Psi_{rk}^{(0)}\right] = -\,[\mathrm{B}_{rr}]^{-1}\,[\mathrm{B}_{rk}]\ \left[\Psi_{kk}^{(0)}\right] \tag{3.34}$$

Comparing this equation with Eq. (3.14), we obtain an initial approximation for the condensation matrix $\left[\hat{R}\right]$ as follows:

$$\left[\hat{R}^{(0)}\right] = -\left[B_{rr}\right]^{-1}\left[B_{rk}\right] \tag{3.35}$$

Using Eq. (3.11b), this equation can be written as

$$\left[\hat{R}^{(0)}\right] = \begin{bmatrix} G_M & 0 \\ 0 & G_K \end{bmatrix} = -\begin{bmatrix} M_{rr}^{-1}\,M_{rk} & 0 \\ 0 & K_{rr}^{-1}\,K_{rk} \end{bmatrix} \tag{3.36}$$

in which submatrices G_M and G_K are identified as the Guyan condensation matrices [19] in terms of the mass and stiffness matrices, respectively. An alternative estimate can be defined by replacing submatrix G_M by submatrix G_K in the above equation as follows

$$\left[\hat{R}^{(0)}\right] = \begin{bmatrix} G_K & 0 \\ 0 & G_K \end{bmatrix} = -\begin{bmatrix} K_{rr}^{-1}\,K_{rk} & 0 \\ 0 & K_{rr}^{-1}\,K_{rk} \end{bmatrix} \tag{3.37}$$

With this initial estimate of the condensation matrix, matrices $\left[\hat{A}\right]$ and $\left[\hat{B}\right]$ of the eigenvalue problem (3.17) can be obtained as

$$\left[\hat{A}\right] = \begin{bmatrix} [\,0\,] & \left[\hat{M}\right] \\ \left[\hat{M}\right] & \left[\hat{C}\right] \end{bmatrix} \tag{3.38a}$$

$$\left[\hat{B}\right] = \begin{bmatrix} \left[\hat{M}\right] & [\,0\,] \\ [\,0\,] & -\left[\hat{K}\right] \end{bmatrix} \tag{3.38b}$$

in which the mass, damping and stiffness matrices have been condensed using Guyan condensation matrix as

$$\left[\hat{M}\right] = [M_{kk}] + [G_K]^T [M_{rk}] + [M_{kr}] [G_K] + [G_K]^T [M_{rr}] [G_K] \tag{3.39a}$$

$$\left[\hat{C}\right] = [C_{kk}] + [G_K]^T [C_{rk}] + [C_{kr}] [G_K] + [G_K]^T [C_{rr}] [G_K] \tag{3.39b}$$

$$\left[\hat{K}\right] = [K_{kk}] + [G_K]^T [K_{rk}] + [K_{kr}] [G_K] + [G_K]^T [K_{rr}] [G_K] \tag{3.39c}$$

In general, better initial estimates of the complex eigenproperties will be obtained when Eq. (3.37) is used. Notice that in both cases, matrix $\left[\hat{R}\right]$ is defined in terms of real matrices and consequently the condensed matrices will be initially real.

With this condensation matrix known, we can compute the matrices of the condensed eigenvalue problem associated with the lower modes, Eq. (3.17), and then obtain an initial approximation of the eigenproperties $\left[\Psi_{kk}^{(0)}\right]$ and $\left[\Omega_k^{(0)}\right]$. This approximate solution can now be used to improve matrix $\left[\hat{R}\right]$. To define the improved estimate for $\left[\hat{R}\right]$ we consider Eq. (3.32b) again, which after reordering terms is written as

$$[\, B_{rr}\ \Psi_{rk}\,] = [A_{rk}\ \Psi_{kk} + A_{rr}\ \Psi_{rk}]\ [\, \Omega_k\,] - [\, B_{rk}\ \Psi_{kk}\,] \tag{3.40}$$

By pre- and post-multiplying by $[B_{rr}]^{-1}$and $[\Psi_{kk}]^{-1}$, respectively, the above equation and recalling the definition of $\left[\hat{R}\right]$, Eq. (3.15), we obtain

$$\left[\hat{R}\right] = [B_{rr}]^{-1} \left[A_{rk} + A_{rr}\ \hat{R}\right]\ [\Psi_{kk}]\ [\, \Omega_k\,]\ [\Psi_{kk}]^{-1} - [B_{rr}]^{-1} [B_{rk}] \tag{3.41}$$

This equation requires the inverse of $[\Psi_{kk}]$, a complex matrix. However, we can use the orthogonality condition of the lower modes to avoid calculating this inverse. We consider the following orthogonality condition

$$[\Psi_{kk}]^{\mathrm{T}} \left[\hat{\mathrm{B}}\right] [\Psi_{kk}] = [\,\Omega_k\,] \tag{3.42}$$

If we post-multiply the above equation by $[\Psi_{kk}]^{-1}$, we get

$$[\,\Omega_k\,] \; [\Psi_{kk}]^{-1} = [\Psi_{kk}]^{\mathrm{T}} \left[\hat{\mathrm{B}}\right] \tag{3.43}$$

By introducing Eq. (3.43) into Eq. (3.41), we obtain the expression

$$\left[\hat{\mathrm{R}}\right] = [\mathrm{B}_{rr}]^{-1} \left[\mathrm{A}_{rk} + \mathrm{A}_{rr}\,\hat{\mathrm{R}}\right] [\Psi_{kk}] \; [\Psi_{kk}]^{\mathrm{T}} \left[\hat{\mathrm{B}}\right] - [\mathrm{B}_{rr}]^{-1} [\mathrm{B}_{rk}] \tag{3.44}$$

The equality in Eq. (3.44) will be identically satisfied if the actual condensation matrix $\left[\hat{\mathrm{R}}\right]$ and eigenvector matrix $[\Phi_{kk}]$ are used in the right hand side of the equation. However, this equation can also be used to define a recursive relationship to iteratively obtain an improved estimate of $\left[\hat{\mathrm{R}}\right]$ as follows

$$\left[\hat{\mathrm{R}}^{(l+1)}\right] = [\,\mathrm{B}_{rr}]^{-1} \left[\mathrm{A}_{rk} + \mathrm{A}_{rr}\,\hat{\mathrm{R}}^{(l)}\right] \left[\Psi_{kk}^{(l)}\right] \left[\Psi_{kk}^{(l)}\right]^{\mathrm{T}} \left[\hat{\mathrm{B}}^{(l)}\right] - [\,\mathrm{B}_{rr}]^{-1} [\,\mathrm{B}_{rk}] \tag{3.45}$$

where superscript (l) refers to the iteration step. The last term on the right hand side of this equation can be identified as the initial approximation $\left[\hat{\mathrm{R}}^{(0)}\right]$. The other term is a correction term that is added to improve this original estimate. Once again this improved condensation matrix is defined in terms of complex eigenvectors, but we will show next that it is always a real matrix.

Consider the case when l = 0. From Eq. (3.45) we can see that the first estimate of the condensation matrix, $\left[\hat{R}^{(1)}\right]$, will be real if the term

$$\left[\Psi_{kk}^{(0)}\right]\left[\Psi_{kk}^{(0)}\right]^{T} \tag{3.46}$$

is real. To prove this, lets consider the orthogonality condition

$$\left[\Psi_{kk}^{(0)}\right]^{T}\left[\hat{A}^{(0)}\right]\left[\Psi_{kk}^{(0)}\right] = \left[I_{k}\right] \tag{3.47}$$

By pre- and post-multiplying the above equation by $\left[\Psi_{kk}^{(0)}\right]^{-T}$ and $\left[\Psi_{kk}^{(0)}\right]^{-1}$, respectively, and then computing its inverse we get that

$$\left[\Psi_{kk}^{(0)}\right]\left[\Psi_{kk}^{(0)}\right]^{T} = \left[\hat{A}^{(0)}\right]^{-1} \tag{3.48}$$

where the matrix $\left[\hat{A}^{(0)}\right]$ is real since the initial condensation matrix is real. Thus, $\left[\hat{R}^{(1)}\right]$ defined from Eq. (3.45) will be real which in turn render the remaining matrices $\left[\hat{A}^{(1)}\right]$ and $\left[\hat{B}^{(1)}\right]$ real. Thus, matrices $\left[\hat{R}^{(l)}\right]$, $\left[\hat{A}^{(l)}\right]$ and $\left[\hat{B}^{(l)}\right]$ involved in all subsequent iterations will also be real. This will also apply to the condensation matrix for the higher modes $\left[\bar{R}^{(l)}\right]$.

The improved condensation matrix $\left[\hat{R}^{(l+1)}\right]$ can be used to define a new condensed eigenvalue problem (3.17). The eigenvector matrix obtained from the solution of this eigenvalue problem is then used to calculate a new condensation matrix by using Eq. (3.45). The procedure is repeated until the desired converge criteria on the eigenvalues at two consecutive iterations steps is achieved.

After the lower modes are obtained, the condensation matrix $\left[\hat{R}\right]$ from the final iteration step can be used in Eq. (3.30) to calculate the condensation matrix for the higher modes. With matrix $[\bar{R}]$ known, the higher modes can be obtained from the solution of their condensed eigenvalue problem (3.23). The complete set of eigenvectors is then computed with Eq. (3.26).

The foregoing procedure allows us to compute the complete set of eigenproperties of a structural system by iteratively solving the eigenvalue problem associated with the lower modes. But as we will show in the next section, it is also possible to compute the eigenproperties by iterating with the higher modes.

3.4 ITERATIVE CONDENSATION PROCESS WITH HIGHER MODES

The initial condensation matrix for the higher modes can be obtained from the eigenvalue problem defined in Eq. (3.19), which is equivalent to the following matrix equations

$$[A_{kk}\ \Psi_{kr} + A_{kr}\ \Psi_{rr}]\ [\Omega_r] = [B_{kk}\ \Psi_{kr} + B_{kr}\ \Psi_{rr}] \tag{3.49a}$$

$$[A_{rk}\ \Psi_{kr} + A_{rr}\ \Psi_{rr}]\ [\Omega_r] = [B_{rk}\ \Psi_{kr} + B_{rr}\ \Psi_{rr}] \tag{3.49b}$$

To obtain an initial estimate for $[\bar{R}]$, consider Eq. (3.49a) and assume that its right hand size is equal to a null matrix. That is,

$$\left[\mathrm{A}_{kk}\ \Psi_{kr}^{(0)}\ +\ \mathrm{A}_{kr}\ \Psi_{rr}^{(0)} \right]\ \left[\Omega_{r}^{(0)} \right] = [\,0\,] \tag{3.50}$$

and hence

$$\left[\mathrm{A}_{kk}\ \Psi_{kr}^{(0)}\ +\ \mathrm{A}_{kr}\ \Psi_{rr}^{(0)} \right] =\ [\,0\,] \tag{3.51}$$

Solving the above equation for $\left[\Psi_{kr}^{(0)} \right]$, we get

$$\left[\Psi_{kr}^{(0)} \right]\ =\ -\ [\mathrm{A}_{kk}]^{-1}\ [\mathrm{A}_{kr}]\ \left[\Psi_{rr}^{(0)} \right] \tag{3.52}$$

Comparing this equation with Eq. (3.20), we obtain the initial approximation for $[\,\overline{\mathrm{R}}\,]$ as

$$\left[\overline{\mathrm{R}}^{(0)} \right] =\ -\ [\mathrm{A}_{kk}]^{-1}\ [\mathrm{A}_{kr}] \tag{3.53}$$

or in terms of the mass and damping submatrices as,

$$\left[\overline{\mathrm{R}}^{(0)} \right]\ =\begin{bmatrix} \mathrm{M}_{kk}^{-1}\ \mathrm{M}_{kr} & \mathrm{M}_{kk}^{-1}\ (\ \mathrm{C}_{kk}\ \mathrm{M}_{kk}^{-1}\ \mathrm{M}_{kr} + \mathrm{C}_{kr}\ ) \\ 0 & \mathrm{M}_{kk}^{-1}\ \mathrm{M}_{kr} \end{bmatrix} \tag{3.54}$$

where the superscript (0) indicate that it is an initial value. Once the initial condensation matrix is known, we can compute the matrices of the condensed eigenvalue problem associated with the higher modes, Eq. (3.23). The solution of this eigenvalue problem provides an initial approximation of the eigenproperties $\left[\Psi_{rr}^{(0)} \right]$ and $\left[\Omega_{r}^{(0)} \right]$. Next we proceed to develop the recursive relationship to improve the initial estimate of $[\,\overline{\mathrm{R}}\,]$.

To develop a recursive equation similar to Eq. (3.45) obtained for the lower modes, consider again Eq. (3.49a). Solving for $[A_{kk}\Psi_{kr}]$ and substituting Eq. (3.20) into its right hand side we obtain

$$[A_{kk}\ \Psi_{kr}] = [\ B_{kk}\ \bar{R} + B_{kr}\ ]\ \ [\Psi_{rr}]\ \ [\ \Omega_r\ ]^{-1} - \ [A_{kr}\ \Psi_{rr}\ ] \tag{3.55}$$

Pre-multiplying by $[A_{kk}]^{-1}$and post-multiplying by $[\Psi_{rr}]^{-1}$the above equation, and after recalling the definition of $[\ \bar{R}]$ in Eq. (3.21), we obtain

$$[\ \bar{R}\ ]= [A_{kk}]^{-1}[\ B_{kk}\ \bar{R} + B_{kr}\ ][\Psi_{rr}]\ [\ \Omega_r\ ]^{-1}[\Psi_{rr}]^{-1} - [A_{kk}]^{-1}[A_{kr}] \tag{3.56}$$

The inverse of $[\Psi_{rr}]$ in this equation also can be obtained from the orthogonality condition

$$[\Psi_{rr}]^{\mathrm{T}}\ [\ \bar{A}\ ]\ \ [\Psi_{rr}] = [\ I_r\ ] \tag{3.57}$$

By pre-multiplying the above equation by $[\Psi_{rr}]^{-1}$ we obtain

$$[\Psi_{rr}]^{-1}= [\Psi_{rr}]^{\mathrm{T}}\ [\ \bar{A}\ ] \tag{3.58}$$

Introducing this equation into Eq. (3.56) we obtain

$$[\ \bar{R}\ ]= [A_{kk}]^{-1}[\ B_{kk}\ \bar{R} + B_{kr}\ ][\Psi_{rr}]\ [\ \Omega_r\ ]^{-1}[\Psi_{rr}]^{\mathrm{T}}[\ \bar{A}\ ] - [A_{kk}]^{-1}[A_{kr}] \tag{3.59}$$

Eq. (3.59) will be satisfied if the actual matrices $[\ \bar{R}\ ]$, $[\Phi_{rr}]$ and $[\ \Lambda_r\ ]$ are introduced in the right hand side. But as in the case of the iterative procedure with lower modes, this equation can also be used to define the recursive equation to improve the estimate of the condensation matrix $[\,\overline{\mathrm{R}}\,]$ as

$$\left[\,\overline{\mathrm{R}}^{(l+1)}\right] = [\,\mathrm{A}_{kk}\,]^{-1}\left[\mathrm{R}_{kr}^{(l)}\right][\,\Psi_{rr}^{(l)}\,][\,\Omega_{r}^{(l)}\,]^{-1}[\,\Psi_{rr}^{(l)}\,]^{\mathrm{T}}[\,\overline{\mathrm{A}}^{(l)}\,] - [\,\mathrm{A}_{kk}\,]^{-1}[\,\mathrm{A}_{kr}\,] \tag{3.60a}$$

where

$$\left[\,\mathrm{R}_{kr}^{(l)}\,\right] = \left[\mathrm{B}_{kk}\,\overline{\mathrm{R}}^{(l)} + \mathrm{B}_{kr}\right] \tag{3.60b}$$

Here again superscript (l) refers to the iteration step. As in Eq. (3.45), the last term on the right hand side of the above equation can be identified as the initial approximation of the condensation matrix and the other term is a correction that is added to the initial approximation to improve it.

Knowing the condensation matrix $[\,\overline{\mathrm{R}}\,]$, the iteration with the higher modes can be performed. In each iteration, the eigenvalue problem (3.23) is solved. This solution is then used to improve the estimate of the condensation matrix by means of Eqs. (3.60a) and (3.60b). The procedure continue until the desire convergence criteria is satisfied. If desired, the condensation matrix for the lower modes is computed using Eq. (3.31) and the lower modes computed from the solution of the eigenvalue problem (3.17).

3.5 STEP-BY-STEP PROCEDURE

The steps of the condensation procedure developed in the previous sections are as follows:

a) Iteration process with lower modes

1. Partition the displacement vector as:

$$\underset{\sim}{x} = \left\{ \begin{array}{c} \underset{\sim}{x}_k \\ \underset{\sim}{x}_r \end{array} \right\} \tag{3.7}$$

2. Calculate an initial value for $\left[\hat{R} \right]$ with:

$$\left[\hat{R}^{(0)} \right] = - \ [B_{rr}]^{-1} \ [B_{rk}] \tag{3.35}$$

or

$$\left[\hat{R}^{(0)} \right] = \begin{bmatrix} G_K & 0 \\ 0 & G_K \end{bmatrix} = - \begin{bmatrix} K_{rr}^{-1} \ K_{rk} & 0 \\ 0 & K_{rr}^{-1} \ K_{rk} \end{bmatrix} \tag{3.37}$$

3. Compute condensed matrices $\left[\hat{A} \right]$ and $\left[\hat{B} \right]$:

$$\left[\hat{A}^{(l)} \right] = [A_{kk}] + \left[\hat{R}^{(l)} \right]^T [A_{rk}] + [A_{kr}] \left[\hat{R}^{(l)} \right] + \left[\hat{R}^{(l)} \right]^T [A_{rr}] \left[\hat{R}^{(l)} \right] \tag{3.18a}$$

$$\left[\hat{B}^{(l)} \right] = [B_{kk}] + \left[\hat{R}^{(l)} \right]^T [B_{rk}] + [B_{kr}] \left[\hat{R}^{(l)} \right] + \left[\hat{R}^{(l)} \right]^T [B_{rr}] \left[\hat{R}^{(l)} \right] \tag{3.18b}$$

4. Solved the eigenvalue problem:

$$\left[\hat{A}^{(l)} \right] \left[\Psi_{kk}^{(l)} \right] \left[\Omega_k^{(l)} \right] = \left[\hat{B}^{(l)} \right] \left[\Psi_{kk}^{(l)} \right] \tag{3.17}$$

5. Check for eigenvalue convergence criterion, such as:

$$\left| \frac{\lambda_i^{(l+1)} - \lambda_i^{(l)}}{\lambda_i^{(l+1)}} \right| \leq \epsilon \qquad \text{for i} = 1, \ldots, \ n_k$$

If criterion is satisfied, go to step 7, otherwise go to step 6.

6. Update condensation matrix:

$$\left[\hat{R}^{(l+1)}\right] = [\,B_{rr}]^{-1}\left[A_{rk} + A_{rr}\,\hat{R}^{(l)}\right]\left[\,\Psi_{kk}^{(l)}\right]\left[\,\Psi_{kk}^{(l)}\right]^{T}\left[\hat{B}^{(l)}\right] - [\,B_{rr}]^{-1}\,[B_{rk}] \quad (3.45)$$

Go to step 3.

7. Compute global eigenvectors:

$$[\,\Psi_k\,] = \begin{bmatrix} \Psi_{kk} \\ \hat{R}^{(l)}\ \Psi_{kk} \end{bmatrix} \quad (3.16)$$

8. If whole set of eigenvectors are desired, then compute the condensation matrix $[\,\bar{R}\,]$:

$$[\,\bar{R}\,] = -\left[\,A_{kk} + \hat{R}^{(l)\,T} A_{rk}\,\right]^{-1}\left[A_{kr} + \hat{R}^{(l)\,T} A_{rr}\right] \quad (3.30)$$

9. Compute condensed matrices $[\,\bar{A}\,]$ and $[\,\bar{B}\,]$:

$$[\,\bar{A}\,] = [\,A_{rr}] + [\,\bar{R}\,]^{T}[\,A_{kr}] + [\,A_{rk}]\,[\,\bar{R}\,] + [\,\bar{R}\,]^{T}[\,A_{kk}]\,[\,\bar{R}\,] \quad (3.24a)$$

$$[\,\bar{B}\,] = [\,B_{rr}] + [\,\bar{R}\,]^{T}[\,B_{kr}] + [\,B_{rk}]\,[\,\bar{R}\,] + [\,\bar{R}\,]^{T}[\,B_{kk}]\,[\,\bar{R}\,] \quad (3.24b)$$

10. Solved the eigenvalue problem:

$$[\bar{\mathrm{A}}]\ [\Psi_{rr}]\ [\Omega_r] = [\bar{\mathrm{B}}]\ [\Psi_{rr}] \tag{3.23}$$

11. Compute global eigenvectors:

$$[\Psi_r] = \begin{bmatrix} \bar{\mathrm{R}}\ \Psi_{rr} \\ \Psi_{rr} \end{bmatrix} \tag{3.22}$$

b) Iteration process with higher modes

1. Partition the displacement vector as:

$$\underset{\sim}{x} = \begin{Bmatrix} \underset{\sim}{x}_k \\ \underset{\sim}{x}_r \end{Bmatrix} \tag{3.7}$$

2. Calculate an initial value for $[\bar{\mathrm{R}}]$ with:

$$\left[\bar{\mathrm{R}}^{(0)}\right] = -\ [\mathrm{A}_{kk}]^{-1}\ [\mathrm{A}_{kr}] \tag{3.53}$$

or

$$\left[\bar{\mathrm{R}}^{(0)}\right] = \begin{bmatrix} \mathrm{M}_{kk}^{-1}\ \mathrm{M}_{kr} & \mathrm{M}_{kk}^{-1}\left(\mathrm{C}_{kk}\ \mathrm{M}_{kk}^{-1}\ \mathrm{M}_{kr} + \mathrm{C}_{kr}\right) \\ 0 & \mathrm{M}_{kk}^{-1}\ \mathrm{M}_{kr} \end{bmatrix} \tag{3.54}$$

3. Compute condensed matrices $[\bar{\mathrm{A}}]$ and $[\bar{\mathrm{B}}]$:

$$\left[\bar{\mathrm{A}}^{(l)}\right] = [\mathrm{A}_{rr}] + \left[\bar{\mathrm{R}}^{(l)}\right]^{\mathrm{T}}[\mathrm{A}_{kr}] + [\mathrm{A}_{rk}]\left[\bar{\mathrm{R}}^{(l)}\right] + \left[\bar{\mathrm{R}}^{(l)}\right]^{\mathrm{T}}[\mathrm{A}_{kk}]\left[\bar{\mathrm{R}}^{(l)}\right] \tag{3.24a}$$

$$\left[\bar{\mathrm{B}}^{(l)}\right] = [\mathrm{B}_{rr}] + \left[\bar{\mathrm{R}}^{(l)}\right]^{\mathrm{T}}[\mathrm{B}_{kr}] + [\mathrm{B}_{rk}]\left[\bar{\mathrm{R}}^{(l)}\right] + \left[\bar{\mathrm{R}}^{(l)}\right]^{\mathrm{T}}[\mathrm{B}_{kk}]\left[\bar{\mathrm{R}}^{(l)}\right] \tag{3.24b}$$

4. Solved the eigenvalue problem:

$$\left[\bar{A}^{(l)}\right] \left[\Psi_{rr}^{(l)}\right] \left[\Omega_{r}^{(l)}\right] = \left[\bar{B}^{(l)}\right] \left[\Psi_{rr}^{(l)}\right] \tag{3.23}$$

5. Check for eigenvalue convergence criterion, such as

$$\left| \frac{\lambda_i^{(l+1)} - \lambda_i^{(l)}}{\lambda_i^{(l+1)}} \right| \leq \epsilon \qquad \text{for i = 1, ... , } n_r$$

If criterion is satisfied, go to step 7, otherwise go to step 6.

6. Update condensation matrix:

$$\left[\bar{R}^{(l+1)}\right] = [A_{kk}]^{-1}\left[R_{kr}^{(l)}\right][\Psi_{rr}^{(l)}][\Omega_r^{(l)}]^{-1}[\Psi_{rr}^{(l)}]^{T}[\bar{A}^{(l)}] - [A_{kk}]^{-1}[A_{kr}] \tag{3.60a}$$

where

$$\left[R_{kr}^{(l)}\right] = \left[B_{kk}\,\bar{R}^{(l)} + B_{kr}\right] \tag{3.60b}$$

Go to step 3.

7. Compute global eigenvectors:

$$[\Psi_r] = \begin{bmatrix} \bar{R}^{(l)}\,\Psi_{rr} \\ \Psi_{rr} \end{bmatrix} \tag{3.22}$$

8. If the whole set of eigenvectors are desired, then compute the condensation matrix $\left[\hat{R}\right]$:

$$\left[\hat{R}\right]^{T} = -\left[B_{kk}\,\bar{R}^{(l)} + B_{kr}\right]\left[B_{rk}\,\bar{R}^{(l)} + B_{rr}\right]^{-1} \tag{3.31}$$

9. Compute condensed matrices $\left[\hat{A}\right]$ and $\left[\hat{B}\right]$:

$$\left[\hat{A}\right] = [A_{kk}] + \left[\hat{R}\right]^{T}[A_{rk}] + [A_{kr}]\left[\hat{R}\right] + \left[\hat{R}\right]^{T}[A_{rr}]\left[\hat{R}\right] \tag{3.18a}$$

$$\left[\hat{B}\right] = [B_{kk}] + \left[\hat{R}\right]^{T}[B_{rk}] + [B_{kr}]\left[\hat{R}\right] + \left[\hat{R}\right]^{T}[B_{rr}]\left[\hat{R}\right] \tag{3.18b}$$

10. Solved the eigenvalue problem:

$$\left[\hat{A}\right][\Psi_{kk}]\,[\Omega_k] = \left[\hat{B}\right][\Psi_{kk}] \tag{3.17}$$

11. Compute global eigenvectors:

$$[\Psi_k] = \begin{bmatrix} \Psi_{kk} \\ \hat{R}\,\Psi_{kk} \end{bmatrix} \tag{3.16}$$

3.6 NUMERICAL RESULTS

To demonstrate the application and convergence properties of the proposed dynamic condensation approach the clamped-clamped beam shown in Figure 3.1 is considered as a numerical example. This structure has been analyzed by Craig and Chung

[15] and consists of two substructures, α and β. In order to construct a system with nonclassical damping matrix it is assumed that damping matrices in the two parts be differently proportioned to their respective stiffness matrices as follows

$$[C_\alpha] = \frac{1}{48}[K_\alpha] \qquad\qquad [C_\beta] = \frac{1}{96}[K_\beta] \tag{3.61}$$

where $[\,C_j\,]$ and $[\,K_j\,]$ are the damping and stiffness matrices respectively of substructure j. The structure is modeled with ten beam finite elements. The beam has a total of 18 degrees of freedom with two degrees of freedom per node, a vertical displacement and a rotation.

Complex eigenvalues of this clamped-clamped beam calculated without any condensation are given in Table 3.1. Since all eigenvalues occur in complex conjugate pairs, only one value of each pair is given. The eigenvalue corresponding to the j^{th} mode is denoted as

$$\lambda_j = -\sigma_j + i\,\theta_j \tag{3.62}$$

in which σ_j and θ_j are the real and imaginary parts respectively. Modal frequencies and damping ratios for each modes also are given in Table 3.1 and are computed as

$$\omega_j = \sqrt{\sigma_j^2 + \theta_j^2} \qquad\qquad \beta_j = \frac{\sigma_j}{\omega_j} \tag{3.63}$$

These values are considered as exact values for comparison purposes.

The results obtained with the condensation approach are evaluated using eigenvalues and eigenvectors errors. Eigenvalue errors are obtained by comparing the exact modal frequencies and damping ratios with those obtained with the condensation approach. The relative error ϵ_ω for modal frequencies is defined as

$$\epsilon_\omega = \frac{(\omega_{appr} - \omega_{exact})}{\omega_{exact}} \text{ x } 100 \tag{3.64}$$

Relative errors for damping ratios, ϵ_β, are computed in a similar way. For the eigenvectors, the percent root-mean-square (RMS) error is used to indicate how well they match with the exact ones. RMS errors are defined as

$$\text{RMS ERROR} = \frac{\left\| \underset{\sim}{\psi}_{appr} - \underset{\sim}{\psi}_{exact} \right\|_2}{\left\| \underset{\sim}{\psi}_{exact} \right\|_2} \text{ x } 100 \tag{3.65}$$

where the 2-norm of the complex vector $\underset{\sim}{\psi}$ is defined as

$$\| \underset{\sim}{\psi} \|_2 = \sqrt{\sum_{j=1}^{n} |\mathrm{Re}(\psi_j)|^2 + |\mathrm{Im}(\psi_j)|^2} \tag{3.66}$$

The displacement vector of the clamped-clamped beam has been partitioned into two sets of nine degrees of freedom each one. Translational degrees of freedom were kept to formulate the eigenvalue problem associated with the lower modes whereas the rotational degrees of freedom were used to compute the higher modes. At each iteration step, the whole set of modes are computed from the solution of the eigenvalue problems (3.17) and (3.23). Then the condensation matrix is updated with Eq. (3.45) when iterating with the lower modes and with Eq. (3.60) when iterating with the higher modes. Tables 3.2 to 3.4 show the results obtained when iterating with the lower modes. A dash in these and other tables indicates that the error is less than 0.0005% and the value is regarded as exact. It is seen that two iterations are enough to obtain all the modal frequencies and damping ratios with absolute errors less than 1%. After four iterations fifteen frequencies and twelve damping ratios are exact. Nonetheless, the RMS error in several eigenvectors, Table 3.4, are considerably big at the beginning of the process but after four iterations only three of them are greater than 1% with 4.7% the largest. On the other hand, Tables 3.5 to 3.7 show the results obtained when iterating with the higher modes. In this case, four iterations are required to reduced the absolute errors below 1% in all modal frequencies and damping ratios. Twelve frequencies and ten damping ratios are exact and five eigenvectors have RMS errors greater than 1% after four iterations. Comparing the errors in these tables we can see that the iterative process with lower modes provide better initial estimate and convergence than the iterative process with higher modes, Figures 3.2 and 3.3.

It is interesting to note that for the first nine modes in this example, obtained from the solution of the eigenvalue problem (3.17), all modal frequencies have positive errors in every iteration step. That means that the approximate lower frequencies are higher than the exact ones and their convergence is monotonically from above, Figure 3.4. However, the errors in the damping ratios may fluctuate and signs may change as the iterative process proceeds as shown in Figure 3.5. Eigenvectors have larger absolute errors than frequencies and damping ratios. In general, higher errors are associated with the higher modes in the spectrum sought, as shown in Figure 3.6. For the other nine modes, which are obtained from the solution of the eigenvalue problem (3.23), all modal frequencies have negative errors in each iteration step. That means that the approximate higher frequencies are lower than the exact ones and their convergence is monotonically from below, as shown in Figure 3.7. As in the case of the lower modes, errors in damping ratios may fluctuate and change signs, Figure 3.8. Similarly, eigenvectors have errors higher than the errors in the corresponding frequencies and damping ratios. Higher errors are now associated with the lower modes in the spectrum sought, Figure 3.9. These observations apply for the both cases of iteration with lower modes as well as higher modes.

It is also of interest to examine the accuracy of the eigenproperties obtained when different sets of coordinates are used. The proper selection of coordinates to be kept in the reduced eigenvalue problem will affect the initial estimate of the condensation matrices and which, in turn, also will affect the convergence rate of the iterative process. To show this, the eigenproperties of the truss structure shown in Figure 3.10 have been obtained with different sets of coordinates. Only the iteration process with lower modes will be presented. In order to have a nonclassically damped system, the truss has been divided into two substructures with their damping matrices defined as

$$[C_\alpha] = \frac{3}{40}\,[K_\alpha] \qquad\qquad [C_\beta] = \frac{1}{40}\,[K_\beta] \tag{3.67}$$

The truss consists of 41 elements and 22 joints. Each joint has two degrees of freedom and the structure has a total 40 degrees of freedom. Table 3.8 shows the first ten exact eigenvalues, modal frequencies and damping ratios of the truss, obtained for the full system without any condensation. Once again only one value of each conjugate pair is given.

Two different ways of selecting the coordinates have been considered. In the first case, the degrees of freedom are ordered according to the magnitude of the stiffness to mass ratios, K_{ii}/M_{ii}, with the smallest ratios located at the first positions. The first n_k degrees of freedom are kept in this case. In the second case, the degrees of freedom are ordered according to Shah and Raymund's procedure [50]. The procedure is briefly described by the following steps. (1) Find a degree of freedom for which the stiffness to mass ratio is the largest. (2) Eliminate this degree of freedom from mass and stiffness matrices by the Guyan reduction method. (3) Apply steps 1 and 2 to the reduced matrices obtained in step 2. (4) Repeat steps 1 to 3 until n_r degrees of freedom are eliminated. The remaining n_k degrees of freedom will be kept. Figure 3.11 shows some of the degrees of freedom of the truss numbered according to Shah and Raymund's procedure. For the first case, coordinates 8, 16, 18 and 19 were kept whereas for the second case, coordinates 1 through 4 were kept. It means that in this example 90 percent of the coordinates have been condensed.

The numerical results for the first case are given in Tables 3.9 and 3.10 whereas the results for the second case are given in Tables 3.11 and 3.12. In case one, the initial estimates of the modal frequencies and damping ratios, Table 3.9, are obviously unacceptable. Errors in the initial estimates of modal frequencies range from 56 to 385% and from 224 to 1406% in damping ratios. However, a radical improvement is observed after the first iteration although the errors for two of the modes are still unacceptable. After four iterations the third mode has the largest errors, 5.5% in the modal frequencies and 39% in the damping ratio. A similar behavior is observed with the eigenvectors, Table 3.10. The second choice of selecting the degrees of freedom is seem to provide better results as seen from the following tables. Errors in the initial estimates of the modal frequencies range from 0.8 to 18.2% and in damping ratios from 1.9 to 13.8%, (Table 3.11). Once again, the errors are considerably reduced after one iteration and after four iterations all complex modes are very close to the exact ones. Comparing the results in these tables we can see that the proper selection of coordinates will indeed affect the convergence rate of the condensation approach. Nonetheless, the iterative procedure is able to reduce the errors significantly in all the eigenproperties no matter what coordinates are selected. If we continue the iteration process we will eventually obtain exact values for all complex modes in the reduced eigenvalue problem.

3.7 SUMMARY AND CONCLUSIONS

This chapter presents a dynamic condensation approach for the calculation of the eigenproperties of nonclassically damped structures. The approach is iterative and can be carried out not only with the lower modes but with the higher modes as well. It starts with the condensation of a selected number of degrees of freedom and an appropriate trial condensation matrix. Guyan's condensation matrix can be used as the trial matrix when seeking the lower modes first. A reduced size eigenvalue problem is formed using the condensation matrix. The solution of the condensed eigenvalue provides enough information to update the condensation matrix which in turn is used to define a better condensed eigenvalue problem. Successive iterations provide better results for the eigenproperties. Usually a few iteration steps provide excellent results. The final condensation matrix can be used to define another complementary eigenvalue problem. The solution of this complementary problem provide the remaining modes.

Two numerical examples are presented to show the effectiveness of the proposed approach. The convergence properties of the method are studied in the first example. The second example is presented to demonstrate the effect of choosing the kept degrees of freedom on the convergence. Although in both cases excellent results were obtained, a careful selection of coordinates can improve the convergence to the final results. That is, with a better selection of the coordinates, less iteration steps are required to achieve a certain level of accuracy in the calculated eigenproperties.

Table 3.1 Exact eigenproperties of the clamped-clamped beam in Figure 3.1.

Mode	Eigenvalue	Modal Frequency	Damping Ratio
1	-0.0004 + i 0.2237	0.224	0.0019
2	-0.0030 + i 0.6169	0.617	0.0049
3	-0.0125 + i 1.2102	1.210	0.0103
4	-0.0332 + i 2.0037	2.004	0.0166
5	-0.0747 + i 3.0018	3.003	0.0249
6	-0.1498 + i 4.2127	4.215	0.0355
7	-0.2630 + i 5.6458	5.652	0.0465
8	-0.4469 + i 7.3033	7.317	0.0611
9	-0.6935 + i 9.0750	9.101	0.0762
10	-1.2359 + i 12.0952	12.158	0.1017
11	-1.8204 + i 14.6402	14.753	0.1234
12	-2.6403 + i 17.7727	17.968	0.1470
13	-4.0126 + i 21.3880	21.761	0.1844
14	-5.7159 + i 25.8828	26.506	0.2156
15	-8.1141 + i 30.2511	31.320	0.2591
16	-13.0760 + i 36.1990	38.488	0.3397
17	-12.4335 + i 40.7452	42.600	0.2919
18	-22.2042 + i 41.4118	46.989	0.4725

Table 3.2 Percent error in modal frequencies of clamped-clamped beam in Figure 3.1 calculated by iterating with lower modes.

Mode	Iteration Step 0	1	2	3	4
1	0.000	--------	--------	--------	--------
2	0.003	0.000	--------	--------	--------
3	0.029	0.000	--------	--------	--------
4	0.145	0.000	--------	--------	--------
5	0.518	0.001	0.000	--------	--------
6	1.427	0.003	0.000	--------	--------
7	3.070	0.033	0.000	--------	--------
8	4.411	0.364	0.044	0.003	0.001
9	1.725	0.201	0.100	0.018	0.013
10	-0.806	-0.047	-0.023	-0.020	-0.012
11	-1.137	-0.118	-0.018	-0.002	0.000
12	-0.369	-0.003	-0.001	0.000	--------
13	-0.087	0.000	-------	-------	--------
14	-0.023	0.000	--------	--------	--------
15	-0.005	0.000	--------	--------	--------
16	-0.001	0.000	--------	--------	--------
17	-0.003	0.000	--------	--------	--------
18	0.000	--------	--------	--------	--------

Table 3.3 Percent error in damping ratios of clamped-clamped beam in Figure 3.1 calculated by iterating with lower modes.

Mode	Iteration Step				
	0	1	2	3	4
1	0.004	0.000	--------	--------	--------
2	-0.043	0.000	--------	--------	--------
3	0.064	0.000	--------	--------	--------
4	-0.227	0.004	0.000	--------	--------
5	-0.694	0.039	0.000	--------	--------
6	-0.346	0.260	-0.001	0.000	--------
7	-5.444	1.284	0.026	0.001	0.000
8	0.191	3.684	0.602	0.196	0.046
9	-4.760	0.803	0.100	0.051	0.038
10	-0.377	-0.840	-0.139	-0.055	-0.026
11	2.316	-0.476	-0.029	0.021	-0.003
12	0.062	-0.192	-0.012	-0.002	-0.001
13	0.109	-0.029	0.000	--------	--------
14	0.005	-0.003	0.000	--------	--------
15	0.020	-0.001	0.000	--------	--------
16	-0.007	0.000	--------	--------	--------
17	0.005	0.000	--------	--------	--------
18	0.001	0.000	--------	--------	--------

Table 3.4 RMS error in eigenvectors of clamped-clamped beam in Figure 3.1 calculated by iteracting with lower modes.

Mode	Iteration Step				
	0	1	2	3	4
1	0.010	0.000	--------	--------	--------
2	0.132	0.002	0.000	--------	--------
3	0.663	0.014	0.001	0.000	--------
4	2.164	0.086	0.005	0.001	0.000
5	5.559	0.368	0.022	0.004	0.002
6	12.434	1.386	0.138	0.043	0.019
7	24.557	4.995	0.824	0.246	0.122
8	42.399	16.997	6.672	3.352	1.595
9	44.783	20.422	10.172	6.553	4.767
10	9.355	4.289	2.177	1.403	1.084
11	8.118	3.018	1.047	0.517	0.205
12	3.411	1.250	0.338	0.167	0.107
13	1.431	0.471	0.091	0.072	0.050
14	0.520	0.204	0.025	0.024	0.023
15	0.369	0.091	0.019	0.017	0.013
16	0.204	0.038	0.010	0.006	0.004
17	0.238	0.073	0.013	0.006	0.005
18	0.129	0.013	0.004	0.003	0.002

Table 3.5 Percent error in modal frequencies of clamped-clamped beam in Figure 3.1 calculated by iterating with higher modes.

Mode	Iteration Step				
	0	1	2	3	4
1	0.020	0.000	--------	--------	--------
2	0.095	0.000	--------	--------	--------
3	0.363	0.000	--------	--------	--------
4	0.899	0.003	0.000	--------	--------
5	1.918	0.027	0.001	0.000	--------
6	3.495	0.152	0.001	0.000	--------
7	5.277	0.614	0.063	0.013	0.002
8	5.721	1.543	0.454	0.164	0.061
9	2.030	0.675	0.226	0.077	0.024
10	-3.153	-1.302	-0.556	-0.220	-0.081
11	-6.582	-1.727	-0.668	-0.238	-0.090
12	-5.486	-0.699	-0.170	-0.028	-0.005
13	-3.690	-0.211	-0.025	-0.001	0.000
14	-2.200	-0.053	-0.002	0.000	--------
15	-1.016	-0.012	0.000	--------	--------
16	-0.026	-0.001	0.000	--------	--------
17	-0.641	-0.004	0.000	--------	--------
18	-0.088	0.000	--------	--------	--------

Table 3.6 Percent error in damping ratios of clamped-clamped beam in Figure 3.1 calculated by iterating with higher modes.

Mode	Iteration Step				
	0	1	2	3	4
1	0.022	0.000	--------	--------	--------
2	0.113	0.000	--------	--------	--------
3	-0.032	0.001	0.000	--------	--------
4	-0.290	0.009	0.006	0.000	--------
5	-1.099	0.027	0.044	0.001	0.000
6	-2.019	0.031	0.241	0.024	0.003
7	4.972	-0.102	0.941	0.301	0.077
8	-1.821	0.505	1.627	1.071	0.598
9	-4.345	-1.425	-0.064	0.128	0.105
10	0.682	-0.123	-0.756	-0.657	-0.406
11	8.102	1.859	-0.554	-0.426	-0.237
12	3.627	0.215	-0.586	-0.180	-0.047
13	3.429	0.062	-0.156	-0.020	-0.002
14	1.039	-0.015	-0.029	-0.002	0.000
15	0.899	0.003	-0.004	0.000	--------
16	-0.243	-0.002	-0.001	0.000	--------
17	0.505	-0.001	-0.001	0.000	--------
18	0.065	0.000	--------	--------	--------

Table 3.7 RMS error in eigenvectors of clamped-clamped beam in Figure 3.1 calculated by iterating with higher modes

Mode	Iteration Step				
	0	1	2	3	4
1	0.126	0.002	0.001	0.000	--------
2	0.660	0.012	0.016	0.004	0.000
3	1.503	0.091	0.025	0.003	0.002
4	3.075	0.415	0.108	0.032	0.024
5	5.589	1.445	0.416	0.068	0.025
6	10.293	4.311	1.490	0.360	0.147
7	19.642	11.467	5.126	2.041	1.141
8	34.777	27.064	15.767	9.784	7.038
9	33.473	28.719	17.831	11.517	8.487
10	18.338	16.885	7.358	7.022	3.667
11	19.975	18.259	6.094	5.667	2.736
12	15.709	11.882	2.974	2.343	0.955
13	10.256	7.917	1.186	0.693	0.197
14	5.763	5.177	0.406	0.182	0.042
15	3.157	2.888	0.140	0.050	0.009
16	2.603	0.693	0.016	0.006	0.001
17	2.913	1.311	0.037	0.013	0.003
18	0.456	0.383	0.011	0.002	0.000

Table 3.8 First ten exact eigenvalues, modal frequencies (rad / sec.) and damping ratios of truss structure in Figure 3.9.

Mode	Eigenvalue	Modal Frequency	Damping Ratio
1	-0.0024 + i 2.2760	0.0228	0.0011
2	-0.0247 + i 5.7412	0.0574	0.0043
3	-0.0281 + i 9.2934	0.0929	0.0030
4	-0.0876 + i 11.534	0.1153	0.0076
5	-0.1809 + i 17.470	0.1747	0.0136
6	-0.3397 + i 23.529	0.2353	0.0144
7	-0.1872 + i 26.176	0.2618	0.0072
8	-0.5136 + i 29.769	0.2977	0.0173
9	-0.5461 + i 32.438	0.3244	0.0141
10	-0.8177 + i 36.778	0.3679	0.0222

Table 3.9 Percent errors in modal frequencies and damping ratios of truss in Figure 3.9 calculated by iterating with lower modes and with kept degrees of freedom selected according to the stiffness to mass ratio.

a) Modal Frequencies

Mode	Iteration Step				
	0	1	2	3	4
1	56.552	0.040	0.014	0.012	0.011
2	151.611	1.883	0.600	0.505	0.451
3	345.142	34.874	13.776	7.869	5.492
4	385.783	121.935	7.539	4.481	3.712

b) Damping Ratios

Mode	Iteration Step				
	0	1	2	3	4
1	224.04	-0.42	-0.760	-0.594	-0.506
2	260.34	3.18	-0.976	-1.076	-1.073
3	1406.84	123.19	-63.803	-50.471	-39.309
4	683.85	-7.42	-23.630	-15.778	-12.363

Table 3.10 RMS errors in eigenvectors of the truss in Figure 3.9 calculated by iterating with lower modes and with kept degrees of freedom selected according to the stiffness to mass ratio

Mode	Iteration Step				
	0	1	2	3	4
1	44.603	0.588	0.155	0.122	0.107
2	76.181	12.329	3.505	2.540	2.097
3	105.775	82.368	24.937	15.707	12.175
4	74.939	61.530	27.180	16.908	13.177

Table 3.11 Percent errors in modal frequencies and damping ratios of truss in Figure 3.9 calculated by iterating with lower modes and with kept degrees of freedom selected according to Shah and Raymund's Method.

a) Modal Frequencies

Mode	Iteration Step				
	0	1	2	3	4
1	0.818	0.000	--------	--------	--------
2	6.852	0.047	0.003	0.000	--------
3	18.191	0.239	0.028	0.004	0.001
4	7.538	0.044	0.003	0.000	--------

b) Damping Ratios

Mode	Iteration Step				
	0	1	2	3	4
1	-2.007	-0.010	-0.000	--------	--------
2	1.947	-1.020	-0.052	-0.005	-0.000
3	-13.784	-3.700	-0.562	-0.116	0.001
4	6.557	-1.515	0.044	0.042	0.000

Table 3.12 RMS errors in eigenvectors of truss in Figure 3.9 calculated by iterating with lower modes and with kept degrees of freedom selected according to Shah and Raymund's Method.

	Iteration Step				
Mode	0	1	2	3	4
1	1.286	0.009	0.001	0.000	--------
2	11.135	1.128	0.216	0.052	0.140
3	27.400	3.556	1.155	0.482	0.199
4	16.638	1.531	0.736	0.407	0.093

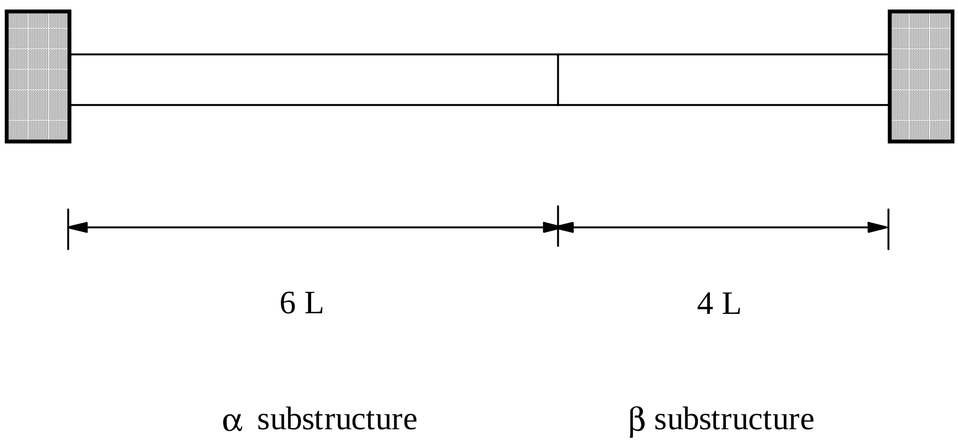

Figure 3.1. Structural configuration of the clamped-clamped beam used in the first numerical example.

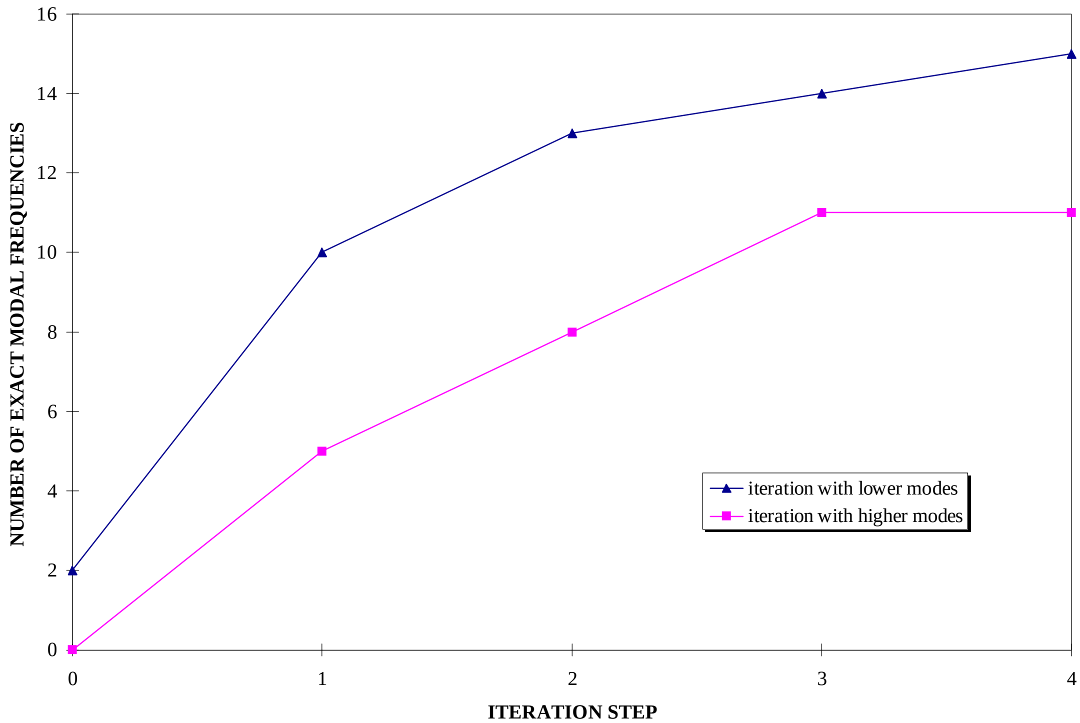

Figure 3.2 Comparison in the number of exact frequencies when iterating with lower modes and higher modes.

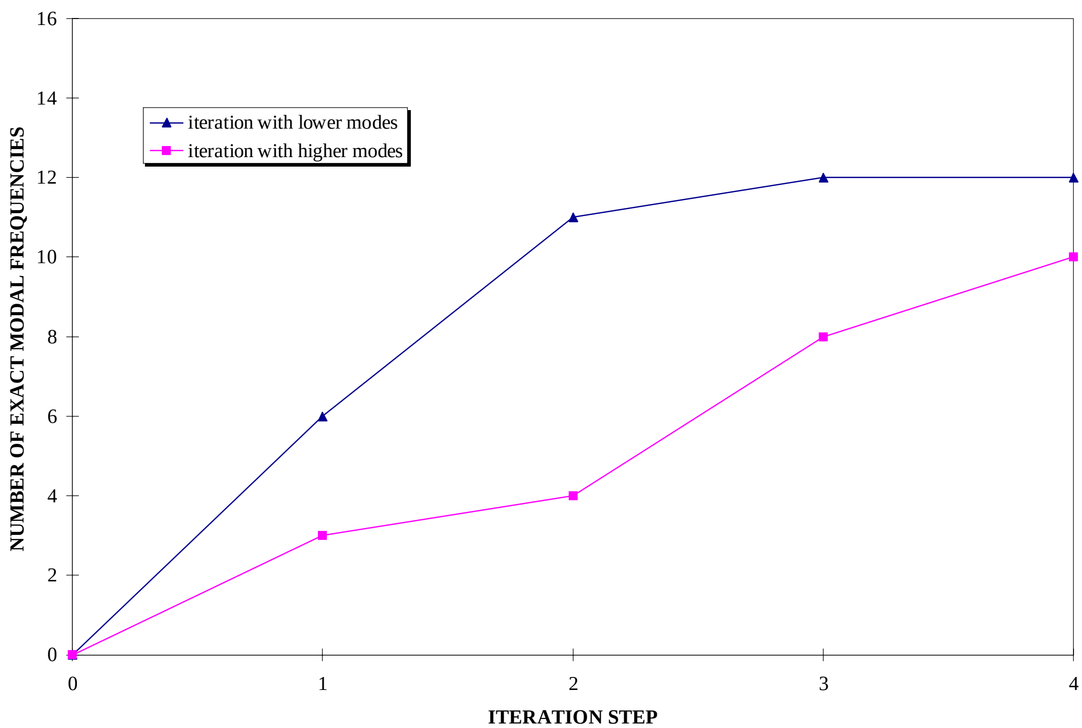

Figure 3.3 Comparison in the number of exact modal damping ratios when iterating with lower modes and higher modes.

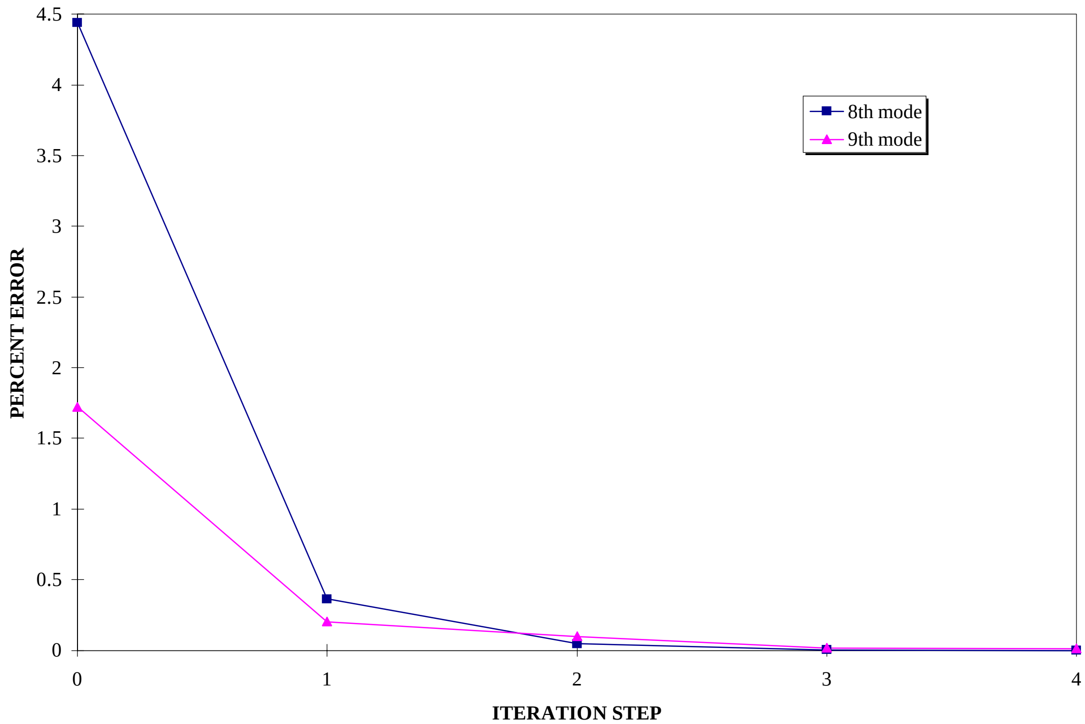

Figure 3.4 Percent errors for the 8^{th} and 9^{th} modal frequencies of the beam in Figure 3.1 obtained from the solution of the eigenvalue problem (3.17).

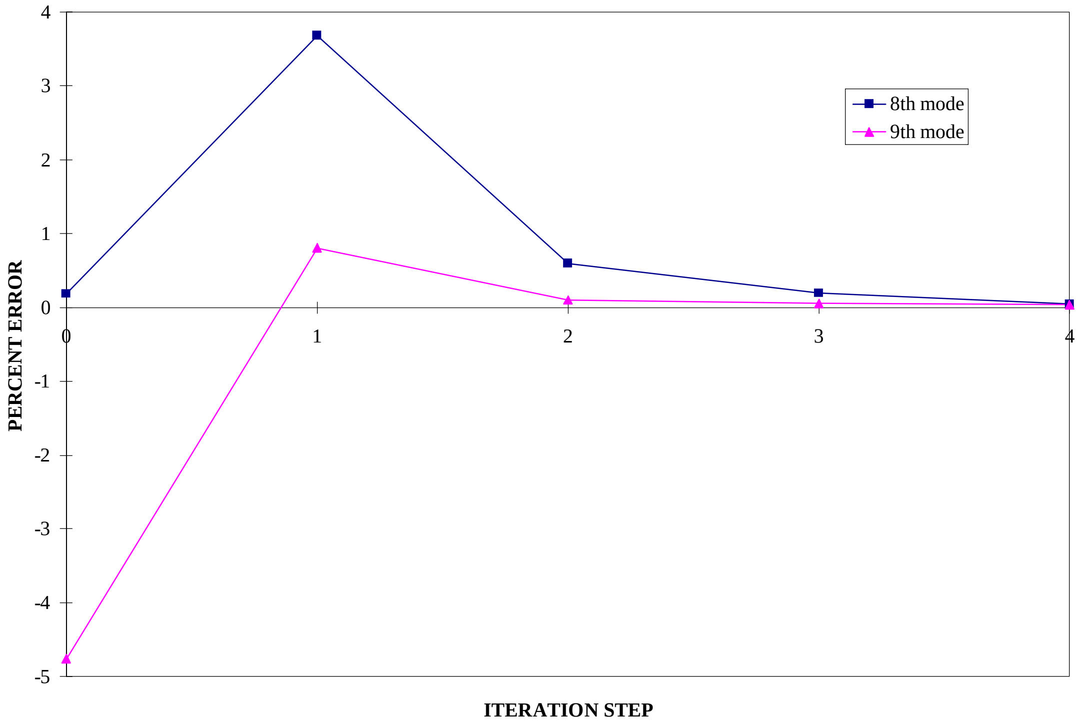

Figure 3.5 Percent errors for the 8^{th} and 9^{th} modal damping ratios of the beam in Figure 3.1 obtained from the solution of the eigenvalue problem (3.17).

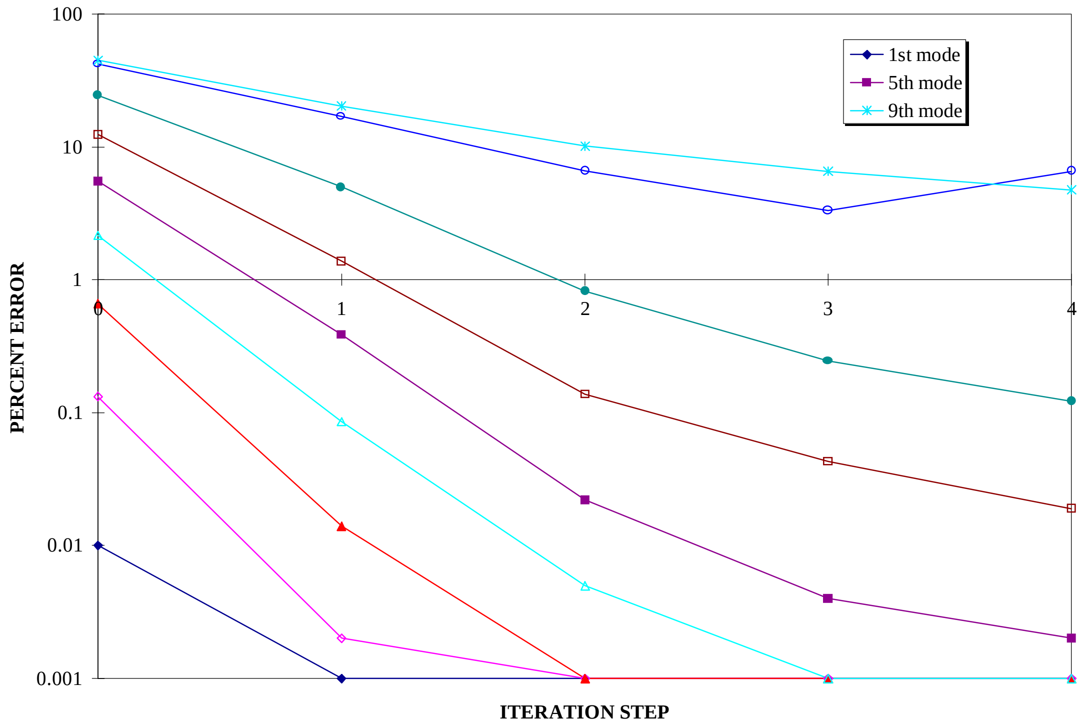

Figure 3.6 Root mean square errors for the eigenvectors of the beam in Figure 3.1 obtained from the solution of the eigenvalue problem (3.17).

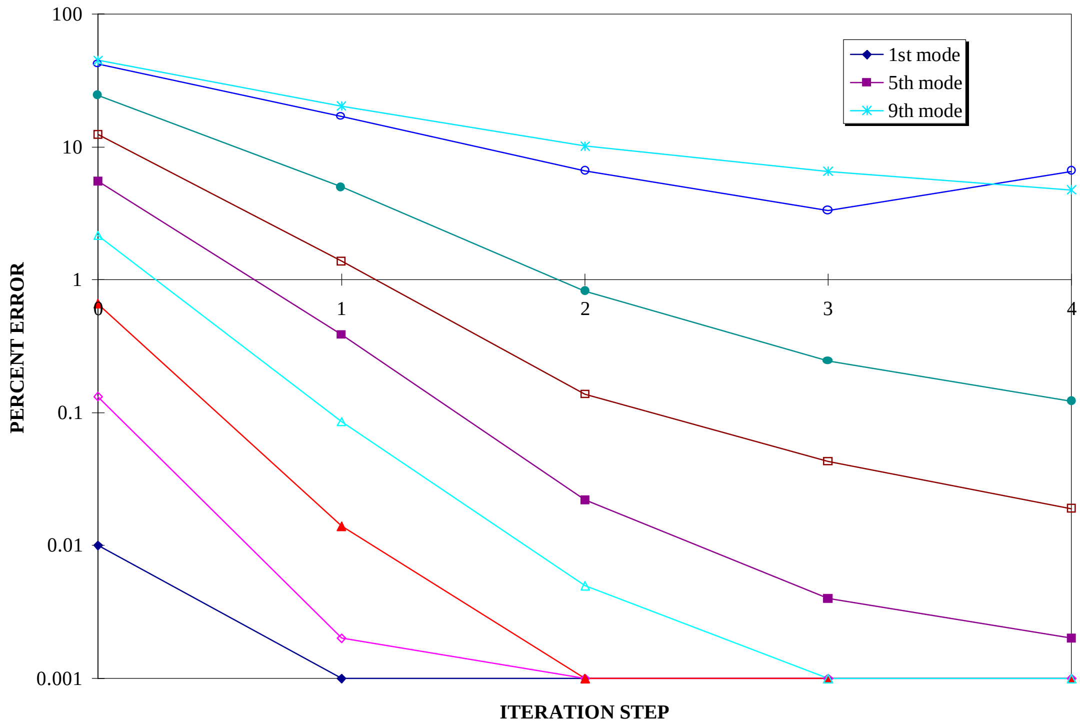

Figure 3.7 Percent errors for the 10^{th} and 11^{th} modal frequencies of the beam in Figure 3.1 obtained from the solution of the eigenvalue problem (3.23).

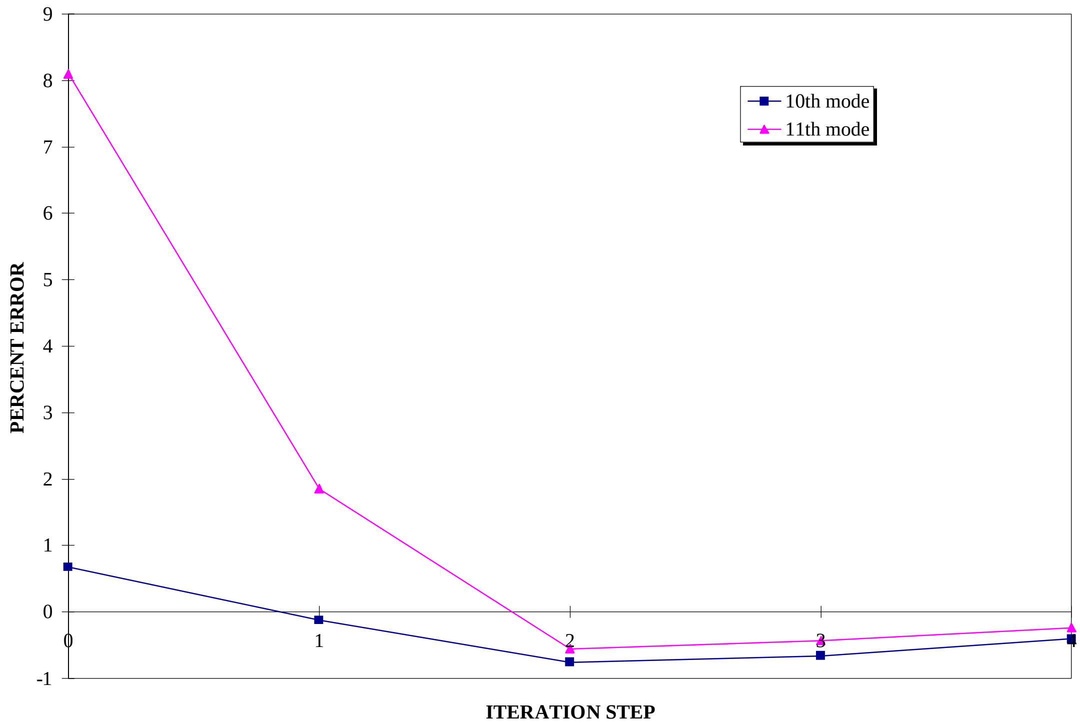

Figure 3.8 Percent errors for the 10^{th} and 11^{th} modal damping ratios of the beam in Figure 3.1 obtained from the solution of the eigenvalue problem (3.23).

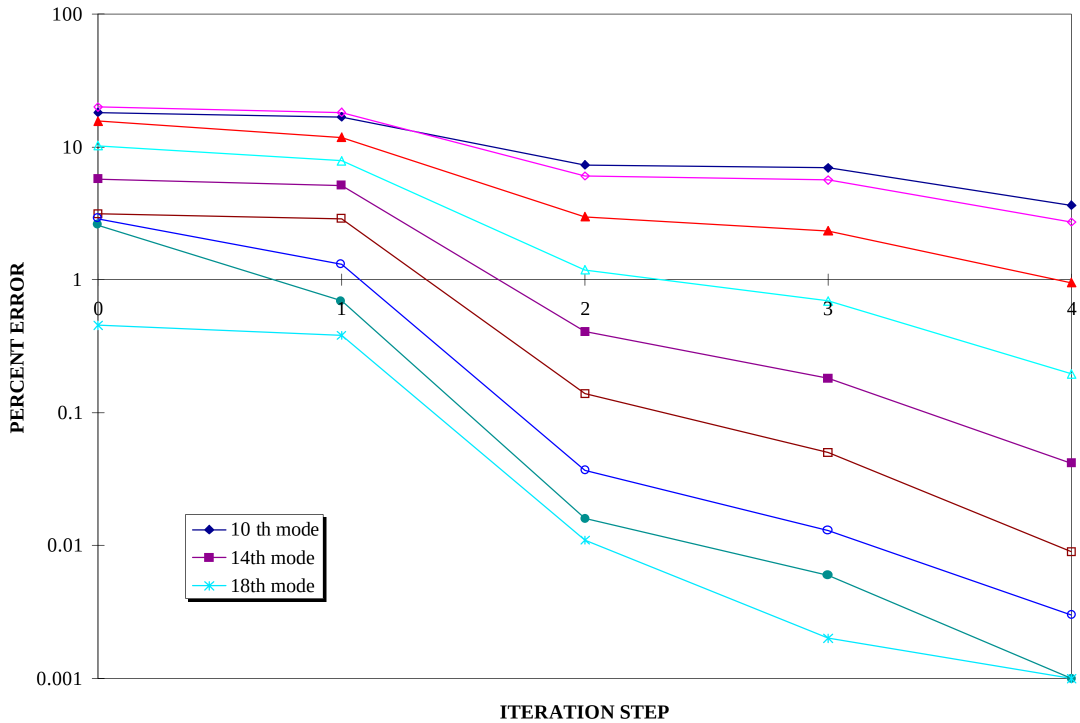

Figure 3.9 Root mean square errors for the eigenvectors of the beam in Figure 3.1 obtained from the solution of the eigenvalue problem (3.23).

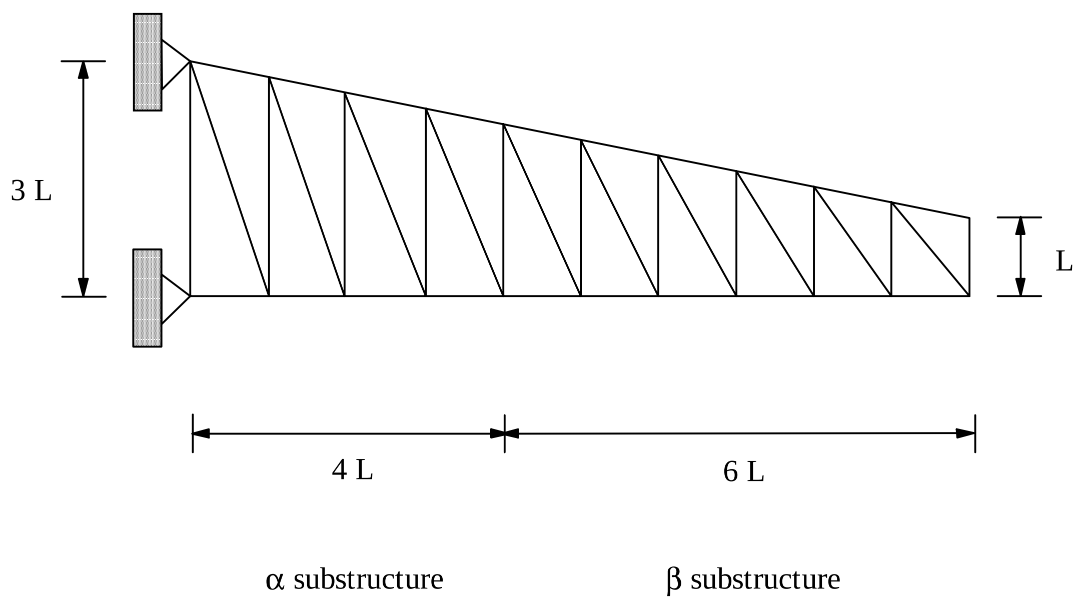

Figure 3.10 Structural configuration of the truss used in the second numerical example.

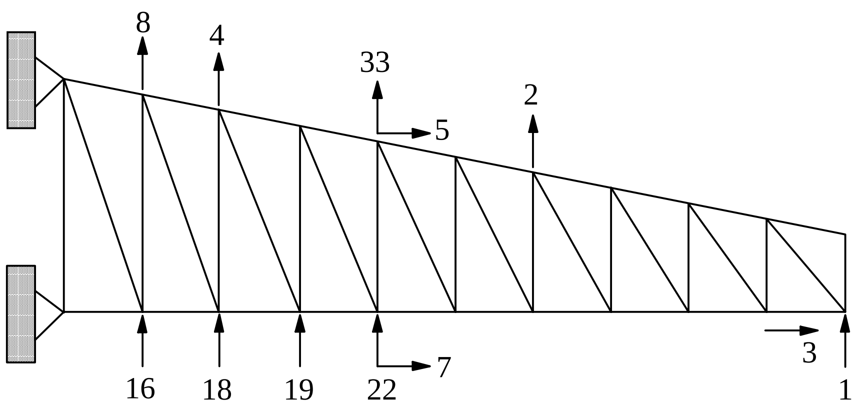

Figure 3.11 Degrees of freedom numbered according to Shah and Raymund's procedure.

CHAPTER IV

DYNAMIC CONDENSATION WITH SUBSTRUCTURING FOR NONCLASSICALLY DAMPED STRUCTURES

4.1 INTRODUCTION

In Chapter 2 we used the condensed structure superposition approach to include the dynamic effect of one part of a structure on another, such as the effect of a floor slab on the supporting frame. The condensation in one of the substructure degrees of freedom was achieved by using a first few modes. That is, the condensed substructure was represented by only a first few modes. It was, however, observed that some of the eigenproperties of the combined structure were not accurate enough. In this chapter we will attempt to improve the accuracy of the eigenproperties by using the iterative approach presented in Chapter 3. That is, we will combine the methods presented in the previous two chapters to obtain more accurate estimates of the combined system eigenproperties.

In Chapter 3 we did not divide the structure into substructures, but just attempted to reduce the size of the eigenvalue problem by direct condensation of the physical degrees of freedom. However, while presenting the numerical results of the condensation approach, it was observed that the method of selecting the kept and reduced physical degrees of freedom in the condensation process had a significant effect on the rate of convergence to the correct eigenproperties. This rate of convergence can be improved if the structure is divided into two or more substructures and each substructure is represented by not its physical coordinates but by its eigenproperties. The selection of the kept degrees of freedom in the synthesized structure corresponding to a first few ordered eigenproperties of the substructure is seen to expedite the convergence to the final results. The details of this combined modal synthesis and condensation approach are also presented in the later part of this chapter.

4.2 CONDENSED SUBSTRUCTURE SUPERPOSITION APPROACH WITH ITERATIONS

We are primarily interested in computing a first few complex modes of a nonclassically damped structural system. As considered in Chapter 2, we again divide the structure into two substructures, identified here as α and β substructures. The α substructure has n degrees of freedom whereas the β substructures has m. They are connected at n_b coordinates and the total number of degrees of freedom of the structural system is $N = n + m - n_b$. In the condensed substructure superposition approach of Chapter 2, we condensed the interior degrees of freedom of one of the two substructures and kept only the degrees of freedom at the interface. This way we could reduce the dimension of the eigenvalue problem of the combined structure to n or m. We can further reduce the size of the eigenvalue problem by condensing the interior degrees of freedom of both substructures. Here, however, we will not use the eigenproperties to define the substructure as was done in Chapter 2. We would rather condense the physical coordinates as in Chapter 3. A first few eigenproperties obtained from the solution of the condensed eigenvalue problem of the combined system will then be used to improve the condensation matrix iteratively to obtain more accurate values.

4.2.1 Condensed Eigenvalue Problem

Consistent with Eq. (2.3), the state vector $\underset{\sim}{y}^j$ of a substructure with its interface coordinates free can be defined as

$$\underset{\sim}{y}^j = \begin{Bmatrix} \underset{\sim}{y}_b^j \\ \underset{\sim}{y}_i^j \end{Bmatrix} \qquad \text{with } j = \alpha, \beta \tag{4.1}$$

in which the boundary and interior degrees of freedom are associated with vectors $\underset{\sim}{y}_b^j$ and $\underset{\sim}{y}_i^j$, respectively. Corresponding substructure state matrices $[\,A^j\,]$ and $[\,B^j\,]$ are then given as

$$[\,A^j\,] = \begin{bmatrix} A_{bb}^j & A_{bi}^j \\ A_{ib}^j & A_{ii}^j \end{bmatrix} \qquad [\,B^j\,] = \begin{bmatrix} B_{bb}^j & B_{bi}^j \\ B_{ib}^j & B_{ii}^j \end{bmatrix} \qquad \text{with j} = \alpha, \beta \tag{4.2}$$

in which submatrices $[A_{lk}]$ and $[B_{lk}]$ have been defined in Eqs. (3.11a) and (3.11b), respectively. According to this partitioning, the global state vector can also be partitioned and written as

$$\underset{\sim}{y} = \begin{Bmatrix} \underset{\sim}{y}_b \\ \underset{\sim}{y}_i^\alpha \\ \underset{\sim}{y}_i^\beta \end{Bmatrix} \tag{4.3}$$

in which $\underset{\sim}{y}_b^\alpha = \underset{\sim}{y}_b^\beta = \underset{\sim}{y}_b$ to satisfy the compatibility conditions at the boundaries and the global state matrices are partitioned as

$$[\mathrm{A}] = \begin{bmatrix} \mathrm{A}_{bb} & \mathrm{A}_{bi} \\ \mathrm{A}_{ib} & \mathrm{A}_{ii} \end{bmatrix} = \begin{bmatrix} \mathrm{A}_{bb}^{\alpha} + \mathrm{A}_{bb}^{\beta} & \mathrm{A}_{bi}^{\alpha} & \mathrm{A}_{bi}^{\beta} \\ \mathrm{A}_{ib}^{\alpha} & \mathrm{A}_{ii}^{\alpha} & 0 \\ \mathrm{A}_{ib}^{\beta} & 0 & \mathrm{A}_{ii}^{\beta} \end{bmatrix} \tag{4.4a}$$

$$[\mathrm{B}] = \begin{bmatrix} \mathrm{B}_{bb} & \mathrm{B}_{bi} \\ \mathrm{B}_{ib} & \mathrm{B}_{ii} \end{bmatrix} = \begin{bmatrix} \mathrm{B}_{bb}^{\alpha} + \mathrm{B}_{bb}^{\beta} & \mathrm{B}_{bi}^{\alpha} & \mathrm{B}_{bi}^{\beta} \\ \mathrm{B}_{ib}^{\alpha} & \mathrm{B}_{ii}^{\alpha} & 0 \\ \mathrm{B}_{ib}^{\beta} & 0 & \mathrm{B}_{ii}^{\beta} \end{bmatrix} \tag{4.4b}$$

In order to condense the interior degrees of freedom of the substructures, the complex eigenproperties of both substructures, or at least a reduced set of them, should be available. If they were indeed available then the condensation matrices can be computed according to Eq. (2.12) as

$$\left[\hat{\mathrm{R}}_{j}\right] = \left[\psi_{ib}^{j}\right] \left[\psi_{bb}^{j}\right]^{-1} \qquad \text{with j} = \alpha,\, \beta \tag{4.5}$$

in which submatrices $\left[\psi_{ib}^{j}\right]$ and $\left[\psi_{bb}^{j}\right]$ contain n_b complex conjugate pairs of eigenvectors. The dimension of the condensation matrix is ($2n_i^j$ x $2n_b$), where n_i^j is the number of interior degrees of freedom of the j substructure. It is noted that here the number of pairs of modes kept to define the condensation matrix has to be equal to the number of boundary degrees of freedom, otherwise the inverse of matrix $\left[\psi_{bb}^{j}\right]$ cannot be computed. In terms of the condensation matrices, the condensed state matrices of each substructure can be defined from Eq. (3.18) as:

$$\left[\hat{\mathrm{A}}_{bb}^{j}\right] = \left[\mathrm{A}_{bb}^{j}\right] + \left[\hat{\mathrm{R}}_{j}\right]^{T} \left[\mathrm{A}_{ib}^{j}\right] + \left[\mathrm{A}_{ib}^{j}\right]^{T} \left[\hat{\mathrm{R}}_{j}\right] + \left[\hat{\mathrm{R}}_{j}\right]^{T} \left[\mathrm{A}_{ii}^{j}\right] \left[\hat{\mathrm{R}}_{j}\right] \tag{4.6a}$$

$$\left[\hat{B}_{bb}^{j}\right] = \left[B_{bb}^{j}\right] + \left[\hat{R}_j\right]^T \left[B_{ib}^{j}\right] + \left[B_{ib}^{j}\right]^T \left[\hat{R}_j\right] + \left[\hat{R}_j\right]^T \left[B_{ii}^{j}\right] \left[\hat{R}_j\right] \tag{4.6b}$$

Now the condensed eigenvalue problem of the combined structure can be written as

$$\left[\hat{A}\right] \left[\Psi_b\right] \left[\Omega_b\right] = \left[\hat{B}\right] \left[\Psi_b\right] \tag{4.7}$$

where the combined, but condensed, state matrices of the system are merely the sum of the state matrices of the two substructures and thus are defined as:

$$\left[\hat{A}\right] = \left[\hat{A}_{bb}^{\alpha}\right] + \left[\hat{A}_{bb}^{\beta}\right] \tag{4.8a}$$

$$\left[\hat{B}\right] = \left[\hat{B}_{bb}^{\alpha}\right] + \left[\hat{B}_{bb}^{\beta}\right] \tag{4.8b}$$

The solution of the eigenvalue problem, Eq. (4.7), will provided approximations for the lowest n_b complex conjugate pairs of modes. It is noted that the modal matrix $[\Psi_b]$ is associated only with the boundary degrees of freedom. To obtain the remaining elements of the eigenvectors associated with the condensed interior degrees of freedom for each substructure, we can use Eq. (4.5) backwards as follows

$$\left[\Psi_i^{j}\right] = \left[\hat{R}_j\right] \left[\Psi_b\right] \qquad \text{with j} = \alpha, \beta \tag{4.9}$$

The complete eigenvectors of the combined structure partitioned consistent with Eq. (4.3) can be defined in terms of the matrix $[\Psi_b]$ simply as:

$$\left[\hat{\Psi}\right] = \begin{bmatrix} \Psi_b \\ \Psi_i^{\alpha} \\ \Psi_i^{\beta} \end{bmatrix} = \begin{bmatrix} \mathrm{I} \\ \hat{\mathrm{R}} \end{bmatrix} \left[\Psi_b\right] \tag{4.10}$$

where

$$\left[\hat{\mathrm{R}}\right] = \begin{bmatrix} \hat{\mathrm{R}}_{\alpha} \\ \hat{\mathrm{R}}_{\beta} \end{bmatrix} \tag{4.11}$$

It is, however, noted that to define the eigenvalue problem of Eq. (4.7), one needs the condensation matrices of the two substructures which in turn need the substructure eigenvectors for their definition. Since the substructure eigenvectors are not available priori, we will have to adopt an iterative procedure similar to the one developed in Chapter 3.

4.2.2 Iterative Procedure

To start the iterative procedure, we need to define an initial estimate for $\left[\hat{\mathrm{R}}\right]$ in Eq. (4.11) as

$$\left[\hat{\mathrm{R}}^{(0)}\right] = \begin{bmatrix} \hat{\mathrm{R}}_{\alpha}^{(0)} \\ \hat{\mathrm{R}}_{\beta}^{(0)} \end{bmatrix} \tag{4.12}$$

As in Chapter 3, we can initially define this in terms of the state matrix $[\mathrm{B}]$ as:

$$\left[\hat{\mathrm{R}}^{(0)}\right] = -\left[\mathrm{B}_{ii}\right]^{-1}\left[\mathrm{B}_{ib}\right] \tag{4.13}$$

in which subscripts i and b are used instead of r and k, respectively. The inverse of matrix $[\mathrm{B}_{ii}]$, can be computed in terms of the $[\mathrm{B}]$ matrices of the individual substructures as

$$\begin{bmatrix} \mathrm{B}_{ii}^{\alpha} & 0 \\ 0 & \mathrm{B}_{ii}^{\beta} \end{bmatrix}^{-1} = \begin{bmatrix} [\mathrm{B}_{ii}^{\alpha}]^{-1} & 0 \\ 0 & \left[\mathrm{B}_{ii}^{\beta}\right]^{-1} \end{bmatrix} \tag{4.14}$$

Thus, the initial condensation matrix for each substructure can be defined as

$$\left[\hat{\mathrm{R}}_{j}^{(0)}\right] = -\left[\mathrm{B}_{ii}^{j}\right]^{-1}\left[\mathrm{B}_{ib}^{j}\right] \qquad \text{with j} = \alpha,\ \beta \tag{4.15}$$

Another approach that could be used to define the initial condensation matrix for each substructure in terms of their stiffness matrices is to use an equation similar to Eq. (3.37)

$$\left[\hat{\mathrm{R}}_{j}^{(0)}\right] = \begin{bmatrix} \mathrm{G}_{K}^{j} & 0 \\ 0 & \mathrm{G}_{K}^{j} \end{bmatrix} = -\begin{bmatrix} \left[\mathrm{K}_{ii}^{j}\right]^{-1}\left[\mathrm{K}_{ib}^{j}\right] & 0 \\ 0 & \left[\mathrm{K}_{ii}^{j}\right]^{-1}\left[\mathrm{K}_{ib}^{j}\right] \end{bmatrix} \tag{4.16}$$

This condensation is equivalent to the static Guyan reduction method. In general, it is seen to provide better results.

Using the initial condensation matrices in Eq. (4.15) or (4.16), one can construct the condensed eigenvalue problem of Eq. (4.7). This can be solved to obtain the initial approximations of the eigenproperties of the combined, but condensed, structure. These eigenproperties can now be used to upgrade the condensation matrix $\left[\hat{\mathrm{R}}\right]$ according to Eq. (3.45). This recursive equation, now written in terms of the substructure's matrices, is given by

$$\left[\hat{\mathrm{R}}_j^{(l+1)}\right] = \left[\mathrm{B}_{ii}^j\right]^{-1}\left[\mathrm{R}_{ib}^{j(l)}\right]\left[\Psi_b^{(l)}\right]\left[\Psi_b^{(l)}\right]^T\left[\hat{\mathrm{B}}^{(l)}\right] - \left[\mathrm{B}_{ii}^j\right]^{-1}\left[\mathrm{B}_{ib}^j\right] \tag{4.17a}$$

where

$$\left[\mathrm{R}_{ib}^{j\,(l)}\right] = \left[\mathrm{A}_{ib}^j + \mathrm{A}_{ii}^j\ \hat{\mathrm{R}}_j^{(l)}\right] \tag{4.17b}$$

and superscript (l) refers to the iteration step. After calculating the improved condensation matrices for each substructure, the condensed matrices $\left[\hat{\mathrm{A}}_{bb}^j\right]$ and $\left[\hat{\mathrm{B}}_{bb}^j\right]$ are obtained using Eq. (4.6). These, in turn, define the new global condensed matrices $\left[\hat{\mathrm{A}}\right]$ and $\left[\hat{\mathrm{B}}\right]$ according to Eq. (4.8) for the eigenvalue problem (4.7). These steps are repeated until a desired converge criterion is satisfied. At the final step, the lowest n_b pairs of complex conjugate pairs of the condensed structure are obtained. These, in turn, can be used to obtain the corresponding full length eigenvectors from Eq. (4.10).

The described procedure is an extension of the iterative condensation process with lower modes presented in Chapter 3 but now utilizing two substructures with the synthesis concept developed in Chapter 2. The fact that the inverse of $[\mathrm{B}_{ii}]$ can be computed using Eq. (4.14) makes it possible to apply it to structures divided into substructures. However, the iterative condensation process with higher modes cannot be used with substructures because the inverse of matrix $[\mathrm{A}_{bb}]$ is required. From Eq. (4.4a) it is observed that this matrix is given as the summation of the substructure matrices $\left[\mathrm{A}_{bb}^j\right]$. In this case, an expression in terms of the substructure matrices to update the condensation matrix $[\bar{\mathrm{R}}]$ is not possible.

Here, only the substructure state matrices $\left[\mathrm{A}_{lk}^j\right]$ and $\left[\mathrm{B}_{lk}^j\right]$ are required. Thus, the eigenproperties of the combined structure can be obtained without ever generating the global state matrices or any of their submatrices. Since no additional approximating assumption is made, same eigenproperties should be obtained with or without substructuring when the same degrees of freedom are kept in the reduced eigenvalue problem.

4.2.3 Step-by-Step Procedure

The steps of the condensation procedure developed in the previous sections are as follows:

1. On the substructure level.

a) Partition of the displacement vector:

$$\underset{\sim}{x}^j = \begin{Bmatrix} \underset{\sim}{x}_b^j \\ \underset{\sim}{x}_i^j \end{Bmatrix} \qquad \text{with } j = \alpha,\ \beta \tag{3.7}$$

b) Calculate an initial value for $\left[\hat{R}_j^{(0)}\right]$ with:

$$\left[\hat{R}_j^{(0)}\right] = -\begin{bmatrix} \left[K_{ii}^j\right]^{-1}\left[K_{ib}^j\right] & 0 \\ 0 & \left[K_{ii}^j\right]^{-1}\left[K_{ib}^j\right] \end{bmatrix} \tag{4.16}$$

c) Compute condensed matrices $\left[\hat{A}_{bb}^j\right]$ and $\left[\hat{B}_{bb}^j\right]$:

$$\left[\hat{A}_{bb}^j\right] = \left[A_{bb}^j\right] + \left[\hat{R}_j\right]^T\left[A_{ib}^j\right] + \left[A_{ib}^j\right]^T\left[\hat{R}_j\right] + \left[\hat{R}_j\right]^T\left[A_{ii}^j\right]\left[\hat{R}_j\right] \tag{4.6a}$$

$$\left[\hat{B}_{bb}^j\right] = \left[B_{bb}^j\right] + \left[\hat{R}_j\right]^T\left[B_{ib}^j\right] + \left[B_{ib}^j\right]^T\left[\hat{R}_j\right] + \left[\hat{R}_j\right]^T\left[B_{ii}^j\right]\left[\hat{R}_j\right] \tag{4.6b}$$

2. On the structure level.

a) Assemble global state matrices:

$$\left[\hat{A}\right] = \left[\hat{A}_{bb}^{\alpha}\right] + \left[\hat{A}_{bb}^{\beta}\right] \qquad (4.8a)$$

$$\left[\hat{B}\right] = \left[\hat{B}_{bb}^{\alpha}\right] + \left[\hat{B}_{bb}^{\beta}\right] \qquad (4.8b)$$

b) Solve the eigenvalue problem:

$$\left[\hat{A}\right] \; [\,\Psi_b\,] \; [\,\Omega_b\,] \; = \; \left[\hat{B}\right] \; [\,\Psi_b\,] \qquad (4.7)$$

c) Check for eigenvalue convergence criterion, such as:

$$\left| \frac{\lambda_i^{(l+1)} - \lambda_i^{(l)}}{\lambda_i^{(l+1)}} \right| \leq \epsilon \qquad \text{for i = 1, ... , 2 } n_b$$

If criterion is satisfied, go to step 4, otherwise go to step 3.

3. On the substructure level.

a) Update condensation matrix:

$$\left[\hat{R}_j^{(l+1)}\right] = \left[B_{ii}^j\right]^{-1} \left[\,R_{ib}^{j(l)}\,\right] \left[\Psi_b^{(l)}\right] \left[\Psi_b^{(l)}\right]^T \left[\hat{B}^{(l)}\right] - \left[B_{ii}^j\right]^{-1} \left[B_{ib}^j\right] \qquad (4.17a)$$

where

$$\left[R_{ib}^{j\,(l)}\right] = \left[A_{ib}^j + A_{ii}^j \; \hat{R}_j^{(l)}\right] \qquad (4.17b)$$

b) Compute new condensed matrices $\left[\hat{A}_{bb}^{j}\right]$ and $\left[\hat{B}_{bb}^{j}\right]$.

c) Go to step 2.

4. On the structure level.

a) Compute global eigenvectors:

$$\left[\hat{\Psi}\right] = \begin{bmatrix} \Psi_b \\ \Psi_i^{\alpha} \\ \Psi_i^{\beta} \end{bmatrix} = \begin{bmatrix} I \\ \hat{R} \end{bmatrix} \left[\Psi_b\right] \tag{4.10}$$

4.3 DYNAMIC CONDENSATION WITH MODAL SYNTHESIS

The second substructuring technique presented here consists of a combination of the mode synthesis approach and the dynamic condensation approach. In a conventional mode synthesis approach [14], the following steps are required. (1) Divide the structure into substructures. (2) Calculate the eigenproperties of the individual substructures. (3) Synthesize some of the eigenproperties along with a set of the so-called component modes of the substructures to obtain a reduced size eigenvalue problem. (4) Solve this eigenvalue problem and obtain the lower modes of the original structure. In this approach, the size is reduced at the substructure level by elimination of the higher modes from any further consideration in the synthesis process. In the approach to be presented here, however, we will use all the eigenproperties of the substructures to define the condensed eigenvalue problem of step 3. To reduce the size of the synthesized eigenvalue problem we apply the dynamic condensation approach presented in Chapter 3. The reduced eigenvalue problem is solved and then updated again iteratively to improve the accuracy of the results. It is specially efficient to apply the dynamic condensation in this case as the selection of the kept degrees of freedom is greatly facilitated by the fact that the substructure frequencies are already known. In the following section, we formulate the approach for a structure divided into two substructures, with fixed interface boundary conditions for one of the substructures and free for the other.

4.3.1 Synthesis of Substructure Eigenproperties

We again consider a structural system that has been divided into two substructures which are identified here as the α and the β substructures. The number of degrees of freedom of the α and β substructures with their interface coordinates free are *n* and *m*, respectively. Substructures are connected at n_b boundary degrees of freedom.

We assume that the undamped eigenproperties of both substructures, one with free interfaces and the other with fixed interfaces, are known from previous analyses. For instance, if the α substructure is chosen as the substructure with free interfaces, the undamped vibration modes can be obtained from the solution of the following eigenvalue problem

$$[\mathrm{M}^{\alpha}]\ [\,\phi^{\alpha}\,]\ [\,\Lambda_{\alpha}\,] = [\,\mathrm{K}^{\alpha}]\ [\,\phi^{\alpha}\,] \tag{4.18}$$

The mass and stiffness matrices of the substructure have been defined in Eqs. (2.4), and the eigenvector matrix $[\,\phi^{\alpha}\,]$ is partitioned as

$$[\,\phi^{\alpha}\,] = \begin{bmatrix} \phi_b^{\alpha} \\ \phi_i^{\alpha} \end{bmatrix} \tag{4.19}$$

in which subscript b and i are again associated with the boundary and interior degrees of freedom respectively. The eigenvectors are assumed to be normalized with respect to the mass matrix of the α substructure. Similarly, the undamped vibration modes of the β substructure, with the boundary degrees of freedom now considered fixed, can be obtained from the eigenvalue problem

$$\left[\mathrm{M}_{ii}^{\beta}\right] \ [\phi^{\beta}] \ [\Lambda_{\beta}] = \left[\mathrm{K}_{ii}^{\beta}\right] \ [\phi^{\beta}] \tag{4.20}$$

Modal matrix $[\phi^{\beta}]$ is also assumed to be normalized with respect to its mass matrix.

The equations of motion of the combined structural system in free vibration can be written as

$$[\mathrm{M}] \ \ddot{\underset{\sim}{x}} + [\mathrm{C}] \ \dot{\underset{\sim}{x}} + [\mathrm{K}] \ \underset{\sim}{x} = \underset{\sim}{0} \tag{4.21}$$

in which the mass and stiffness matrices are given in Eqs. (2.6) and (2.7), and similarly, the damping matrix is partitioned as follows,

$$[\mathrm{C}] = \begin{bmatrix} \mathrm{C}_{bb} & \mathrm{C}_{bi} \\ \mathrm{C}_{ib} & \mathrm{C}_{ii} \end{bmatrix} = \begin{bmatrix} \mathrm{C}_{bb}^{\alpha} + \mathrm{C}_{bb}^{\beta} & \mathrm{C}_{bi}^{\alpha} & \mathrm{C}_{bi}^{\beta} \\ \mathrm{C}_{ib}^{\alpha} & \mathrm{C}_{ii}^{\alpha} & 0 \\ \mathrm{C}_{ib}^{\beta} & 0 & \mathrm{C}_{ii}^{\beta} \end{bmatrix} \tag{4.22}$$

We will express these equations of motion in terms of the eigenproperties of the substructures. To accomplish this, we introduce the following transformation of coordinates,

$$\underset{\sim}{x} = [\mathrm{U}] \ \underset{\sim}{z} \tag{4.23}$$

where

$$[\mathrm{U}] = \begin{bmatrix} \phi^{\alpha} & 0 \\ 0 & \phi^{\beta} \end{bmatrix} = \begin{bmatrix} \phi_b^{\alpha} & 0 \\ \phi_i^{\alpha} & 0 \\ 0 & \phi^{\beta} \end{bmatrix} \tag{4.24}$$

into Eq. (4.21). After pre-multiplying by $[\mathrm{U}]^{\mathrm{T}}$, we obtain the following transformed equations of motion,

$$[\mathrm{M}^*]\ \ddot{\underset{\sim}{z}} + [\mathrm{C}^*]\ \dot{\underset{\sim}{z}} + [\mathrm{K}^*]\ \underset{\sim}{z} = \underset{\sim}{Q} \tag{4.25}$$

where the new mass, damping and stiffness matrices are given by the following expressions,

$$[\mathrm{M}^*] = \begin{bmatrix} \phi^{\alpha\mathrm{T}}\mathrm{M}^{\alpha}\ \phi^{\alpha} + \phi_b^{\alpha\mathrm{T}}\mathrm{M}_{bb}^{\beta}\ \phi_b^{\alpha} & \phi_b^{\alpha\mathrm{T}}\ \mathrm{M}_{bi}^{\beta}\ \ \phi^{\beta} \\ \phi^{\beta\mathrm{T}}\mathrm{M}_{ib}^{\beta}\ \phi_b^{\alpha} & \phi^{\beta\mathrm{T}}\ \mathrm{M}_{ii}^{\beta}\ \ \phi^{\beta} \end{bmatrix} \tag{4.26a}$$

$$[\mathrm{C}^*] = \begin{bmatrix} \phi^{\alpha\mathrm{T}}\mathrm{C}^{\alpha}\ \phi^{\alpha} + \phi_b^{\alpha\mathrm{T}}\mathrm{C}_{bb}^{\beta}\ \phi_b^{\alpha} & \phi_b^{\alpha\mathrm{T}}\ \mathrm{C}_{bi}^{\beta}\ \ \phi^{\beta} \\ \phi^{\beta\mathrm{T}}\mathrm{C}_{ib}^{\beta}\ \phi_b^{\alpha} & \phi^{\beta\mathrm{T}}\ \mathrm{C}_{ii}^{\beta}\ \ \phi^{\beta} \end{bmatrix} \tag{4.26b}$$

$$[\mathrm{K}^*] = \begin{bmatrix} \phi^{\alpha\mathrm{T}}\mathrm{K}^{\alpha}\ \phi^{\alpha} + \phi_b^{\alpha\mathrm{T}}\mathrm{K}_{bb}^{\beta}\ \phi_b^{\alpha} & \phi_b^{\alpha\mathrm{T}}\ \mathrm{K}_{bi}^{\beta}\ \ \phi^{\beta} \\ \phi^{\beta\mathrm{T}}\mathrm{K}_{ib}^{\beta}\ \phi_b^{\alpha} & \phi^{\beta\mathrm{T}}\ \mathrm{K}_{ii}^{\beta}\ \ \phi^{\beta} \end{bmatrix} \tag{4.26c}$$

Utilizing the orthonormal properties of the modal matrices $[\phi^{\alpha}]$ and $[\phi^{\beta}]$, the above equations can be written as

$$[\mathrm{M}^*] = \begin{bmatrix} \mathrm{I}_{\alpha} + \phi_b^{\alpha\mathrm{T}}\mathrm{M}_{bb}^{\beta}\ \phi_b^{\alpha} & \phi_b^{\alpha\mathrm{T}}\ \mathrm{M}_{bi}^{\beta}\ \ \phi^{\beta} \\ \phi^{\beta\mathrm{T}}\mathrm{M}_{ib}^{\beta}\ \phi_b^{\alpha} & \mathrm{I}_{\beta} \end{bmatrix} \tag{4.27a}$$

$$[\mathrm{C}^*] = \begin{bmatrix} \Delta_\alpha + \phi_b^{\alpha\mathrm{T}} \mathrm{C}_{bb}^{\beta}\, \phi_b^{\alpha} & \phi_b^{\alpha\mathrm{T}}\, \mathrm{C}_{bi}^{\beta}\ \ \phi^{\beta} \\ \phi^{\beta\mathrm{T}} \mathrm{C}_{ib}^{\beta}\, \phi_b^{\alpha} & \Delta_\beta \end{bmatrix} \tag{4.27b}$$

$$[\mathrm{K}^*] = \begin{bmatrix} \Lambda_\alpha + \phi_b^{\alpha\mathrm{T}} \mathrm{K}_{bb}^{\beta}\, \phi_b^{\alpha} & \phi_b^{\alpha\mathrm{T}}\, \mathrm{K}_{bi}^{\beta}\ \ \phi^{\beta} \\ \phi^{\beta\mathrm{T}} \mathrm{K}_{ib}^{\beta}\, \phi_b^{\alpha} & \Lambda_\beta \end{bmatrix} \tag{4.27c}$$

in which $[\ \mathrm{I}_j\ ]$ is an identity matrix, $[\,\Lambda_j\,]$ is a diagonal matrix containing the eigenvalues of the j substructure, and $[\,\Delta_j\,]$ is defined as

$$[\,\Delta_j\,] = [\ \phi^j\ ]^{\mathrm{T}} \left[\mathrm{C}_{ii}^{j}\right] [\ \phi^j\ ] \tag{4.28}$$

The matrix $[\,\mathrm{C}\,]$ can be classically or nonclassically damped. However, if the j substructure is classically damped, then matrix $[\,\Delta_j\,]$ becomes diagonal with coefficients equal to $2\ \xi_l^j\ \omega_l^j$, where ω_l^j and ξ_l^j are the modal frequency and the damping ratio, respectively, of the l^{th} mode of the j substructure.

It is noted that these transformed equations of motion remain of order N since all modes have been used in the transformation process. In the next section we will explain how we can obtain the complex modes of the combined structure by solving a reduced size eigenvalue problem.

4.3.2 Dynamic Condensation

In general, the equations (4.25) will still be coupled. To obtain the eigenproperties of the combined system, we will rewrite Eq. (4.25) in the state vector form. The eigenvalue problem of this state equation is

$$[\mathrm{A}^*]\ [\Psi^*]\ [\Omega] = [\mathrm{B}^*]\ [\Psi^*] \tag{4.29}$$

in which

$$[A^*] = \begin{bmatrix} [\,0\,] & [M^*] \\ [M^*] & [C^*] \end{bmatrix} \tag{4.30a}$$

$$[B^*] = \begin{bmatrix} [M^*] & [\,0\,] \\ [\,0\,] & -[K^*] \end{bmatrix} \tag{4.30b}$$

and $[\Omega]$ is a diagonal matrix containing the $2N$ eigenvalues and $[\Psi^*]$ is the modal matrix containing the eigenvectors of the transformed structural system. Eigenvectors of the original system can be computed using the transformation of coordinates defined in Eq. (4.23) as follows

$$[\Psi] = \begin{bmatrix} U & 0 \\ 0 & U \end{bmatrix} [\Psi^*] \tag{4.31}$$

We do not wish to solve the full eigenvalue problem of Eq. (4.29) but only a condensed one to reduce the size of the problem. To condense, we first make the choice about the coordinates to be kept and reduced. This choice has a significant impact on the efficiency of the procedure. This will be shown by a numerical example later. If we partition the displacement vector $\underset{\sim}{z}$ as indicated by Eq. (3.7),

$$\underset{\sim}{z} = \begin{Bmatrix} \underset{\sim}{z}_k \\ \underset{\sim}{z}_r \end{Bmatrix} \tag{4.32}$$

and rearrange the transformed state matrices such that

$$[\mathrm{A}^*] = \begin{bmatrix} \mathrm{A}_{kk} & \mathrm{A}_{kr} \\ \mathrm{A}_{rk} & \mathrm{A}_{rr} \end{bmatrix} \tag{4.33a}$$

$$[\mathrm{B}^*] = \begin{bmatrix} \mathrm{B}_{kk} & \mathrm{B}_{kr} \\ \mathrm{B}_{rk} & \mathrm{B}_{rr} \end{bmatrix} \tag{4.33b}$$

then the dynamic condensation approach developed in Chapter 3 can be directly applied to the transformed structural system represented by Eq. (4.29). Following the step-by-step procedure described in Section 3.5, the desired eigenproperties of the transformed system can be obtained. Eigenvectors of the original system are then computed by using Eq. (4.31). It is of interest to note that with this substructuring technique, we can use the iteration process with lower modes as well as with higher modes. In addition to that, the number of degrees of freedom to be kept in the reduced size eigenvalue problem does not have to be equal to the number of boundary degrees of freedom.

4.4 NUMERICAL RESULTS

The truss structure considered in the previous chapter will be utilized here to present the numerical results of the dynamic condensation methods introduced in this chapter. The truss has been divided into two substructure as indicated Figure 4.1. The total number of degrees of freedom of the two substructures with their interface coordinates free are 16 and 28, respectively. They are connected at 4 boundary coordinates. The combined structure has a total of 40 degrees of freedom.

We consider first the condensed substructure superposition approach with iterations. As we mentioned earlier, the dimension of the reduced eigenvalue problem is determined by the number of the boundary degrees of freedom between the substructures. From Figure 3.10 we can see that coordinates 5, 7, 22 and 33, numbered according to

Shah and Raymund's procedure, are kept in the reduced eigenvalue problem. Since the condensed eigenvalue problem is of size 4 (the number of degrees of freedom at the interface), in this case, we will get the first four pairs of complex and conjugate eigenproperties of the truss. Table 4.1 shows the percent errors obtained in modal frequencies and damping ratios calculated from the complex eigenvalues and Table 4.2 shows the RMS errors in the four eigenvectors. It is noted that the initial estimates of the eigenproperties are poor, but after one iteration the errors are reduced noticeably. Almost exact values are obtained after four iterations.

The results obtained with the dynamic condensation with modal synthesis are given next. Eigenproperties of the α and β substructures were calculated with interface coordinates free and fixed, respectively. The first five natural frequencies of each substructure are listed in Table 4.3. The transformed combined system was reduced to a size of 4, thus providing the lowest four modes; this amounts of a reduction in the size by 90% of the degrees of freedom.

To demonstrate the effect of the choice of the kept degrees of freedom on the efficiency of the procedure two different ways of choosing the kept generalized coordinates in the reduced eigenvalue problem have been considered. In the first case, the system matrices are directly formed as indicated in Eqs. (4.27a-c), and the first four coordinates of the transformed structure are kept. These correspond to the coordinates at the interface of the substructures. In the second case, the system matrices were reordered according to the magnitudes of the natural frequencies of the uncoupled α and β substructure in Eq. (4.27c). From the magnitude of the frequencies indicated in Table 4.3, we see that in this method of selecting coordinates only one coordinate of the α substructure and three of the β substructure are kept.

Tables 4.4 and 4.5 show the results obtained for the first case. It is noted that the initial estimate of the eigenproperties are completely off the mark with large errors. They are significantly improved after one iteration, where only the fourth mode, has rather a high error. The errors are, however, drastically reduced when the selection is made according to the second approach, as is seen from the results in Tables 4.6 and 4.7; with the exception of the damping ratios of the third and fourth modes, the initial estimates of the results in the second case are excellent. After four iterations the first three modes can be considered as exact and the fourth is very close to being an exact one also. From the results we can conclude that better results and faster convergence will be obtained when the system matrices are reordered according to the magnitude of the natural frequencies of the uncoupled substructures.

4.5 SUMMARY AND CONCLUSIONS

In this chapter, the dynamic condensation approach presented in Chapter 3 is applied to structures divided into substructures. Two substructuring techniques are considered. One is based on the condensed substructure superposition approach developed in Chapter 2. The other technique is a combination of the well known modal synthesis approach and the dynamic condensation method.

In the condensed substructure superposition approach with iterations, the substructures' mass, damping and stiffness submatrices are only required. The interior degrees of freedom are condensed at substructure level initially using the static condensation approach. This reduction approach can be refined by using the iterative approach presented here. In the iterative approach the eigenproperties of the condensed problem are successively used. In this approach, the dimension of the eigenvalue problem of the combined structure is reduced to the number of boundary degrees of freedom. A numerical example is presented to demonstrate the implementation and effectiveness of the method.

In the combined mode synthesis and condensation approach each substructure is described by its eigenproperties. The case of free and fixed boundary conditions at the interface of the two substructures was considered. Physical coordinates of the combined structure are transformed into generalized coordinates before the iterative condensation process described in Chapter 3 is implemented. Examples are presented which illustrate the effectiveness of the proposed method. It is found that a better convergence is obtained when the kept coordinates are selected according to the magnitude of the eigenvalues of the constituent substructures.

Table 4.1 Percent errors in modal frequencies and damping ratios of the truss in Figure 3.9 calculated with the condensed substructure superposition approach with iterations.

a) Modal Frequencies

Mode	Iteration Step				
	0	1	2	3	4
1	12.889	0.001	0.000	--------	--------
2	25.994	0.059	0.010	0.004	0.003
3	15.930	0.189	0.020	0.003	0.001
4	185.147	3.202	1.040	0.705	0.526

b) Damping Ratios

Mode	Iteration Step				
	0	1	2	3	4
1	32.986	-0.136	-0.009	0.001	0.001
2	33.252	-0.990	-0.025	0.054	0.052
3	46.034	-0.420	-0.053	-0.021	-0.014
4	256.894	4.117	-5.894	-4.394	-3.593

Table 4.2 RMS errors in eigenvectors of truss in Figure 3.9 calculated with the condensed substructure superposition approach with iterations.

Mode	Iteration Step				
	0	1	2	3	4
1	12.753	0.023	0.005	0.003	0.002
2	21.169	1.161	0.299	0.152	0.099
3	21.932	2.250	0.634	0.245	0.114
4	65.533	11.829	4.788	2.000	1.576

Table 4.3 First five natural frequencies in rad/sec of the α substructure with free interface coordinates, and the β substructure with fixed interface coordinates.

Mode	α Substructure	β Substructure
1	0.0568	0.0449
2	0.1662	0.1161
3	0.2000	0.1624
4	0.2875	0.2327
5	0.3383	0.3443

Table 4.4 Percent errors in modal frequencies and damping ratios of truss in Figure 3.9 calculated with the dynamic condensation approach with modal synthesis. Kept degrees of freedom selected without any reordering.

a) Modal Frequencies

Mode	Iteration Step				
	0	1	2	3	4
1	19.692	0.004	0.002	0.001	0.001
2	37.209	0.504	0.189	0.112	0.072
3	20.535	0.346	0.051	0.010	0.002
4	61.116	14.126	6.027	3.461	2.304

b) Damping Ratios

Mode	Iteration Step				
	0	1	2	3	4
1	75.883	-0.375	-0.246	-0.141	-0.087
2	73.168	-1.235	-1.209	-0.748	-0.480
3	51.596	-2.370	-0.213	0.036	0.048
4	187.802	35.883	13.875	7.137	4.549

Table 4.5 RMS errors in eigenvectors of truss in Figure 3.9 calculated with the dynamic condensation approach with modal synthesis. Kept degrees of freedom selected without any reordering.

Mode	Iteration Step				
	0	1	2	3	4
1	35.921	0.193	0.167	0.125	0.097
2	55.454	3.336	2.052	1.557	1.232
3	36.183	5.429	2.251	1.084	0.597
4	98.325	49.473	33.018	24.262	19.165

Table 4.6 Percent errors in modal frequencies and damping ratios of truss in Figure 3.9 calculated with the dynamic condensation approach with modal synthesis. Kept degrees of freedom selected according to the magnitudes of the uncoupled frequencies of the substructures.

a) Modal Frequencies

	Iteration Step				
Mode	0	1	2	3	4
1	0.026	0.000	--------	--------	--------
2	0.362	0.003	0.000	--------	--------
3	1.609	0.026	0.001	0.000	--------
4	1.674	0.262	0.050	0.010	0.002

b) Damping Ratios

	Iteration Step				
Mode	0	1	2	3	4
1	-0.529	-0.002	0.000	--------	--------
2	0.322	-0.053	0.000	--------	--------
3	-11.884	-0.653	-0.041	-0.003	-0.000
4	-20.209	-6.107	-2.203	-0.674	-0.235

Table 4.7 RMS errors in eigenvectors of the truss in Figure 3.9 calculated with the dynamic condensation approach with modal synthesis. Kept degrees of freedom selected according to the magnitudes of the uncoupled frequencies of the substructures.

Mode	Iteration Step				
	0	1	2	3	4
1	0.017	0.003	0.000	--------	--------
2	0.759	0.064	0.007	0.001	0.000
3	1.539	0.230	0.040	0.008	0.002
4	6.678	2.971	1.384	0.714	0.373

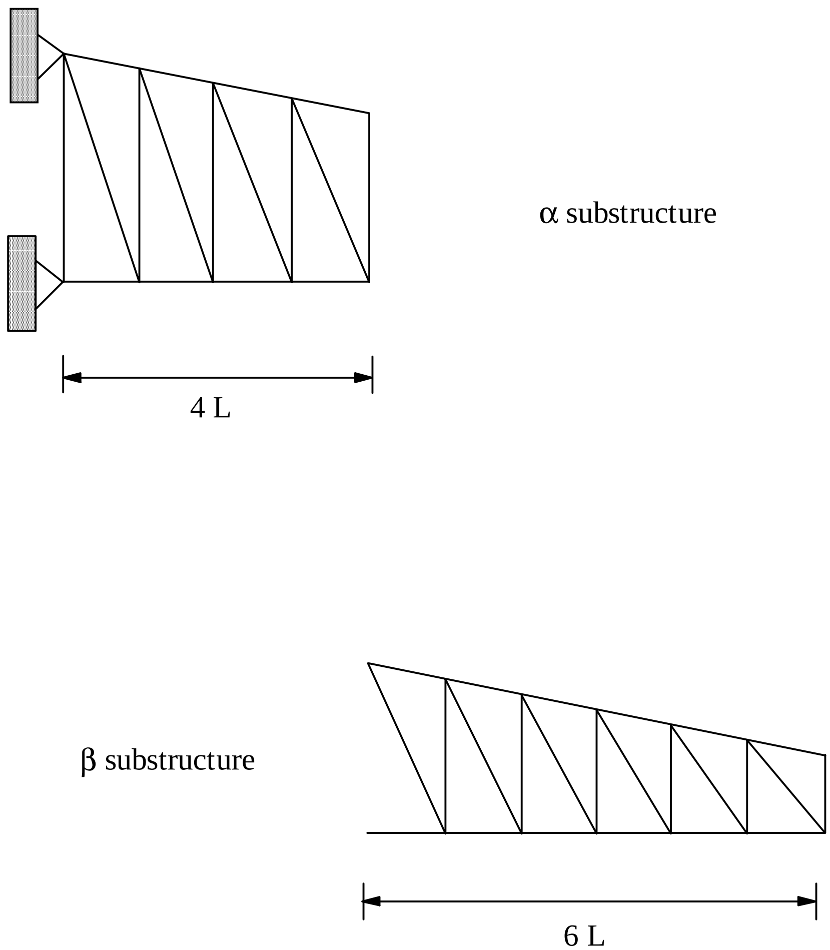

Figure 4.1 The α substructure with free interface boundary conditions and the β substructure with fixed boundary condition for the truss in Figure 3.9.

CHAPTER V

DYNAMIC CONDENSATION APPROACH FOR CLASSICALLY DAMPED STRUCTURES

5.1 INTRODUCTION

In the previous chapters we presented a dynamic condensation approach for nonclassically damped structures. As quite often the structures are modeled as classically damped, in this chapter we will specialize the expressions of this analytical procedure to make it applicable to classically damped structures. The expressions for the dynamic condensation approach and also for the two condensation methods with substructuring considered in Chapter 4 are given. The performance of the proposed approach is demonstrated with numerical examples for classically damped systems.

5.2 DYNAMIC CONDENSATION FOR CLASSICAL DAMPING

The eigenproperties of the structural system with classical damping can be obtained from the solution of the eigenvalue problem

$$[M]\ [\Phi]\ [\Lambda] = [K]\ [\Phi] \tag{5.1}$$

in which $[\mathrm{M}]$ and $[\mathrm{K}]$ are positive definite matrices, $[\Lambda]$ is a diagonal matrix containing N real eigenvalues and $[\Phi]$ is the (N x N) eigenvector matrix. Eigenvectors can be normalized such that

$$[\Phi]^{\mathrm{T}}\,[\mathrm{M}]\;[\Phi] \;=\; [\;\mathrm{I}\;] \tag{5.2a}$$

$$[\Phi]^{\mathrm{T}}\,[\mathrm{K}]\;[\Phi] \;=\; [\Lambda] \tag{5.2b}$$

where $[\;\mathrm{I}\;]$ is an unity matrix.

As in the case of nonclassically damped systems, we are interested in solve two reduced size eigenvalue problems instead of solving this one directly. Once again, we have to partition the displacement vector $\underset{\sim}{\mathrm{x}}$ as indicated in Eq. (3.7),

$$\underset{\sim}{\mathrm{x}} = \begin{Bmatrix} \underset{\sim}{\mathrm{x}}_k \\ \underset{\sim}{\mathrm{x}}_r \end{Bmatrix} \tag{5.3}$$

in which $\underset{\sim}{\mathrm{x}}_k$ will contain the degrees of freedom to be kept in the eigenvalue problem associated with the lower modes and $\underset{\sim}{\mathrm{x}}_r$ will contains the remaining degrees of freedom, those to be kept in the eigenvalue problem associated with the higher modes. The selection of the degrees of freedom can be done with any of the analytical procedures available in the literature [2,8,17,28,44,50,54,57,64]. Corresponding to this partition of the displacement vector, the mass and stiffness matrices are also partitioned as

$$[\mathrm{M}] \;=\; \begin{bmatrix} \mathrm{M}_{kk} & \mathrm{M}_{kr} \\ \mathrm{M}_{rk} & \mathrm{M}_{rr} \end{bmatrix} \tag{5.4a}$$

$$[\mathrm{K}] \;=\; \begin{bmatrix} \mathrm{K}_{kk} & \mathrm{K}_{kr} \\ \mathrm{K}_{rk} & \mathrm{K}_{rr} \end{bmatrix} \tag{5.4b}$$

where submatrices M_{ij} and K_{ij} have a dimension (n_i x n_j), with i,j = k,r.

After the corresponding partition of the modal matrices in Eq. (5.1), the eigenvalue problem corresponding to the n_k lower modes can be written as

$$\begin{bmatrix} M_{kk} & M_{kr} \\ M_{rk} & M_{rr} \end{bmatrix} \begin{bmatrix} \Phi_{kk} \\ \Phi_{rk} \end{bmatrix} [\Lambda_k] = \begin{bmatrix} K_{kk} & K_{kr} \\ K_{rk} & K_{rr} \end{bmatrix} \begin{bmatrix} \Phi_{kk} \\ \Phi_{rk} \end{bmatrix} \tag{5.5}$$

whereas the eigenvalue problem corresponding to the n_r higher modes can be written as

$$\begin{bmatrix} M_{kk} & M_{kr} \\ M_{rk} & M_{rr} \end{bmatrix} \begin{bmatrix} \Phi_{kr} \\ \Phi_{rr} \end{bmatrix} [\Lambda_r] = \begin{bmatrix} K_{kk} & K_{kr} \\ K_{rk} & K_{rr} \end{bmatrix} \begin{bmatrix} \Phi_{kr} \\ \Phi_{rr} \end{bmatrix} \tag{5.6}$$

It is noted that these eigenvalue problems are similar to the ones obtained for nonclassically damped structures, Eqs. (3.13) and (3.19), reproduced here as:

$$\begin{bmatrix} A_{kk} & A_{kr} \\ A_{rk} & A_{rr} \end{bmatrix} \begin{bmatrix} \Psi_{kk} \\ \Psi_{rk} \end{bmatrix} [\Omega_k] = \begin{bmatrix} B_{kk} & B_{kr} \\ B_{rk} & B_{rr} \end{bmatrix} \begin{bmatrix} \Psi_{kk} \\ \Psi_{rk} \end{bmatrix} \tag{3.13}$$

$$\begin{bmatrix} A_{kk} & A_{kr} \\ A_{rk} & A_{rr} \end{bmatrix} \begin{bmatrix} \Psi_{kr} \\ \Psi_{rr} \end{bmatrix} [\Omega_r] = \begin{bmatrix} B_{kk} & B_{kr} \\ B_{rk} & B_{rr} \end{bmatrix} \begin{bmatrix} \Psi_{kr} \\ \Psi_{rr} \end{bmatrix} \tag{3.19}$$

where now

$$[A_{ij}] = [M_{ij}] \qquad [B_{ij}] = [K_{ij}] \qquad \text{with i, j = k, r} \tag{5.7a}$$

$$[\Psi_{ij}] = [\Phi_{ij}] \qquad [\Omega_i] = [\Lambda_i] \qquad \text{with i, j = k, r} \tag{5.7b}$$

Of course, here the dimensions of the submatrices are (n_i x n_j) instead of ($2n_i$ x $2n_j$) and the eigenproperties are real. To obtain the dynamic condensation for classically damped structures we can follow the formulation similar to the one presented in Chapter 3. This procedure will show that the expressions obtained for nonclassically damped structures are directly applicable to classically damped if the submatrices are replaced as indicated in Eqs. (5.7a) and (5.7b). These equations with replacement of the submatrices according to Eqs. (5.7a) and (5.7b) are presented in the following sections.

5.2.1 Condensed Eigenvalue Problems

The condensed eigenvalue problem associated with the lower modes is given by the following expression

$$\left[[\ ]\hat{M} \right] \; [\Phi_{kk}] \; [\Lambda_k] = \left[\hat{K} \right] \; [\Phi_{kk}] \tag{5.8}$$

where the condensed matrices $\left[\hat{M} \right]$ and $\left[\hat{K} \right]$ are

$$[\hat{M}] = [M_{kk}] + [\hat{R}]^T [M_{rk}] + [M_{kr}] \left[\hat{R} \right] + \left[\hat{R} \right]^T [M_{rr}] \left[\hat{R} \right] \tag{5.9a}$$

$$\left[\hat{K} \right] = [K_{kk}] + \left[\hat{R} \right]^T [K_{rk}] + [K_{kr}] \left[\hat{R} \right] + \left[\hat{R} \right]^T [K_{rr}] \left[\hat{R} \right] \tag{5.9b}$$

The condensation matrix for the lower modes $\left[\hat{R} \right]$ is defined as

$$\left[\hat{R} \right] = [\Phi_{rk}] \; [\Phi_{kk}]^{-1} \tag{5.10}$$

The condensed eigenvalue problem associated with the higher modes is given by

$$[\bar{M}]\ [\Phi_{rr}]\ [\Lambda_r] = [\bar{K}]\ [\Phi_{rr}] \tag{5.11}$$

where the condensed matrices $[\bar{M}]$ and $[\bar{K}]$ are

$$[\bar{M}] = [M_{rr}] + [\bar{R}]^T [M_{kr}] + [M_{rk}]\ [\bar{R}] + [\bar{R}]^T [M_{kk}]\ [\bar{R}] \tag{5.12a}$$

$$[\bar{K}] = [K_{rr}] + [\bar{R}]^T [K_{kr}] + [K_{rk}]\ [\bar{R}] + [\bar{R}]^T [K_{kk}]\ [\bar{R}] \tag{5.12b}$$

The condensation matrix for the higher modes $[\bar{R}]$ is now defined as

$$[\bar{R}] = [\Phi_{kr}]\ [\Phi_{rr}]^{-1} \tag{5.13}$$

The relationships between the condensation matrices obtained from the orthogonality conditions of the eigenvector matrix $[\Phi]$, Eqs. (5.2a) and (5.2b), are

$$[\bar{R}] \;=\; -\left[M_{kk} + \hat{R}^T M_{rk}\right]^{-1} \left[M_{kr} + \hat{R}^T M_{rr}\right] \tag{5.14}$$

$$\left[\hat{R}\right]^T = -\left[K_{kk}\ \bar{R} + K_{kr}\right]\ \left[K_{rk}\ \bar{R} + K_{rr}\right]^{-1} \tag{5.15}$$

Using the solution of the condensed eigenvalue problems (5.8) and (5.10), we can obtain the complete set of real eigenproperties of the structural system by means of the following equation,

$$[\Phi] = \begin{bmatrix} \Phi_{kk} & \Phi_{kr} \\ \Phi_{rk} & \Phi_{rr} \end{bmatrix} = \begin{bmatrix} \Phi_{kk} & \bar{R}\ \Phi_{rr} \\ \hat{R}\ \Phi_{kk} & \Phi_{rr} \end{bmatrix} \tag{5.16}$$

However, once again the condensation matrices cannot be defined since the eigenvectors are unknown. In the next sections we present the iterative procedures to compute the condensation matrices for lower and higher modes.

5.2.2 Iterative Condensation Processes

The initial approximation for the condensation matrix for lower modes can be computed as

$$\left[\hat{R}^{(0)}\right] = -[K_{rr}]^{-1}[K_{rk}] \tag{5.17}$$

where the superscript (0) indicate that it is an initial value. This condensation matrix is the same as the static condensation proposed by Guyan [19]. The recursive relationship to iteratively obtain improved estimate of $\left[\hat{R}\right]$ is

$$\left[\hat{R}^{(l+1)}\right] = [K_{rr}]^{-1}\left[R_{rk}^{j\,(l)}\right]\left[\Phi_{kk}^{(l)}\right]\left[\Phi_{kk}^{(l)}\right]^{T}\left[\hat{R}^{(l)}\right] - [K_{rr}]^{-1}[K_{rk}] \tag{5.18a}$$

where

$$\left[R_{rk}^{j\,(l)}\right] = \left[M_{rk} + M_{rr}\hat{R}^{(l)}\right] \tag{5.18b}$$

The last term on the right hand side of Eq. (5.18a) can be identified as the initial approximation $\left[\hat{R}^{(0)}\right]$ and the other one is a correction term that is added to improve this original estimate. This iterative procedure will improve the initial condensation matrix. Superscript *(l)* refers to the iteration step.

When the higher modes are used in the condensation process, then the initial approximation of the condensation matrix is written as

$$\left[\bar{\mathrm{R}}^{(0)}\right] = -\left[\mathrm{M}_{kk}\right]^{-1}\left[\mathrm{M}_{kr}\right] \tag{5.19}$$

The recursive equation to improve the estimate of the condensation matrix $[\bar{\mathrm{R}}]$ is

$$\left[\bar{\mathrm{R}}^{(l+1)}\right] = \left[\mathrm{M}_{kk}\right]^{-1}\left[\mathrm{R}_{kr}^{(l)}\right]\left[\Phi_{rr}^{(l)}\right]\left[\Lambda_{r}^{(l)}\right]^{-1}\left[\Phi_{rr}^{(l)}\right]^{\mathrm{T}}\left[\bar{\mathrm{M}}^{(l)}\right]$$

$$-\left[\mathrm{M}_{kk}\right]^{-1}\left[\mathrm{M}_{kr}\right] \tag{5.20a}$$

where

$$\left[\mathrm{R}_{kr}^{(l)}\right] = \left[\mathrm{K}_{kk}\,\bar{\mathrm{R}}^{(l)} + \mathrm{K}_{kr}\right] \tag{5.20b}$$

Here again superscript (l) refers to the iteration step. As in Eq. (5.18), the last term on the right hand side of the above equation can be identified as the initial approximation of the condensation matrix. The other term represents a correction that is added to improve the initial approximation. A step-by-step procedure for both iteration processes is similar to the one presented in Section 3.5 with a proper substitution of the submatrices as indicated in Eqs. (5.7a) and (5.7b).

5.2.3 Numerical Results

The frame structure considered in Chapter 2 will be used here to verify the effectiveness of the dynamic condensation approach presented in the preceding sections. Only the results obtained with the iteration process with lower modes are included.

Again two different ways of selecting the kept degrees of freedom were considered. In the first case, the n_k degrees of freedom with the smallest stiffness to mass ratios were selected, whereas the kept coordinates of the second case were arbitrarily selected. In both cases only 8 of the 102 coordinates were kept. Figure 5.1 shows these degrees of freedom for both cases. First eight coordinates correspond to the first case and the remaining eight correspond to the second case. It can be suspected that these groups of coordinates may not lead to reasonably approximations of the lower modes since all coordinates kept pertain to the horizontal displacements.

The natural frequencies calculated at different iteration steps for the first case are listed in Table 5.1. Percent errors are also given in the table immediately below the frequencies, in parentheses. Again the frequencies with errors less than 0.005% are regarded as exact. At the iteration step '0', corresponding to the Guyan reduction method, all frequencies are unacceptable with errors ranging from 12 and 72%. However, after the first iteration the frequencies are improved noticeably with errors bellow 7% with two of them being essentially exact. All frequencies have errors less than 1% after the third iteration. As observed with the nonclassical damped structures, all frequencies have positive errors in all the iteration steps. It means that the convergence of the lower modes is from the above.

The eigenproperties calculated with the dynamic condensation approach were also used to compute the response quantities identified in Tables 2.5 and 2.6. Normalized root mean square values for the shear forces, bending moments and displacements are given in Tables 5.2 to 5.4. A value close to 1.00 indicates that the response is close to the exact response. The ground excitations, defined by the Kanai-Tajimi spectral density function with parameters given in Table 2.4, have been considered. The results have been obtained for (a) horizontal excitation only, (b) vertical excitation only and (c) combined horizontal and vertical excitations. It is observed from Tables 5.2 to 5.4 that all response quantities computed with the Guyan's condensation are poor. However, the results are improved considerable as the iteration process proceeds.

For the second case where the kept coordinates were selected arbitrarily, the natural frequencies calculated at different iteration steps are listed in Table 5.5. A dash in this and the following tables indicates that the particular frequency was not even remotely approximated in the iteration step. Four of the first five frequencies were obtained with errors less than 4%. But, no approximation of the fourth frequency, 44.54 rad/sec, was obtained. The rest of the calculated frequencies are completely off the mark. It was only after the third iteration than an approximation of the fourth frequency was obtained. Two iterations steps later, however, all eight frequencies have an error below 3%. However, the exact eigenproperties can still be obtained by performing a few more iterations.

These results clearly indicate that it is important to choose the kept degrees of freedom properly and not just arbitrarily. An arbitrary choice may even lead to missing a few modes from the spectrum and it can slow down the convergence significantly. Next we show what effect it has in the calculation response.

In Table 5.6 we present the normalized force and displacement response values obtained for the input applied in the horizontal direction only. It is noted the response values are very accurate even though the frequencies had very large errors in a first few iterations. However, if we observe the results presented in Table 5.7 which are for the input applied in the vertical direction, we observe that errors are very large. This is due to the fact that in the first case the response contributions came from those frequencies which could be calculated accurately even by a simple static condensation. In the case of vertical excitation, the frequencies which contribute to the response can only be calculated after several iterations have been performed. In Table 5.8 we show similar results, but now for the input applied in both directions. Here the errors are not as large as they were in the case of vertical excitation only but are also not as small as for the horizontal input only. Actually, these errors depend upon the relative contribution of the two inputs. What these results indicate is that to calculate all the responses accurately it is necessary to choose the kept coordinates properly. Otherwise many more iterations may be required to obtain the modes as well as the response accurately.

5.3 CONDENSED SUBSTRUCTURE SUPERPOSITION APPROACH WITH ITERATIONS

The expressions developed in Section 4.2 for the dynamic condensation of nonclassically damped structures can also be used with classically damped systems if the substitution for various matrices is made according to Eqs. (5.7a) and (5.7b). Next, we present these equations for their ready use.

To start, the initial condensation matrix is defined in terms of the substructure matrices as follow

$$\left[\hat{\mathrm{R}}_j^{(0)}\right] = -\left[\mathrm{K}_{ii}^j\right]^{-1}\left[\mathrm{K}_{ib}^j\right] \qquad \text{with j} = \alpha,\ \beta \tag{5.21}$$

Using these condensation matrices, the condensed mass and stiffness matrices for each substructure are defined as :

$$\left[\hat{\mathrm{M}}_{bb}^j\right] = \left[\mathrm{M}_{bb}^j\right] + \left[\hat{\mathrm{R}}_j\right]^{\mathrm{T}}\left[\mathrm{M}_{ib}^j\right] + \left[\mathrm{M}_{ib}^j\right]^{\mathrm{T}}\left[\hat{\mathrm{R}}_j\right] + \left[\hat{\mathrm{R}}_j\right]^{\mathrm{T}}\left[\mathrm{M}_{ii}^j\right]\left[\hat{\mathrm{R}}_j\right] \tag{5.22a}$$

$$\left[\hat{K}_{bb}^{j}\right] = \left[K_{bb}^{j}\right] + \left[\hat{R}_{j}\right]^{T} \left[K_{ib}^{j}\right] + \left[K_{ib}^{j}\right]^{T} \left[\hat{R}_{j}\right] + \left[\hat{R}_{j}\right]^{T} \left[K_{ii}^{j}\right] \left[\hat{R}_{j}\right] \tag{5.22b}$$

The condensed eigenvalue problem of the combined structure is

$$\left[\hat{M}\right] \left[\Phi_b\right] \left[\Lambda_b\right] = \left[\hat{K}\right] \left[\Phi_b\right] \tag{5.23}$$

where the mass and stiffness matrices are defined in terms of the substructure matrices as:

$$\left[\hat{M}\right] = \left[\hat{M}_{bb}^{\alpha}\right] + \left[\hat{M}_{bb}^{\beta}\right] \tag{5.24a}$$

$$\left[\hat{K}\right] = \left[\hat{K}_{bb}^{\alpha}\right] + \left[\hat{K}_{bb}^{\beta}\right] \tag{5.24b}$$

The solution of this eigenvalue problem will provide the approximations of the first n_b modes of the combined structures. To improve their accuracy, we will use Eq. (5.18) to update the substructures' condensation matrices $\left[\hat{R}_j\right]$. This recursive equation, here written in terms of the substructure submatrices, is given by

$$\left[\hat{R}_{j}^{(l+1)}\right] = \left[K_{ii}^{j}\right]^{-1} \left[R_{ib}^{j(l)}\right] \left[\Phi_{b}^{(l)}\right] \left[\Phi_{b}^{(l)}\right]^{T} \left[\hat{K}^{(l)}\right] - \left[K_{ii}^{j}\right]^{-1} \left[K_{ib}^{j}\right] \tag{5.25a}$$

where

$$\left[R_{ib}^{j(l)}\right] = \left[M_{ib}^{j} + M_{ii}^{j}\ \hat{R}_{j}^{(l)}\right] \tag{5.25b}$$

and superscript (l) refers to the iteration step. New global matrices $\left[\hat{M}\right]$ and $\left[\hat{K}\right]$ are computed with this improved substructure condensation matrix and eigenvalue problem

(5.23) is solved again. The lowest n_b modes of the combined structure are obtained by repeating the procedure until a desired convergence criterion is satisfied.

The elements of the eigenvectors corresponding to the interior degrees of freedom of each substructure can be obtained from

$$\left[\Phi_i^j \right] = \left[\hat{R}_j \right] [\, \Phi_b \,] \qquad \text{with j} = \alpha, \beta \tag{5.26}$$

Thus, the complete eigenvectors of the combined structure can be stated as

$$[\, \Phi \,] = \begin{bmatrix} \Phi_b \\ \Phi_i^\alpha \\ \Phi_i^\beta \end{bmatrix} = \begin{bmatrix} I \\ \hat{R}_\alpha \\ \hat{R}_\beta \end{bmatrix} [\, \Phi_b \,] \tag{5.27}$$

5.3.1 Numerical Results

The frame structure considered in Chapter 2 will be also used in this section to present numerical results obtained by the condensed substructure superposition approach with iterations. The structure has been divided into two substructure, Figure 2.2. The 3-Dimensional frame is considered as the α substructure and the cross structure as the β substructure. The 24 boundary degrees of freedom has been kept to define the reduced eigenvalue problem.

Natural frequencies obtained for different iterations steps are listed in Table 5.9. Percent errors are also shown in the table in parenthesis. For iteration step '0', which corresponds to Guyan's reduction scheme, percent errors ranged from 0.08 to 196, with only the first 7 frequencies having an error below 5%. It is observed that after the first iteration the maximum percent error has been reduced to 90 and now 10 of the frequencies are acceptable. As the iteration process continues, the results improve considerably and after 5 iterations 20 frequencies had an error below 5%.

In Table 5.10, we show the results for the normalized shear, bending moment and displacements obtained for horizontal input. The accuracy of these results is excellent even at '0' iteration step. What it means is that the modes which primarily contributed to these responses for this input were accurately calculated even in the very first iteration. This is, however, not the case for the response calculated for the vertical input shown in Table 5.11; where some of responses obtained with the Guyan reduction are poor with percent errors up to 40%. After the first iteration these errors are reduced to 5%. More iterations, of course, reduce the errors even further. Table 5.12 shows the results for the case of the inputs applied in both directions. The errors in this case are in between the errors for the previous two cases. The largest error obtained at iteration step '0' is 15% but after the first iteration it is reduced to 2%. In general, the results obtained here with only one iteration are much better than those obtained in Chapter 2 with the condensed substructure superposition approach without iteration, Tables 2.7 and 2.8.

5.4 DYNAMIC CONDENSATION WITH MODAL SYNTHESIS

In this section we specialize the substructuring technique presented in Chapter 4 for nonclassically damped structures for classically damped structures. We again assume that the undamped eigenproperties of the α substructure with free interfaces are $[\,\Lambda_\alpha\,]$ and $[\,\phi^\alpha\,]$, and the undamped eigenproperties of the β substructure with fixed interfaces are $[\,\Lambda_\beta\,]$ and $[\,\phi^\beta\,]$. Modal matrices are assumed normalized with respect to their respective mass matrices.

For classically damped systems, we can ignore the damping matrix while calculating the eigenproperties. That is, we consider the following undamped equation in free vibration as

$$[\mathrm{M}]\ \ddot{\underset{\sim}{x}} + [\mathrm{K}]\ \underset{\sim}{x} = \underset{\sim}{0} \tag{5.28}$$

As in the case of nonclassically damped structures, we express these equations in terms of the eigenproperties of the substructures. For this, we introduced the transformation of coordinates given in Eq. (4.23),

$$\underset{\sim}{x} = [\mathrm{U}]\ \underset{\sim}{z} = \begin{bmatrix} \phi^{\alpha} & 0 \\ 0 & \phi^{\beta} \end{bmatrix} \underset{\sim}{z} \tag{5.29}$$

into Eq. (5.28). After pre-multiply it by $[\mathrm{U}]^{\mathrm{T}}$, the following transformed equations of motion are obtained

$$[\mathrm{M}^{*}]\ \ddot{\underset{\sim}{z}} + [\mathrm{K}^{*}]\ \underset{\sim}{z} = \underset{\sim}{0} \tag{5.30}$$

where the transformed mass and stiffness matrices are given by Eqs. (4.27a) and (4.27c), which are repeated as:

$$[\mathrm{M}^{*}] = \begin{bmatrix} \mathrm{I}_{\alpha} + \phi_b^{\alpha\mathrm{T}} \mathrm{M}_{bb}^{\beta}\ \phi_b^{\alpha} & \phi_b^{\alpha\mathrm{T}}\ \mathrm{M}_{bi}^{\beta}\ \ \phi^{\beta} \\ \phi^{\beta\mathrm{T}} \mathrm{M}_{ib}^{\beta}\ \phi_b^{\alpha} & \mathrm{I}_{\beta} \end{bmatrix} \tag{4.27a}$$

$$[\mathrm{K}^{*}] = \begin{bmatrix} \Lambda_{\alpha} + \phi_b^{\alpha\mathrm{T}} \mathrm{K}_{bb}^{\beta}\ \phi_b^{\alpha} & \phi_b^{\alpha\mathrm{T}}\ \mathrm{K}_{bi}^{\beta}\ \ \phi^{\beta} \\ \phi^{\beta\mathrm{T}} \mathrm{K}_{ib}^{\beta}\ \phi_b^{\alpha} & \Lambda_{\beta} \end{bmatrix} \tag{4.27c}$$

The dynamic condensation presented in section 5.2 can now be applied to reduce the size of the problem. We partition the transformed matrices $[\mathrm{M}^*]$ and $[\mathrm{K}^*]$ according to the kept and reduced degrees of freedom as follows

$$[\mathrm{M}^*] = \begin{bmatrix} \mathrm{M}_{kk} & \mathrm{M}_{kr} \\ \mathrm{M}_{rk} & \mathrm{M}_{rr} \end{bmatrix} \tag{5.31a}$$

$$[\mathrm{K}^*] = \begin{bmatrix} \mathrm{K}_{kk} & \mathrm{K}_{kr} \\ \mathrm{K}_{rk} & \mathrm{K}_{rr} \end{bmatrix} \tag{5.31b}$$

The transformation of Eq. (5.28) expressed in terms of the physical coordinates to Eq. (5.30) expressed in terms of the modal coordinates provides a very convenient way of selecting the kept and reduced degrees of freedom for a very efficient convergence, as will be shown by the numerical example. The iteration process either with lower modes or with higher modes can be carried out to obtain the eigenproperties of the transformed structural system. The full eigenvectors of the original system can be obtained in terms of the eigenvectors of the reduced system as follows:

$$[\Phi] = [\mathrm{U}]\ [\Phi^*] \tag{5.32}$$

5.4.1 Numerical Results

Once again we will use the frame structure shown in Figure 2.1 as our numerical example. Only the results obtained by iterating with lower modes are presented. To demonstrate the effect of the choice of the kept coordinates on the efficiency of the approach, here two different ways of selecting these coordinates have been considered. In the first case, coordinates are selected according to the transformed stiffness to mass ratios. The n_k coordinates with the lowest ratios are chosen as the kept degrees of freedom to define the eigenvalue problem associated with the lower modes. In the second case, the coordinates are selected according to the magnitudes of the eigenvalues of the uncoupled substructures, $[\Lambda_\alpha]$ and $[\Lambda_\beta]$. In this case, the transformed mass and stiffness matrices are reordered according to the magnitude of the eigenvalues, so that the smallest eigenvalue is located at the first position and the largest at the last in Eq. (4.27c). Coordinates located in the first n_k positions are chosen as the kept coordinates. Lowest natural frequencies of α and β substructures with the boundary degrees of freedom free and fixed, respectively, are given in Table 5.13. In both cases, eight coordinates were kept.

Table 5.14 shows the natural frequencies obtained for the first case. Percent errors are also shown in parenthesis in the table, but only when the approximated frequency corresponds to one of the exact modes. It is of interest to observe that at iteration step '0', corresponding to the Guyan reduction, four of the first eight frequencies are completely missing. These missed frequencies are the first, second, seventh and eighth frequencies. However, good approximations were obtained for the rest of the frequencies, including the twelfth and fifteenth frequencies. After the first iteration, poor approximations of the first and second frequencies were obtained and the percent errors of the rest of the frequencies were reduced to less than 1. All frequencies are acceptable after five iteration with six of them being exact. However, the seventh and eighth were still missing after the fifth iteration. Thus, in general, this choice of the kept coordinates is not acceptable.

Next we show the normalized root mean square responses obtained for the first case in Tables 5.15 to 5.17. Since we obtained poor approximations of the first two modes at all iteration steps, the accuracy of the responses which seem to have significant contribution from these modes for the horizontal input are also poorly calculated. On the other hand, all response quantities computed for the vertical input, Table 5.16, have errors below 5% with one iteration and are improved as the iteration process is repeated. Table 5.17 shows the results obtained for the combined input. Similar to the observations we made earlier when discussed the results in Tables 5.10 to 5.12, accuracy of these results is between the accuracy of the results in the two previous tables.

The results obtained for the second choice of coordinates are presented now. Since the first eight frequencies of the α substructures were the lowest, all eight kept coordinates belonged to the α substructure in this case. Natural frequencies calculated at different iteration steps are listed in Table 5.18. Even for the Guyan reduction, i.e., iteration step '0', most of the frequencies are almost exact, except that the fourth frequency has an error of 12% and the seventh mode is completely missing. With one iteration the error of the fourth frequency is reduced to less than 1%. After five iterations, seven of the frequencies are exact, however, the seventh mode is still missing. This frequency can be obtained eventually if we continue the iteration process for several steps more. Responses are almost exact for all iteration steps for horizontal input, Tables 5.19. Whereas for the vertical input, Table 5.20, the percent error ranged from 1 to 25 for Guyan reduction and is reduced to less than 2 after three iterations when a better approximation of the fourth mode is obtained. The missing frequency does not seem to be contributing to the response in these cases. Table 5.21 shows the results obtained for the combined input. Comparing the results obtained for the two sets of coordinates used here, we can see that the second choice provides better convergence than the first one.

5.5 SUMMARY AND CONCLUSIONS

In this chapter, the dynamic condensation method for nonclassically damped structures developed earlier is specialized to make it applicable to classically damped structures. It is found that the expressions obtained in previous chapters can be directly used for classically damped systems if we properly replace the matrices. This replacement is indicated by Eqs. (5.7a) and (5.7b).

Several sets of numerical results are presented to show the effectiveness of the condensation methods. Two set of degrees of freedom were considered with the general dynamic condensation method. In both cases, the eigenproperties and responses obtained with the Guyan's reduction method or the static condensation approach, are not accurate in all cases. Results are significantly improved by applying the proposed iterative approach. It is shown that the results are significantly improved in the condensed substructure superposition approach even by performing a single iteration. In general, it is better to increase the number of iteration than to increase the size of the condensed problem in order to improve the accuracy of the calculated response. It is also shown that the choice of the kept coordinate in dynamic condensation process is greatly facilitated by transformation of the physical coordinates to modal coordinates. That is, the modal synthesis and dynamic condensation methods can be combined to improve the efficiency and accuracy of a structural eigenvalue analysis.

Table 5.1 Frequencies (in rad/sec) of the frame in Figure 2.1 calculated with the dynamic condensation approach. Degrees of freedom selected according to the stiffness to mass ratio.

Mode	Iteration Step			
	0	1	3	5
1	13.99	12.39	12.39	12.39
	(12.88)	(0.00)		
2	13.99	12.39	12.39	12.39
	(12.88)	(0.00)		
3	18.88	17.71	17.71	17.71
	(12.28)	(0.01)	(0.00)	
4	76.71	46.21	44.85	44.64
	(72.23)	(3.75)	(0.70)	(0.22)
5	81.47	63.37	61.63	61.49
	(32.56)	(3.10)	(0.29)	(0.05)
6	89.75	75.33	72.61	72.19
	(24.55)	(4.53)	(0.77)	(0.18)
7	94.06	76.57	76.61	72.19
	(30.52)	(6.26)	(0.77)	(0.18)
8	94.06	76.57	72.97	72.78
	(29.29)	(6.26)	(0.32)	(0.05)

Table 5.2 Normalized root mean square responses for the frame of Figure 2.1 under horizontal ground excitations. Eigenproperties obtained with the dynamic condensation approach. Degrees of freedom selected according to the stiffness to mass ratios.

Node	Iteration Step			
	0	1	3	5
Shear Forces				
9	0.5010	0.9960	0.9996	1.0000
11	1.8070	1.0141	1.0008	1.0000
14	0.5010	0.9946	0.9997	1.0000
18	0.4900	0.9916	0.9999	1.0000
Bending Moments				
11	0.4900	0.9964	0.9997	1.0000
14	0.5259	1.0070	0.9996	1.0000
16	0.4967	0.9944	0.9998	1.0000
18	0.4971	0.09921	0.9998	1.0000
Horizontal Displacements				
7	1.0700	1.0039	1.0002	1.0000
11	0.8318	1.0003	1.0000	1.0000
21	0.8072	0.9994	1.0000	1.0000

Table 5.3 Normalized root mean square responses for the frame of Figure 2.1 under vertical ground excitations. Eigenproperties obtained with the dynamic condensation approach. Degrees of freedom selected according to the stiffness to mass ratios.

Node	Iteration Step			
	0	1	3	5
Shear Forces				
9	0.0000	0.7650	0.9099	0.9538
11	0.7744	1.6660	1.3620	1.1142
14	0.0000	0.7430	0.9068	0.9553
18	0.0000	0.6340	0.8910	0.9449
Bending Moments				
11	0.1371	0.6990	0.8307	0.9199
14	0.0584	0.8250	0.9423	0.9724
16	0.1578	0.3780	0.7900	0.8880
18	0.0616	0.7780	0.9367	0.9700
Vertical Displacements				
7	0.000	0.7674	0.9101	0.9539
14	0.1036	0.8890	0.9698	0.9881
21	0.0787	0.8231	0.9502	0.9774

Table 5.4 Normalized root mean square responses for the frame of Figure 2.1 under combines horizontal and vertical ground excitations. Eigenproperties obtained with the dynamic condensation approach. Degrees of freedom selected according to the stiffness to mass ratios.

Node	Iteration Step			
	0	1	3	5
Shear Forces				
9	0.3560	0.8890	0.9562	0.9773
11	1.7910	1.0330	1.0101	1.0052
14	0.4540	0.9541	0.9836	0.9915
18	0.3720	0.8596	0.9555	0.9772
Bending Moments				
11	0.4836	0.9880	0.9954	0.9976
14	0.0793	0.8271	0.9429	0.9727
16	0.4820	0.9664	0.9876	0.9931
18	0.3409	0.8834	0.9664	0.9840

Table 5.5 Frequencies (in rad/sec) of the frame in Figure 2.1 calculated with the dynamic condensation approach. Degrees of freedom selected arbitrarily.

Mode	Iteration Step			
	0	1	3	5
1	12.47 (0.62)	12.39 (0.00)	12.39	12.39
2	12.47 (0.62)	12.39 (0.00)	12.39	12.39
3	17.75 (0.23)	17.71 (0.00)	17.71	17.71
4	------	------	45.63 (2.45)	45.41 (1.94)
5	63.65 (3.56)	61.59 (0.21)	61.46 (0.00)	61.46
6	------	------	------	74.15 (2.90)
7	------	------	------	74.15 (2.90)
8	------	78.33 (7.67)	75.67 (4.02)	74.46 (2.36)
9	496.98	107.07	78.37	------
10	496.98	108.54	78.37	------
11	512.32	108.54	------	------
12	545.88	------	------	------

Table 5.6 Normalized root mean square responses for the frame of Figure 2.1 under horizontal ground excitations. Eigenproperties obtained with the dynamic condensation approach. Degrees of freedom selected arbitrarily.

Node	Iteration Step			
	0	1	3	5
Shear Forces				
9	1.0440	0.9992	1.0001	1.0000
11	0.9415	0.9998	1.0000	1.0000
14	1.0427	1.0002	1.0000	1.0000
18	1.0408	1.0000	1.0000	1.0000
Bending Moments				
11	1.0210	1.0002	1.0000	1.0000
14	1.0720	1.0012	1.0003	1.0000
16	1.0440	1.0000	1.0000	1.0000
18	1.0381	1.0007	1.0000	1.0000
Horizontal Displacements				
7	0.9852	1.0000	1.0000	1.0000
11	1.0034	1.0001	1.0000	1.0000
21	0.9739	0.9998	1.0000	1.0000

Table 5.7 Normalized root mean square responses for the frame of Figure 2.1 under vertical ground excitations. Eigenproperties obtained with the dynamic condensation approach. Degrees of freedom selected arbitrarily.

Node	Iteration Step			
	0	1	3	5
Shear Forces				
9	0.0000	0.3350	0.9489	0.9513
11	0.0000	0.3250	0.9047	0.9273
14	0.0000	0.3250	0.9557	0.9605
18	0.0000	0.2770	0.9527	0.9561
Bending Moments				
11	0.0000	0.3430	0.9465	0.9688
14	0.0000	0.2249	0.9445	0.9523
16	0.0000	0.5316	0.9512	1.0328
18	0.0000	0.1971	0.9529	0.9604
Vertical Displacements				
7	0.0000	0.3354	0.9486	0.9513
14	0.0000	0.1481	0.9356	0.9529
21	0.0000	0.1770	0.9503	0.9529

Table 5.8 Normalized root mean square responses for the frame of Figure 2.1 under combined horizontal and vertical ground excitations. Eigenproperties obtained with the dynamic condensation approach. Degrees of freedom selected arbitrarily.

Node	Iteration Step			
	0	1	3	5
Shear Forces				
9	0.7420	0.7480	0.9751	0.9762
11	0.9311	0.9912	0.9954	0.9984
14	0.9436	0.9156	0.9914	0.9921
18	0.7910	0.7820	0.9805	0.9963
Bending Moments				
11	1.0067	0.9879	0.9986	0.9991
14	0.1097	0.2461	0.9451	0.9529
16	1.0096	0.9764	0.9969	1.0022
18	0.7057	0.6954	0.9750	0.9789

Table 5.9 Frequencies (in rad/sec) of the frame in Figure 2.1 calculated with the condensed substructure superposition approach with iterations.

Mode	Iteration Step			
	0	1	3	5
1	12.41	12.39	12.39	12.39
	(0.08)	(0.00)		
2	12.41	12.39	12.39	12.39
	(0.08)	(0.00)		
3	17.75	17.71	17.71	17.71
	(0.25)	(0.00)		
4	46.49	44.54	44.54	44.54
	(4.38)	(0.01)	(0.00)	
5	63.81	61.50	61.47	61.47
	(3.82)	(0.07)	(0.01)	(0.00)
6	75.03	72.36	72.08	72.07
	(4.12)	(0.42)	(0.03)	(0.02)
7	75.03	72.36	72.08	72.07
	(4.12)	(0.42)	(0.03)	(0.02)
8	76.96	72.98	72.80	72.77
	(5.79)	(0.31)	(0.07)	(0.00)
9	104.69	96.73	95.75	95.61
	(9.65)	(1.30)	(0.28)	(0.14)
10	104.69	96.73	95.75	95.61
	(9.65)	(1.30)	(0.28)	(0.14)
11	151.24	119.94	111.03	109.92
	(40.13)	(11.13)	(2.88)	(1.84)
12	241.71	129.65	121.03	119.72
	(104.2)	(9.52)	(2.24)	(1.13)

Table 5.9 Frequencies (in rad/sec) of the frame in Figure 2.1 calculated with the condensed substructure superposition approach with iterations.. Cont.

Mode	Iteration Step			
	0	1	3	5
13	241.71	136.48	124.57	123.11
	(99.81)	(12.82)	(2.98)	(1.41)
14	285.78	138.35	128.98	126.07
	(135.4)	(13.97)	(6.25)	(4.22)
15	285.78	138.35	128.98	126.07
	(135.4)	(13.97)	(6.25)	(4.22)
16	299.78	156.94	131.84	128.69
	(137.5)	(24.34)	(4.46)	(1.22)
17	370.99	233.27	131.84	128.69
	(191.8)	(83.48)	(3.70)	(1.22)
18	376.34	241.96	132.04	129.46
	(196.0)	(90.31)	(3.86)	(2.57)
19	376.34	241.96	142.03	137.94
	(182.9)	(81.91)	(6.78)	(3.71)
20	379.26	292.48	231.62	231.50
	(56.84)	(20.96)	(0.07)	(0.02)
21	379.26	292.48	279.41	275.75
	(56.84)	(20.96)	(15.55)	(14.01)
22	504.38	365.26	279.41	275.75
	(108.6)	(51.06)	(15.55)	(14.01)
23	520.58	402.37	313.36	291.67
	(98.53)	(53.45)	(19.51)	(11.24)
24	578.73	517.46	314.38	303.31
	(107.8)	(85.78)	(12.87)	(8.90)

Table 5.10 Normalized root mean square responses for the frame of Figure 2.1 under horizontal ground excitations. Eigenproperties obtained with the condensed substructure superposition approach with iterations.

Node	Iteration Step			
	0	1	3	5
Shear Forces				
9	0.031	0.0017	1.0002	1.0001
11	0.9394	0.9997	0.9999	1.0000
14	1.0561	1.0003	1.0002	1.0001
18	0.9986	1.0000	1.0000	1.0000
Bending Moments				
11	1.0198	1.0002	1.0000	1.0000
14	1.5164	1.0063	1.0041	1.0028
16	1.0521	1.0001	1.0000	1.0000
18	0.9985	0.9984	0.9999	1.0000
Horizontal Displacements				
7	0.9817	1.0000	1.0000	1.0000
11	0.9989	1.0000	1.0000	1.0000
21	0.9992	1.0000	1.0000	1.0000

Table 5.11 Normalized root mean square responses for the frame of Figure 2.1 under vertical ground excitations. Eigenproperties obtained with the condensed substructure superposition approach with iterations.

Node	Iteration Step			
	0	1	3	5
Shear Forces				
9	0.9621	1.0390	1.0380	1.0380
11	0.7177	0.9776	0.9833	0.9842
14	1.1262	1.0229	1.0226	1.0207
18	0.5831	0.9555	0.9671	0.9678
Bending Moments				
11	1.0562	1.0187	1.0181	1.0174
14	1.0626	1.0168	1.0159	1.0154
16	1.0389	0.9801	0.9836	0.9838
18	0.7545	0.9872	0.9892	0.9898
Vertical Displacements				
7	0.9710	1.0373	1.0333	1.0247
14	1.0086	1.0126	1.0119	1.0116
21	0.8408	0.9951	0.9944	0.9944

Table 5.12 Normalized root mean square responses for the frame of Figure 2.1 under combined horizontal and vertical ground excitations. Eigenproperties obtained with the condensed substructure superposition approach with iterations.

Node	Iteration Step			
	0	1	3	5
Shear Forces				
9	1.0091	1.0162	1.0150	1.0147
11	0.9349	0.9993	0.9999	1.0000
14	1.0690	1.0042	1.0041	1.0033
18	0.8485	0.9813	0.9861	0.9868
Bending Moments				
11	1.0209	1.0007	1.0006	1.0006
14	1.0685	1.0170	1.0160	1.0155
16	1.0512	0.9989	0.9978	0.9988
18	0.8758	0.9937	0.9950	0.9955

Table 5.13 First ten natural frequencies in rad/sec of the α substructure with free interface coordinates, and the β substructure with fixed interface coordinates.

Mode	α Substructure	β Substructure
1	3.78	11.3
2	3.78	18.6
3	4.29	18.6
4	5.61	18.8
5	7.74	21.8
6	8.39	21.8
7	8.45	22.8
8	8.80	22.8
9	8.80	25.0
10	9.91	25.0

Table 5.14 Frequencies (in rad/sec) of the frame in Figure 2.1 calculated with the dynamic condensation with modal synthesis. Degrees of freedom selected according to the transformed stiffness to mass ratio.

Mode	Iteration Step			
	0	1	3	5
1	------	15.27	13.24	12.91
		(23.21)	(6.78)	(4.16)
2	------	15.27	13.24	12.91
		(23.21)	(6.78)	(4.16)
3	17.71	17.71	17.71	17.71
	(0.01)	(0.00)		
4	17.71	17.71	17.71	17.71
	(0.01)	(0.00)		
5	61.48	61.46	61.46	61.46
	(0.03)	(0.00)		
6	72.95	72.75	72.06	72.06
	(1.24)	(0.97)	(0.01)	(0.00)
7	------	------	------	------
8	------	------	------	------
12	118.48	118.39	118.38	118.38
	(0.08)	(0.01)	(0.00)	
---	119.71	------	------	------
---	119.71	------	------	------
15	121.47	121.40	121.40	121.40
	(0.06)	(0.01)	(0.00)	

Table 5.15 Normalized root mean square responses for the frame of Figure 2.1 under horizontal ground excitations. Eigenproperties obtained with the dynamic condensation with modal synthesis. Degrees of freedom selected according to the transformed stiffness to mass ratio.

Node	Iteration Step			
	0	1	3	5
Shear Forces				
9	4.8176	4.3168	2.5332	2.1516
11	1.3244	1.6562	1.1888	1.1168
14	1.5268	1.7480	1.2342	1.1518
18	3.0626	0.4888	0.6190	0.6789
Bending Moments				
11	1.3305	1.6313	1.1759	1.1069
14	4.8413	3.3802	2.0472	1.7772
16	0.8033	1.1333	0.9256	0.9142
18	0.4390	1.4491	1.0930	1.0434
Horizontal Displacements				
7	1.3358	1.6525	1.1867	1.1153
11	1.3427	1.6542	1.1876	1.1159
21	1.3410	1.6537	1.1873	1.1157

Table 5.16 Normalized root mean square responses for the frame of Figure 2.1 under vertical ground excitations. Eigenproperties obtained with the dynamic condensation with modal synthesis. Degrees of freedom selected according to the transformed stiffness to mass ratio.

Node	Iteration Step			
	0	1	3	5
Shear Forces				
9	1.9897	1.0114	1.0007	1.0000
11	0.9497	1.0004	1.0000	1.0000
14	1.0119	1.0157	1.0009	1.0000
18	1.1415	1.0434	1.0023	1.0001
Bending Moments				
11	1.0348	1.0206	1.0028	1.0001
14	1.0092	1.0149	1.0011	1.0000
16	1.1975	1.0538	1.0023	1.0001
18	1.0710	1.0274	1.0015	1.0001
Vertical Displacements				
7	0.9904	1.0115	1.0007	1.0000
14	1.0064	1.0141	1.0008	1.0000
21	1.0448	1.0221	1.0012	1.0001

Table 5.17 Normalized root mean square responses for the frame of Figure 2.1 under combined horizontal and vertical ground excitations. Eigenproperties obtained with the dynamic condensation with modal synthesis. Degrees of freedom selected according to the transformed stiffness to mass ratio.

Node	Iteration Step			
	0	1	3	5
Shear Forces				
9	3.4935	3.1490	1.9329	1.6830
11	1.3172	1.6445	1.1849	1.1144
14	1.4472	1.6398	1.1953	1.1258
18	2.4439	0.7729	1.8033	0.8297
Bending Moments				
11	1.3232	1.6175	1.1714	1.1041
14	1.1198	1.0673	1.0174	1.0113
16	0.8345	1.1283	0.9308	0.9200
18	0.8402	1.2402	1.0448	1.0203

Table 5.18 Frequencies (in rad/sec) of the frame in Figure 2.1 calculated with the dynamic condensation with modal synthesis. Degrees of freedom selected according to the magnitudes of the uncoupled frequencies of the substructures.

Mode	Iteration Step			
	0	1	3	5
1	12.40	12.39	12.39	12.39
	(0.04)	(0.00)		
2	12.40	12.39	12.39	12.39
	(0.04)	(0.00)		
3	17.71	17.71	17.71	17.71
	(0.01)	(0.00)		
4	49.94	44.70	44.54	44.54
	(12.12)	(0.37)	(0.00)	
5	61.52	61.46	61.46	61.46
	(0.10)	(0.00)		
6	72.84	72.13	72.06	72.06
	(1.08)	(0.09)	(0.00)	
7	-------	-------	-------	-------
8	72.95	72.76	72.75	72.75
	(0.13)	(0.02)	(0.01)	(0.00)
--	346.80	273.26	137.88	134.10

Table 5.19 Percent errors in modal frequencies and damping ratios of the truss in Figure 3.9 calculated with the condensed substructure superposition approach with iterations.

Node	Iteration Step			
	0	1	3	5
Shear Forces				
9	1.0024	1.0000	1.0000	1.0000
11	1.0034	1.0000	1.0000	1.0000
14	1.0027	1.0003	1.0000	1.0000
18	1.0027	1.0000	1.0000	1.0000
Bending Moments				
11	1.0026	1.0001	1.0000	1.0000
14	1.0046	1.0014	1.0008	1.0000
16	1.0024	1.0001	1.0000	1.0000
18	1.0025	1.0001	1.0000	1.0000
Horizontal Displacements				
7	1.0030	1.0002	1.0000	1.0000
11	1.0027	1.0000	1.0000	1.0000
21	1.0026	1.0005	1.0000	1.0000

Table 5.20 Normalized root mean square responses for the frame of Figure 2.1 under vertical ground excitations. Eigenproperties obtained with the dynamic condensation with modal synthesis. Degrees of freedom selected according to the magnitudes of the uncoupled frequencies of the substructures.

Node	Iteration Step			
	0	1	3	5
Shear Forces				
9	1.1259	1.0780	1.0101	1.0051
11	1.2992	1.1287	1.0156	1.0019
14	1.0857	1.0628	1.0083	1.0013
18	0.8759	1.0021	1.0011	1.0000
Bending Moments				
11	1.0368	1.0490	1.0065	1.0006
14	1.1007	1.0677	1.0087	1.0012
16	0.7506	0.9539	0.9947	0.9993
18	0.9986	1.0339	1.0045	1.0007
Vertical Displacements				
7	1.1333	1.0833	1.0167	1.0067
14	1.2151	1.0723	1.0094	1.0014
21	1.0454	1.0500	1.0063	1.0007

Table 5.21 Normalized root mean square responses for the frame of Figure 2.1 under combined horizontal and vertical ground excitations. Eigenproperties obtained with the dynamic condensation with modal synthesis. Degrees of freedom selected according to the magnitudes of the uncoupled frequencies of the substructures.

Node	Iteration Step			
	0	1	3	5
Shear Forces				
9	1.0654	1.0394	1.0052	1.0007
11	1.0109	1.0030	1.0003	1.0000
14	1.0181	1.0118	1.0015	1.0004
18	0.9514	1.0007	1.0000	1.0000
Bending Moments				
11	1.0178	1.0157	1.0144	1.0142
14	1.0997	1.0671	1.0086	1.0012
16	0.9881	0.9971	0.9996	0.9999
18	1.0004	1.0184	1.0024	1.0003

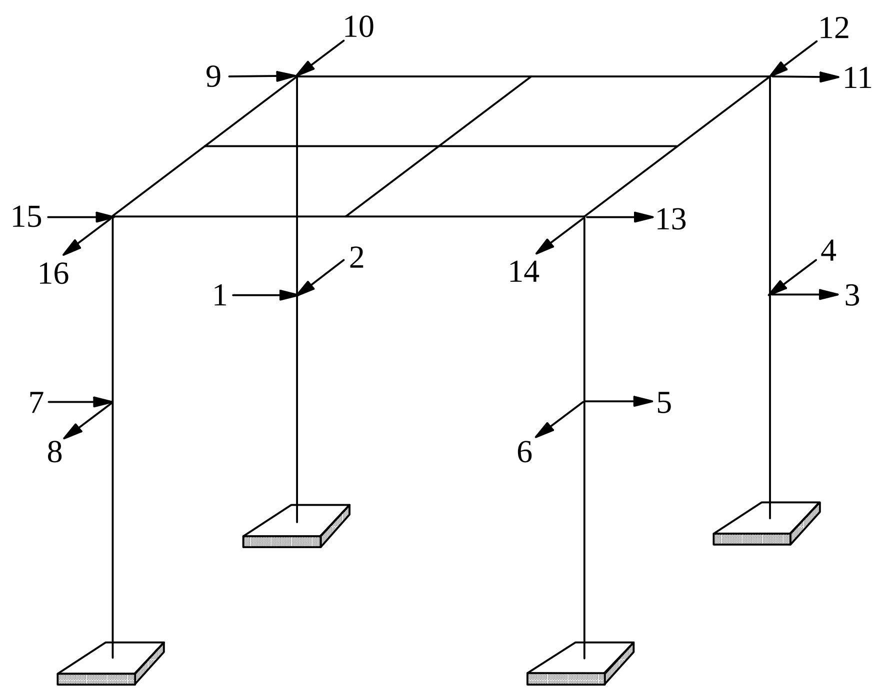

Figure 5.1 Kept degrees of freedom for frame example problem.

CHAPTER VI

SEISMIC RESPONSE OF FLEXIBLE FLOOR STRUCTURES

6.1 INTRODUCTION

In this chapter we present various numerical results obtained for a structure with flexible floors. First, we demonstrate the applicability of the dynamic condensation approach developed in the previous chapter to this type of structures. Then, the influence of the out-of-plane flexibility of the floor slabs on the response of primary and secondary systems subjected to vertical ground motions is investigated. The accuracy achieved by using the currently employed approximate procedures to analyze the problem of flexible floor slab structures is examined in the final sections of the chapter.

The structural properties for the three-story building selected for this study were obtained from Reference 37. The plan dimensions of the floor slabs are 24 x 24 ft. They are supported along its four edges by monolithic concrete beam-column frames. The columns are 18 x 18 in. and the beams are 22 in. deep and 12 in. wide. The slab thickness is 7 in. The first story height is 16 ft, and the remaining two stories are 12 ft each. The properties of the structure are: modulus of elasticity = 3200 ksi, Poisson ratio = 0.15, and mass density = 0.00267 slugs/in^3. A plan and elevation of the building is shown in Figure 6.1.

In the analytical model of the structure we consider the floors to be rigid in their own plane but flexible in the transverse direction. As a consequence, each in-plane rigid floor slab has three common degrees of freedom, two horizontal displacements and a rotation about the vertical axis. The floor slabs were modeled by rectangular finite element thin plates with three degrees of freedom per node: a vertical displacement and two rotations about the horizontal axes. The supporting frame was modeled by beam finite elements and columns with axial and bending deformations.

Since the structure is symmetric with respect to two centroidal axes and it is only subjected to vertical ground motions, the finite element model will consist of only one quarter of each floor and the degrees of freedom associated with the rigid floor assumptions will not be included. Each floor was modeled by 25 plate elements with 96 degrees of freedom per floor as shown in Figure 6.2, which add to a total of 288 degrees of freedom for the three floors. The first 15 natural frequencies and vertical participation factors obtained from the solution of the full eigenvalue problem are listed in Table 6.1. These values will be considered as the exact values for comparison purposes.

6.2 EVALUATION OF CONDENSATION PROCEDURES WITH FLEXIBLE FLOOR STRUCTURES

The three-story building shown in Figure 6.1 was assumed to be classically damped with a modal damping ratio of 5% for all modes. The approximate eigenproperties were obtained by solving iteratively the eigenvalue problem of Eq. (5.8) with the condensed mass and stiffness matrices defined according to Eqs. (5.9). Nine vertical displacements coordinates, three per floor, were arbitrarily selected to define the reduced eigenvalue problem. They correspond to nodes 6, 7 and 8 of each floor indicated

Figure 6.2. This represents a reduction of about 97 % of the total number of degrees of freedom.

The natural frequencies calculated at different iteration steps are listed in Table 6.2. Once again, the errors in percent are given in the table immediately below the frequencies and a dash indicates that the error is less than 0.005%. At the iteration step '0', corresponding to the Guyan reduction method, good results were obtained for the frequencies, with errors ranging from 2.5% for the fourth mode to 6.15 % for the seventh mode. After one iteration, the error has been reduced for all frequencies to less than 0.1%, and the exact values were obtained in the next iteration.

The root mean square values for the displacements, accelerations, and bending moments at nodes 1, 6 and 7 in Figure 6.2, and the shear forces at node 1 and the axial forces in the columns were computed using as input a vertical ground motion defined by the Kanai-Tajimi spectral density function. The responses computed with the exact eigenproperties are listed in Tables 6.3.

The normalized root mean square response values for the displacements are presented in Table 6.4. The results for nodes 6 and 7 are good with errors less than 5% for iteration step '0', and become almost exact in the next iteration. However, for node 1, the errors obtained with the Guyan reduction were at least 25%, which went down to 8% after one iteration and improved as the iteration process was repeated. In the case of the accelerations shown in Table 6.5, the results are good from the beginning with errors ranging from 1 to 6%, where the largest errors correspond to node 1. After five iterations, the errors have been reduced by half. Nevertheless, it is noted that when computing shear forces and bending moments for the slabs and axial forces for the columns, the results for the Guyan reduction are very inaccurate. For the shear forces shown in Table 6.7, the results have at least a 33% error, and the axial forces provided in

Table 6.8 have at least a 20 % error. In the case of the bending moments listed in Table 6.6, the errors are even higher with at least a 10% for node 1, 40% for node 7, and 150 % for node 6. However, a substantial improvement in the accuracy of the responses after the first iteration is observed, with the errors reduced to less than 5%. After five iterations, all the responses are almost exact.

Figures 6.3 to 6.8 show the effect of the dynamic condensation approach in the computation of acceleration floor response spectra for an oscillator located at node 4 and at node 6 of any floor. The damping ratio of the oscillator is 1 % and the interaction effects between the building and the oscillator have been ignored. It is clear from the figures that the peaks for the floor spectra using the Guyan reduction will occur at different frequencies, although close, with respect to those computed using exact eigenproperties. Of course, this was expected since the frequencies obtained from the Guyan reduction are different but close to the exact ones. However, the maximum accelerations for the oscillator at node 4 shown in Figures 6.3 to 6.5, are smaller than the exact values with an error of at least 15%. For the oscillator at node 6, the maximum accelerations shown in Figures 6.6 to 6.8, are greater than the exact values but the errors are less than 5%. The other peaks of the spectrum are also shifted or were not computed with the Guyan reduction. On the other hand, the floor spectrum obtained after the first iteration follows very closely the exact spectrum in all cases. The only difference between the exact and condensed spectra is observed in the regions with frequencies smaller than the building's frequencies or at the higher frequencies where no peaks exist.

6.3 THE EFFECT OF FLOOR FLEXIBILITY ON THE DYNAMIC RESPONSE

In the current practice, the lumped mass model is commonly used to compute the seismic responses. The assumption that the floors are rigid is implicit in this model and thus, for a given floor elevation, the response will be the same at all regions of the floor. In general, the rigid behavior assumption is adequate to describe the in-plane response of the floor. For seismic excitations with vertical components, however, the flexibility of the floor slabs in the out-of-plane direction may play a significant role and it can result in an increase in the responses near the center of the floor. Therefore, ignoring the floor flexibility in such cases may result in an underestimation of the seismic response of the structure and secondary systems. The influence of the floor flexibility on the seismic response is investigated in this section.

To illustrate the importance of the floor flexibility, we analyzed the structure shown in Figure 6.1 considering flexible slabs and compared it with the results obtained from the lumped mass model, Figure 6.9. The maximum displacement and maximum acceleration for each floor, which occur at the center of the slab, and the axial force for each column have been computed for both models. The root mean square responses for the flexible slabs model are listed in Table 6.9. The natural frequencies of the lumped mass model are listed in Table 6.10 and the normalized responses for this case are presented in Figure 6.10. These results have been normalized with respect to the corresponding maximum values shown in Table 6.9 obtained from the flexible slab analysis. It is observed that when the slabs are considered flexible, the displacements are 20 times the values computed using the lumped mass model, the accelerations are 3 times and the axial forces at least 1.2 times larger.

The influence of the floor flexibility in the calculation of acceleration floor response spectra is presented next. Once again, all the floor spectra have been developed for oscillator damping ratio of 1 % and the interaction effects between the building and the oscillator has been ignored. Figures 6.11 to 6.13 show the floor spectra when the oscillator is located in the first, second and third floor, respectively. In each figure we present the floor spectra when the floors are considered flexible and the oscillator is located at different nodes of a given floor. It is interesting to observed that the floor spectra computed with the oscillator at different locations on the same floor have similar shapes but different peak amplitudes. It is also found that the oscillator has a maximum acceleration when it is located at the center of the floor, that is in node 6. In addition, each figure includes the floor spectra when the floors are considered rigid. In all three cases, the spectra for rigid floor model are quite different from those obtained with flexible floor model. They not only have less number of peaks and at different frequencies compared to those obtained when the floors are considered flexible, but also the acceleration of the oscillator is significantly underestimated.

As another example, we analyzed the same building of Figure 6.1 with the floors changed by 16 ft square slabs. As it can be seen in Table 6.11, the structure has now higher natural frequencies. The floors are now more rigid in the out-of-plane direction as a consequence. The responses when the floors are considered flexible are presented in Table 6.12. The normalized responses for the lumped mass model are shown in Figure 6.14 and its frequencies are listed in Table 6.13. In this example the difference between both models has been reduced compared to those shown in Figure 6.10. The axial forces are almost the same, the accelerations are no more than 1.6 times the values computed using the lumped mass model, and the displacements are about 6 times larger. If we reduce even more the plan dimensions of the floors or make them more rigid in some other way, we should expect the responses calculated with both models to be in closer agreement, with the lumped mass model always underestimating the responses.

In the case of the acceleration floor response spectra shown in Figures 6.15 to 6.17, the difference in the results are considerable. The peaks have been shifted to the higher frequencies but, once again they occur at frequencies different than those obtained when the floors are considered flexible. Moreover, the accelerations are smaller. It is noted, however, that for the flexible floor model, the first two peaks are closer to each other. The peak in the lumped mass model does not coincide with any of the peaks in the flexible floor model. If we reduce even more the floors lateral dimensions or make them more rigid, we can expect the first two peaks in the flexible floor spectra approach each other, and also approach the peak in the lumped mass model. The shape of the floor spectra in the flexible and rigid floor models will be different and the maximum acceleration of the oscillator with the lumped mass model will be smaller.

These results clearly indicate the importance of including the out-of-plane flexibility of the floors when computing seismic responses of structures subjected to vertical ground excitations. In general, the rigid floor model underestimates the responses and the corresponding acceleration floor response spectra show different peaks with smaller amplitudes. The flexibility of the floors should therefore be appropriately taken into account in the seismic design of secondary systems.

6.4 EVALUATION OF CURRENTLY USED APPROXIMATE METHODS

As mentioned in Chapter I, there are several approximate methods being utilized in practice to include the floor flexibility in the analytical model of a structure. In this section we will evaluate the accuracy of the results predicted by two popular methods used to consider the floor flexibility effects: the cascade approach and the modified lumped mass method. The structure shown in Figure 6.1 has been analyzed once again, now using these two approaches. The root mean square responses for the finite element model of the structure with flexible slabs are listed in Table 6.14. The maximum bending moments and shear forces for the slabs are also included in this table.

6.4.1 The Cascade Approach

In the cascade approach, the floor slabs are first assumed to be completely rigid. A vertical seismic analysis of a lumped mass model of the structure is performed and the acceleration at a desired floor elevation is obtained. This acceleration is then used as the vertical excitation for a detailed finite element model of the flexible floor. In this way the floor flexibility is included in the analytical model but the dynamic interaction effects between the different floors are ignored. A summary of the equations used to compute the seismic responses with the cascade approach is presented in Appendix A.

Each floor has been modeled as a thin plate with beams along its four edges and point supported at the corners. The stiffness of the columns has been included by means of rotational springs. Due to the symmetry of the structure, only one quarter of the floor was modeled using 25 plate elements. The lower 10 natural frequencies and their respective vertical modal participation factors for each floor are listed in Tables 6.15 to 6.17. We observe that the natural frequencies of the different floors have slight differences because of small variations in the support column stiffness. Some of these frequencies are close to the frequencies of the combined structure. In fact, the fundamental frequency of each floor was quite close to one of the first three frequencies of the whole structure calculated with flexible floors slabs and supporting frame.

Figure 6.18 shows the responses obtained with the cascade approach. These results have been normalized with respect to the corresponding values obtained for the coupled frame and flexible slab model. Since all the normalized responses are greater than 1.0, the cascade approach overestimate all the responses. In the case of the displacements and shear forces, a difference of about 10 to 15% is observed. However, the maximum difference goes up to 25% and 60% for the bending moments and the accelerations, respectively. It is also noted that the difference in the results for the third floor are greater than those of the other two floors.

The acceleration floor response spectra computed for all three floors by the cascade approach and by the flexible floor analysis are presented in Figures 6.19 to 6.21. The oscillator has been placed at the center of the slab and it has a 1% damping ratio. It is noted that, for a given floor, both spectra have peaks at almost the same frequencies. However, the amplitude of these peaks are greater for the cascade approach. It is also noted that the difference in the spectra of the third floor are greater than those of the other two floors. The cascade approach again overestimates the responses.

6.4.2 The Modified Lumped Mass Method

In the modified lumped mass method, the mass of each floor is divided into two parts, one representing the center region of the floor and the other the remaining part of the floor. The center region of each floor is modeled by an equivalent single degree of freedom oscillator. Its equivalent mass and stiffness are calculated from the eigenproperties of the dominant mode of the flexible slab model. This single degree of freedom oscillator is then combined with the conventional lumped mass model. In this way, the floor flexibility and the interaction effects are approximately included in the analytical model.

To compute the equivalent mass and stiffness of the single degree of freedom oscillator of each floor of the structure shown in Figure 6.1, we first have to calculate their eigenproperties. Each floor was modeled as explained in the previous section. The first natural frequencies for each floor are presented in Table 6.15. The equivalent mass of any floor is obtained as,

$$m_e = 1/\phi^2 \tag{6.1}$$

where ϕ is the value of the eigenvector of the first mode of the floor associated with the vertical displacement at the center of the floor. The equivalent stiffness is then computed as,

$$k_e = \omega^2 m_e \tag{6.2}$$

where ω is the lowest natural frequency of the floor. The natural frequencies of the modified lumped mass model, Figure 6.22, which are obtained by combining the lumped mass model and the oscillators described above, are listed in Table 6.18. The table shows that the first three frequencies are very close to the first three frequencies of the flexible floor model and the other three are greater than those obtained from the lumped mass model listed in Table 6.10.

The normalized responses obtained from the modified lumped mass model are presented in Figure 6.23. It is observed that the displacements and acceleration responses for the modified lumped mass model are about 0.6 to 0.75 of the response values for the flexible floor model. The column axial force values in the modified lumped mass model are about 0.8 to 0.85 of the corresponding values in the flexible floor model. It is seen from Figure 6.24 that, when compared with the results obtained with the conventional lumped mass model, the new results show a definite improvement. Nevertheless, the responses are still significantly underestimated.

Similar improvements are also observed in the values of the acceleration floor response spectra for all three floors, displayed in Figures 6.25 to 6.27, although the peaks at the higher frequencies in the floor spectra are missed in the modified lumped mass model results. Also, the acceleration of the oscillator is underestimated.

6.5 SUMMARY AND CONCLUSIONS

The numerical results presented in the first part of this chapter demonstrate the effectiveness of the dynamic condensation approach when applied to structures with flexible floors. Although the master degrees of freedom were selected arbitrarily, the responses computed with the eigenproperties calculated with the condensed eigenvalue problem are very good, even though some of them were obtained by carrying out only one iteration.

The influence of the out-of-plane flexibility of the floor slabs when the structure is subjected to vertical ground excitations was investigated. The seismic response of a structure modeled with flexible floors was compared with the response of the lumped mass model, assuming its floors to be rigid. The difference in the results are considerable, especially when computing floor response spectra. It was demonstrated that as the floors of a structure become more rigid, the difference in the results are reduced and the assumption that the floor is rigid is more justified in this situation. It was also shown that the lumped mass model will usually underestimate the response.

Finally, the accuracy of the cascade approach and the modified lumped mass method to effectively analyze flexible floor slab structures was examined. With the cascade approach, one only has to prepare a detailed finite element model of the floor that needs to be analyzed. The interaction effects between the different parts of the structure are not included in the analytical model. The numerical results demonstrated that the cascade approach always overestimates the response, especially when calculating accelerations.

In the modified lumped mass method, the flexibility of the floor slabs and dynamic interaction effects are approximately included in the analytical model by adding a single degree of freedom oscillator, representing the center of each floor, to the lumped mass model. However, the numerical results showed that the calculated response accuracy improved when compared with the conventional lumped mass model results, but they were underestimated.

Table 6.1 Natural frequencies and participation factors for the structure in Figure 6.1 obtained from the flexible floor slab model.

Mode	Frequency in rad/sec	Participation Factor
1	49.53	5.30
2	54.24	-2.03
3	55.76	8.89
4	109.70	0.00
5	123.12	0.00
6	133.42	0.00
7	145.84	-5.71
8	156.75	-2.14
9	160.49	-1.95
10	331.13	4.37
11	341.17	0.00
12	349.58	0.00

Table 6.2 Frequencies (in rad/sec) of the structure in Figure 6.1 calculated by the dynamic condensation approach.

	Iteration Step			
Mode	0	1	3	5
1	51.40	49.53	49.53	49.53
	(3.78)	(0.00)		
2	56.67	54.24	54.24	54.24
	(4.48)	(0.00)		
3	58.39	55.77	55.77	55.77
	(4.72)	(0.00)		
4	112.48	109.71	109.70	109.70
	(2.53)	(0.01)	(0.00)	
5	127.01	123.15	123.13	123.13
	(3.15)	(0.02)	(0.00)	
6	138.22	133.47	133.43	133.43
	(3.59)	(0.03)	(0.00)	
7	154.81	146.00	145.84	145.84
	(6.15)	(0.11)	(0.00)	
8	164.65	156.84	156.76	156.76
	(5.03)	(0.05)	(0.00)	
9	168.11	160.56	160.50	160.50
	(4.74)	(0.04)	(0.00)	

Table 6.3 Exact root mean square responses for structure in Figure 6.1 obtained from the flexible floor slab model.

Node	Floor		
	0	1	3
Displacements (in inches)			
1	0.00099	0.00149	0.00173
6	0.02300	0.02673	0.02958
7	0.00733	0.00805	0.01065
Accelerations (in g units)			
11	0.057	0.591	0.060
14	0.166	0.207	0.185
18	0.077	0.086	0.089
Slab Bending Moments (in lb-ft)			
1	2686	3335	2576
6	3390	4092	4017
7	1839	2323	1896
Slab Shear Forces (in lbs)			
1	184	224	192
Column Axial Forces (in lbs)			
1	5121	3415	1846

Table 6.4 Normalized root mean square displacements of the structure in Figure 6.1 calculated by the dynamic condensation approach.

Node	Iteration Step			
	0	1	3	5
First Floor				
1	0.7442	0.9224	0.9345	0.9655
6	0.9591	1.0001	0.9983	0.9990
7	0.9651	1.0063	1.0042	1.0040
Second Floor				
1	0.7460	0.9256	0.9383	0.9690
6	0.9598	1.0003	0.9984	0.9990
7	0.9644	1.0069	1.0050	1.0040
Third Floor				
1	0.7512	0.9289	0.9411	0.9706
6	0.9629	0.9997	0.9984	0.9990
7	0.9676	1.0049	1.0037	1.0032

Table 6.5 Normalized root mean square accelerations of the structure in Figure 6.1 calculated by the dynamic condensation approach.

Node	Iteration Step			
	0	1	3	5
First Floor				
1	0.9757	0.9814	0.9827	0.9874
6	1.0246	0.9994	0.9983	0.9991
7	1.0131	1.0003	0.9991	0.9994
Second Floor				
1	0.9534	0.9635	0.9661	0.9670
6	1.0325	0.9984	0.9973	0.9985
7	1.0159	0.9977	0.9966	0.9976
Third Floor				
1	0.9404	0.9541	0.9574	0.9654
6	1.0135	0.9967	0.9963	0.9977
7	1.0019	0.9969	0.9966	0.9973

Table 6.6 Normalized root mean square bending moments of the structure in Figure 6.1 calculated by the dynamic condensation approach.

Node	Iteration Step			
	0	1	3	5
First Floor				
1	0.8692	0.9991	0.9993	0.9995
6	2.5746	1.0048	0.9901	0.9953
7	0.5934	0.9943	0.9949	0.9953
Second Floor				
1	0.8707	1.0099	1.0102	1.0100
6	2.5898	1.0057	0.9903	0.9956
7	0.6086	0.9934	0.9943	0.9961
Third Floor				
1	0.8953	1.0094	1.0090	1.0083
6	2.4937	1.0006	0.9896	0.9945
7	0.5596	0.9904	0.9915	0.9917

Table 6.7 Normalized root mean square shear forces of the structure in Figure 6.1 calculated by the dynamic condensation approach.

Floor	Iteration Step			
	0	1	3	5
1	0.6596	0.9786	0.9891	0.9904
2	0.6708	0.9888	0.9990	0.9993
3	0.6573	0.9892	0.9984	0.9993

Table 6.8 Normalized root mean square axial forces of the structure in Figure 6.1 calculated by the dynamic condensation approach.

Floor	Iteration Step			
	0	1	3	5
1	0.7793	0.9659	0.9786	0.9807
2	0.7891	0.9809	0.9945	0.9955
3	0.8197	0.9818	0.9914	0.9920

Table 6.9 Maximum root mean square responses for the structure in Figure 6.1 obtained from the flexible floor slab model.

Response	Floor 1	Floor 2	Floor 3
Displacement in inches	0.02300	0.02673	0.02958
Acceleration in g units	0.166	0.207	0.185
Axial Force in lbs	5121	3415	1846

Table 6.10 Natural frequencies and participation factors of the structure of Figure 6.1 obtained from the lumped mass model.

Mode	Frequency in rad/sec	Participation Factor
1	144.27	25.85
2	414.84	6.09
3	616.52	-1.85

Table 6.11 Natural frequencies and participation factors for the structure in Figure 6.1 with 16 ft square slabs obtained from the flexible floor slab model.

Mode	Frequency in rad/sec	Participation Factor
1	112.55	6.23
2	124.67	4.32
3	128.69	3.81
4	226.34	0.00
5	258.96	0.00
6	260.10	-4.97
7	296.04	0.00
8	322.99	-0.24
9	334.87	-1.11
10	511.35	2.02
11	612.79	0.00
12	667.75	0.23

Table 6.12 Maximum root mean square responses for structure in Figure 6.1 with 16 ft square slabs obtained from the flexible floor slab model.

Response	Floor		
	1	2	3
Displacement in inches	0.00300	0.00327	0.00433
Acceleration in g units	0.091	0.107	0.121
Axial Force in lbs	2467	1646	824

Table 6.13 Natural frequencies and participation factors of the structure of Figure 6.1 with 16 ft square slabs obtained from the lumped mass model.

Mode	Frequency in rad/sec	Participation Factor
1	188.13	19.98
2	537.26	4.67
3	795.30	-1.35

Table 6.14 Maximum root mean square responses for structure in Figure 6.1 obtained from the flexible floor slab model.

Response	Floor		
	1	2	3
Displacement in inches	0.02300	0.02673	0.02958
Acceleration in g units	0.166	0.207	0.185
Bending Moment in lb-ft	3390	4092	4017
Shear Force in lbs	184	224	192
Axial Force in lbs	5121	3415	1846

Table 6.15 Natural frequencies of first floor of the structure in Figure 6.1.

Mode	Frequency in rad/sec	Participation Factor
1	55.57	5.76
2	126.01	0.00
3	163.45	-3.09
4	349.50	0.00
5	357.30	0.16
6	493.54	0.78
7	578.67	0.00
8	680.59	-0.46
9	806.66	0.00
10	808.01	-0.02

Table 6.16 Natural frequencies of second floor of the structure in Figure 6.1.

Mode	Frequency in rad/sec	Participation Factor
1	56.38	5.74
2	129.19	0.00
3	165.67	-3.17
4	354.12	0.00
5	357.31	0.15
6	523.45	1.10
7	682.95	0.00
8	765.57	0.78
9	806.71	0.00
10	811.19	-0.17

Table 6.17 Natural frequencies of third floor of the structure in Figure 6.1.

Mode	Frequency in rad/sec	Participation Factor
1	52.08	5.76
2	116.19	0.00
3	158.51	-3.09
4	349.68	0.00
5	357.30	0.16
6	493.54	0.78
7	578.67	0.00
8	680.59	-0.46
9	806.66	0.00
10	808.01	-0.02

Table 6.18 Natural frequencies and participation factors of the structure in Figure 6.1 obtained from the modified lumped mass model.

Mode	Frequency in rad/sec	Participation Factor
1	51.64	8.68
2	55.23	7.87
3	56.23	5.44
4	163.19	22.59
5	461.16	5.45
6	682.94	-1.62

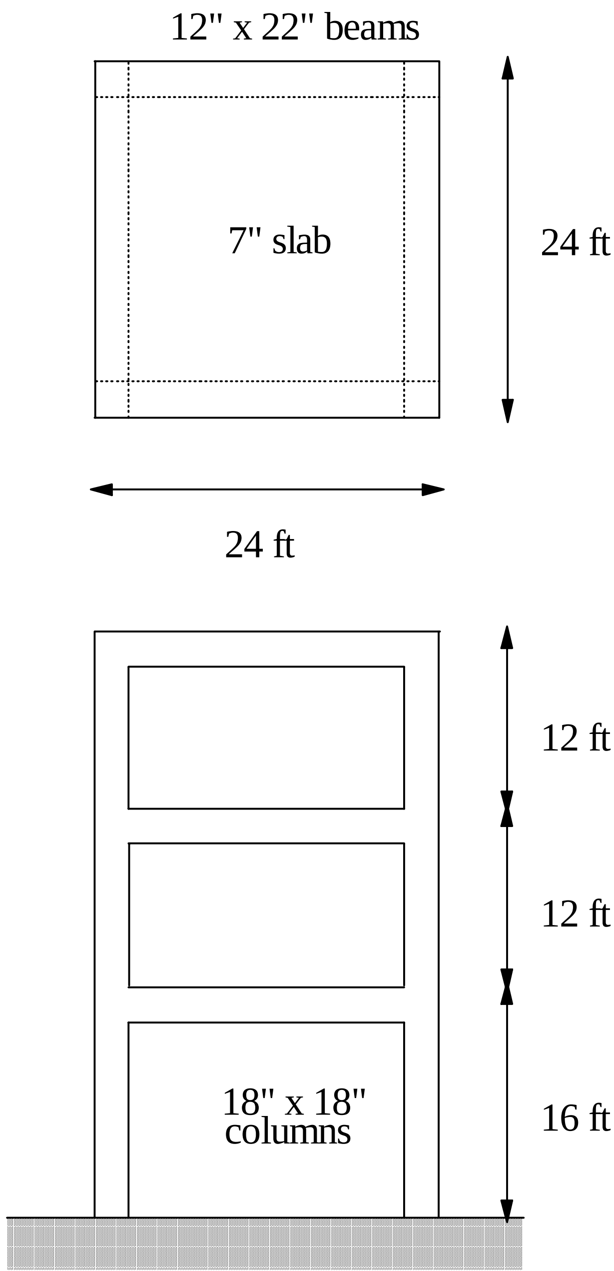

Figure 6.1 Configuration of the three-story building used in the numerical results.

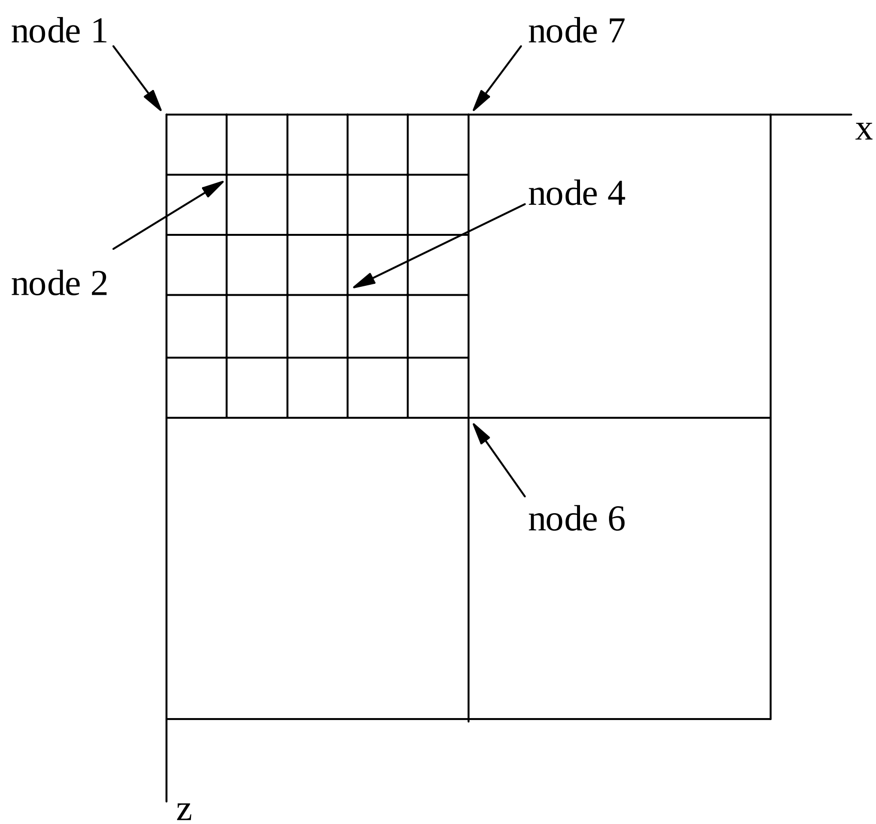

Figure 6.2 Finite element model of a typical floor slab of building in figure 6.1

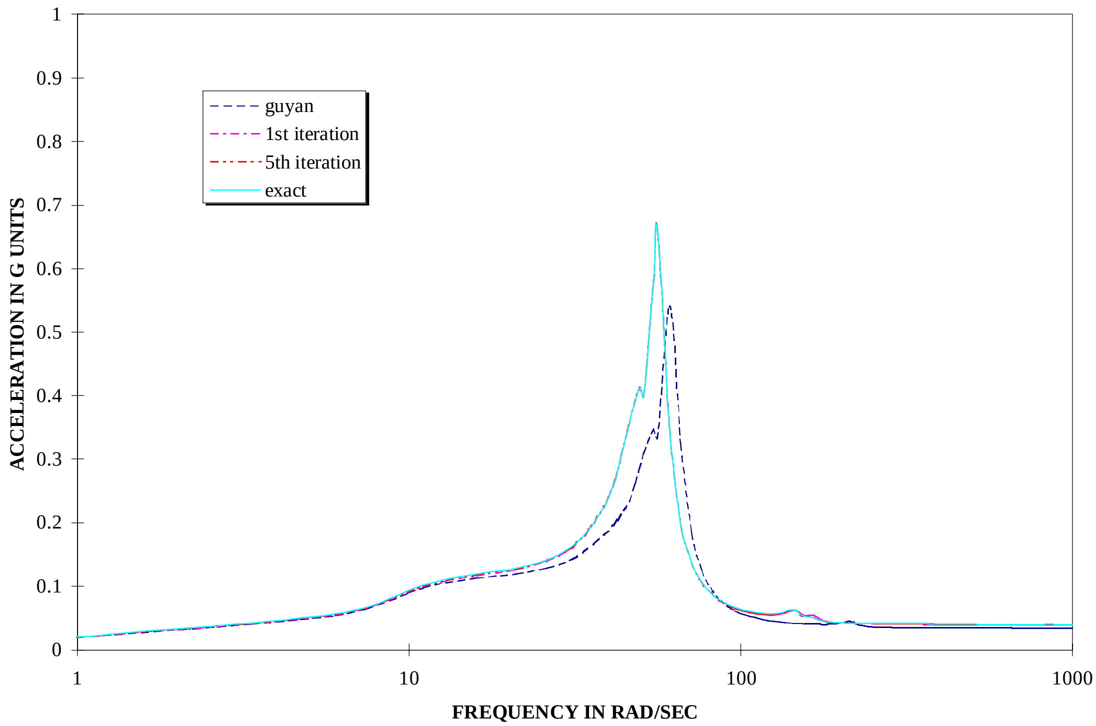

Figure 6.3 Floor spectra for an oscillator at node 4 of the first floor calculated at different iteration steps.

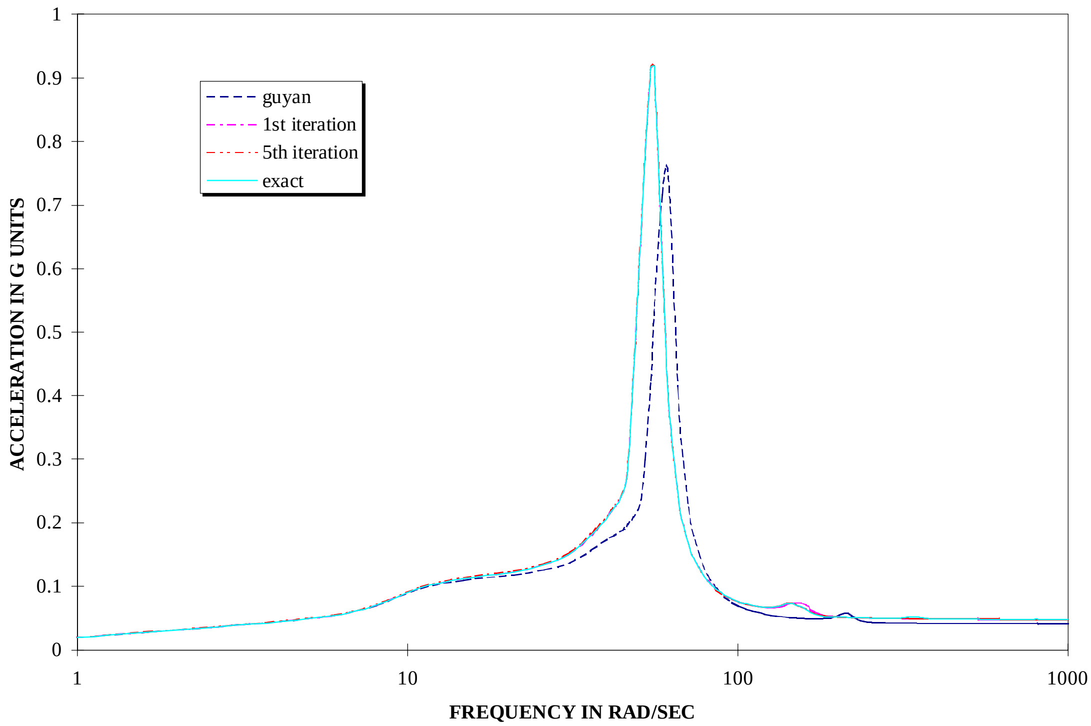

Figure 6.4 Floor spectra for an oscillator at node 4 of the second floor calculated at different iteration steps.

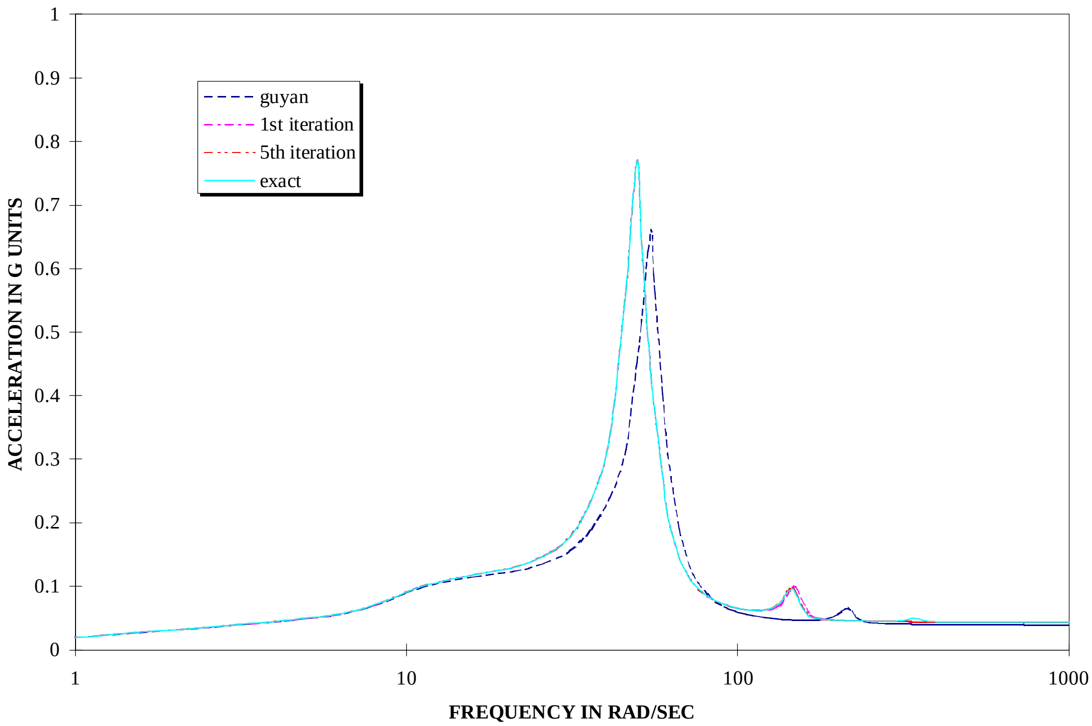

Figure 6.5 Floor spectra for an oscillator at node 4 of the third floor calculated at different iteration steps.

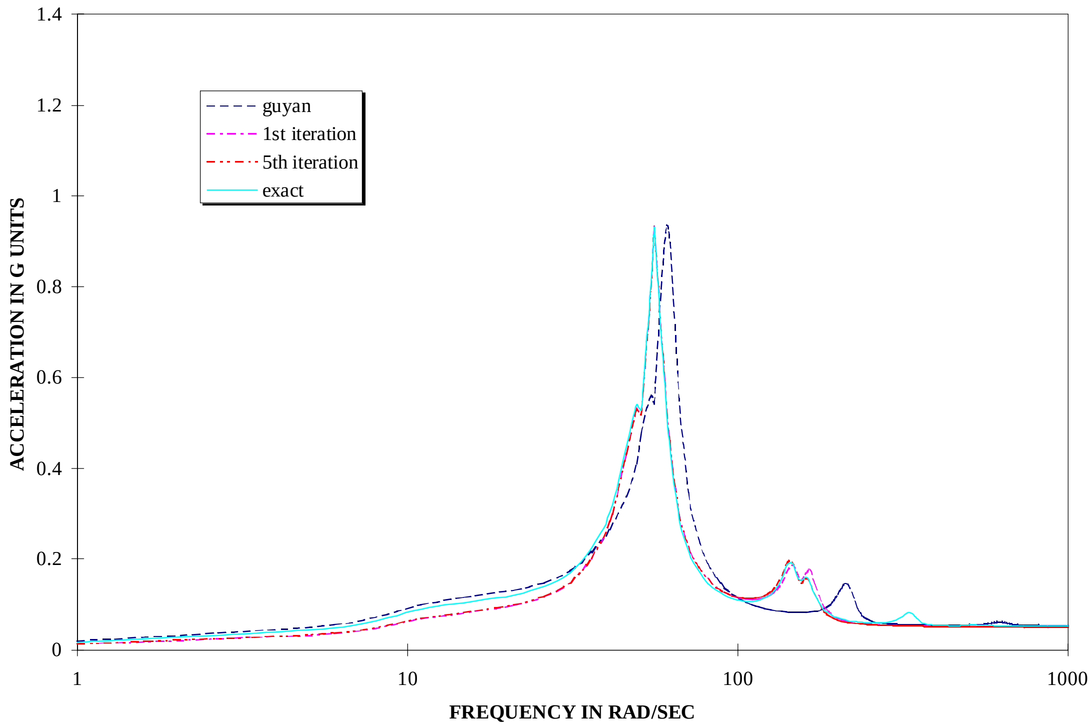

Figure 6.6 Floor spectra for an oscillator at node 6 of the first floor calculated at different iteration steps.

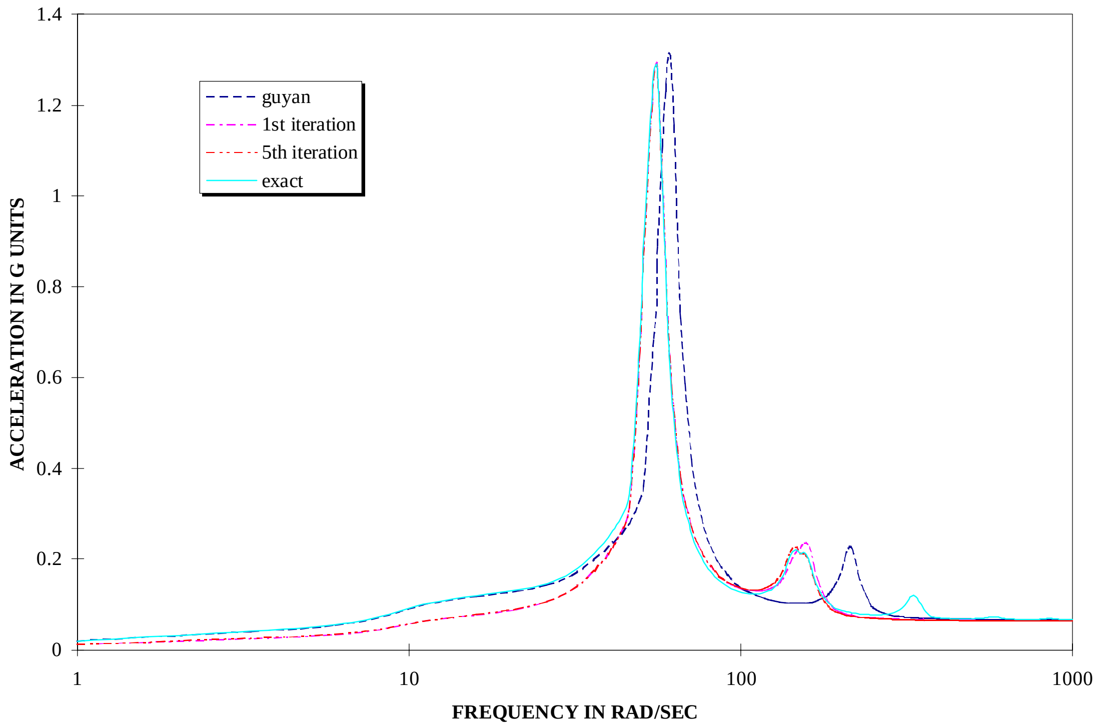

Figure 6.7 Floor spectra for an oscillator at node 6 of the second floor calculated at different iteration steps.

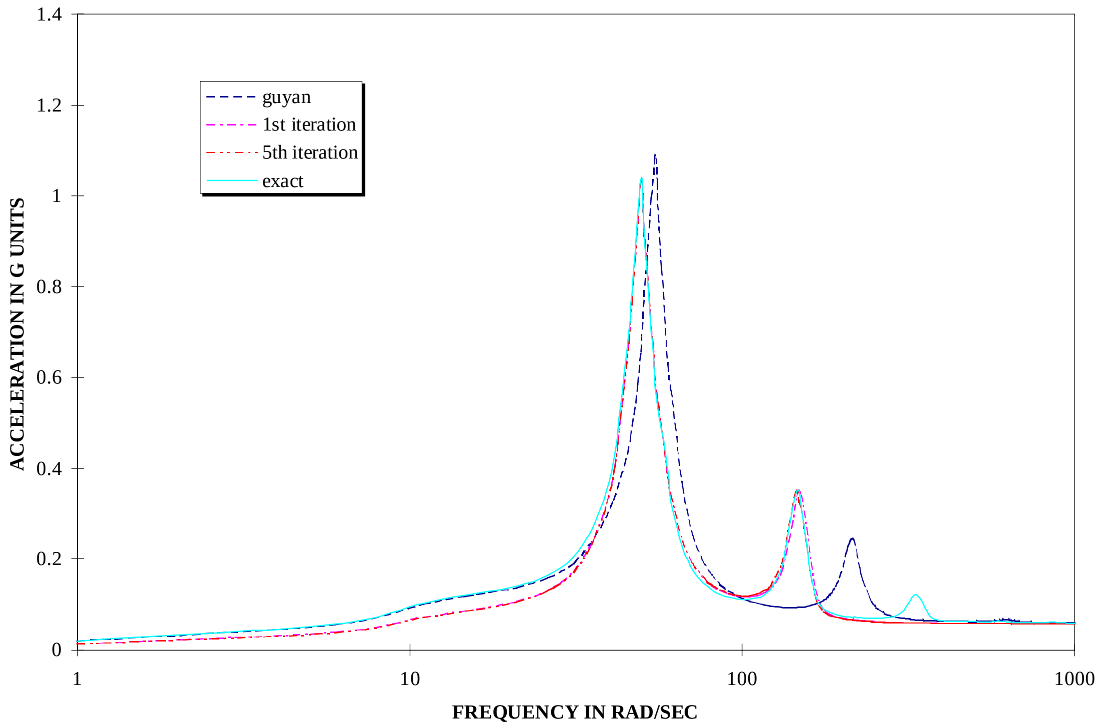

Figure 6.8 Floor spectra for an oscillator at node 6 of the third floor calculated at different iteration steps.

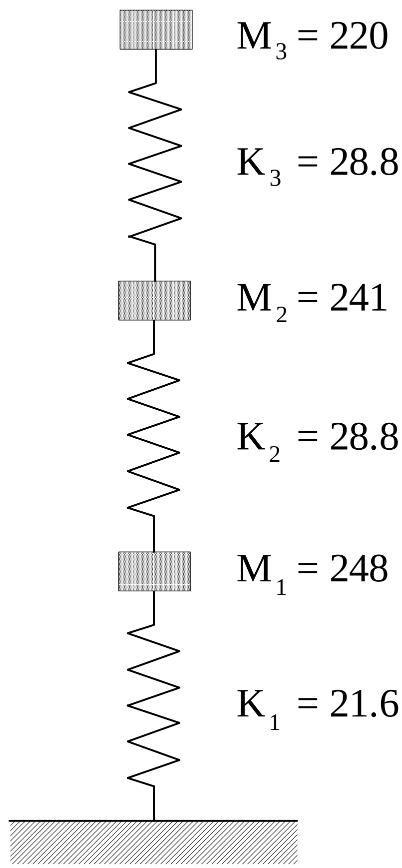

Figure 6.9 Lumped mass model of the structure in Figure 6.1. (Stiffness K in kips/in, and mass M in kips-s^2 / in)

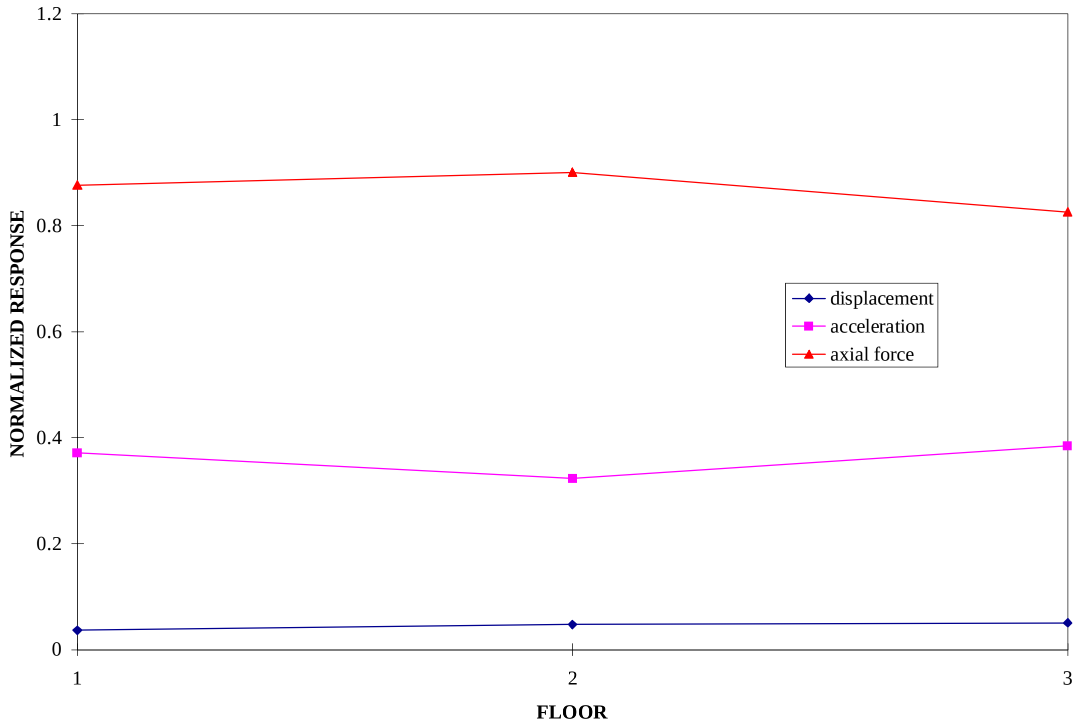

Figure 6.10 Normalized responses obtained for the 24 ft square slabs building using the lumped mass model.

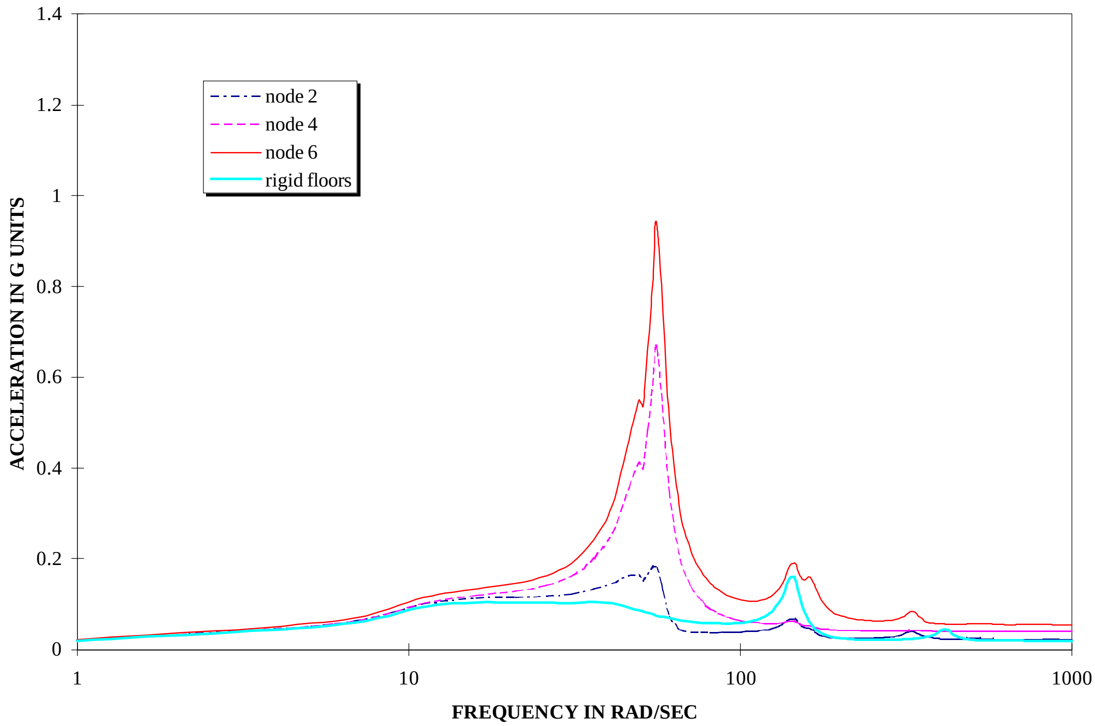

Figure 6.11 Comparison of floor spectra for the first floor of the 24 ft square slabs building calculated at different locations of the flexible floor model and the rigid floor model.

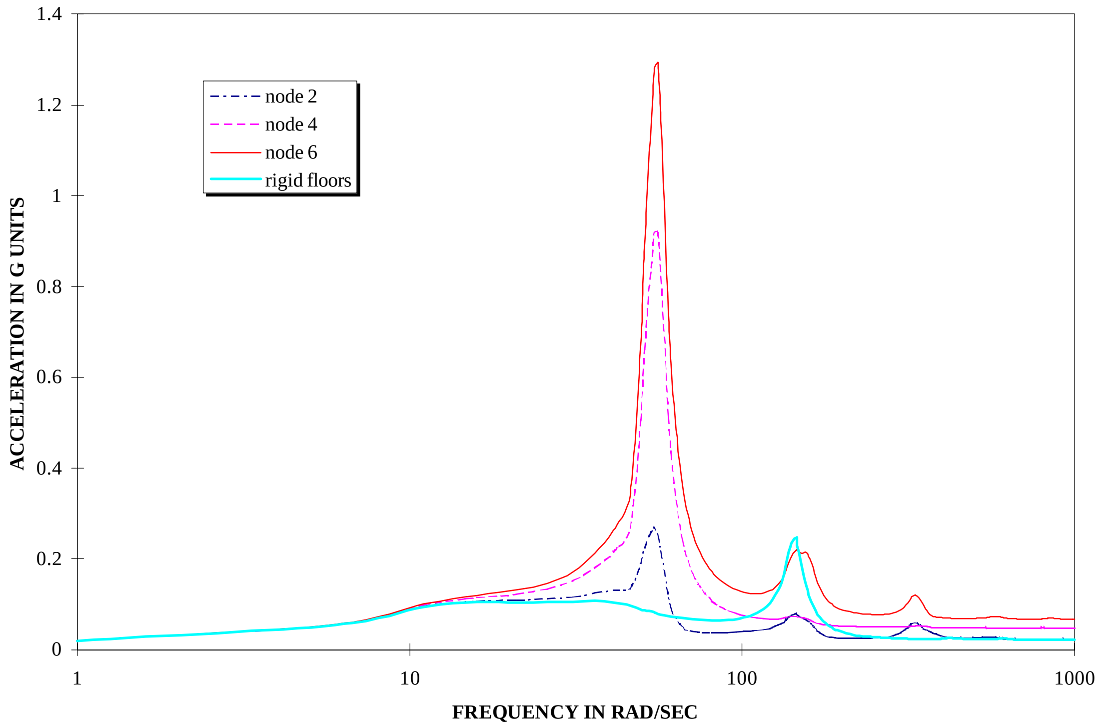

Figure 6.12 Comparison of floor spectra for the second floor of the 24 ft square slabs building calculated at different locations of the flexible floor model and the rigid floor model.

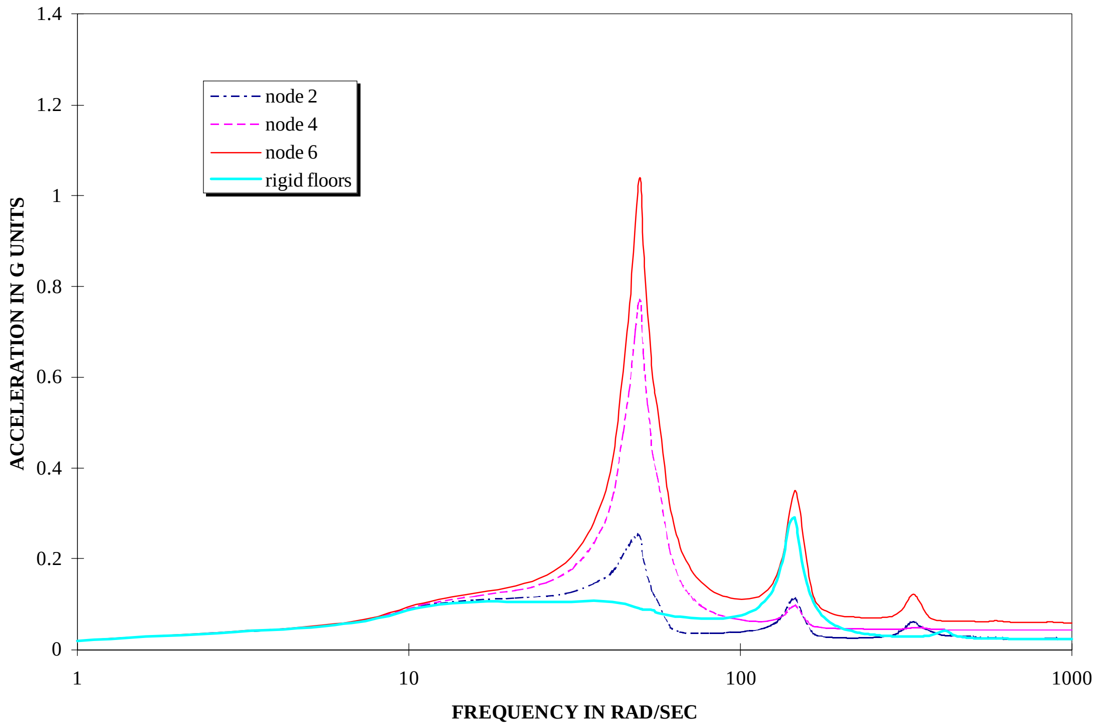

Figure 6.13 Comparison of floor spectra for the third floor of the 24 ft square slabs building calculated at different locations of the flexible floor model and the rigid floor model.

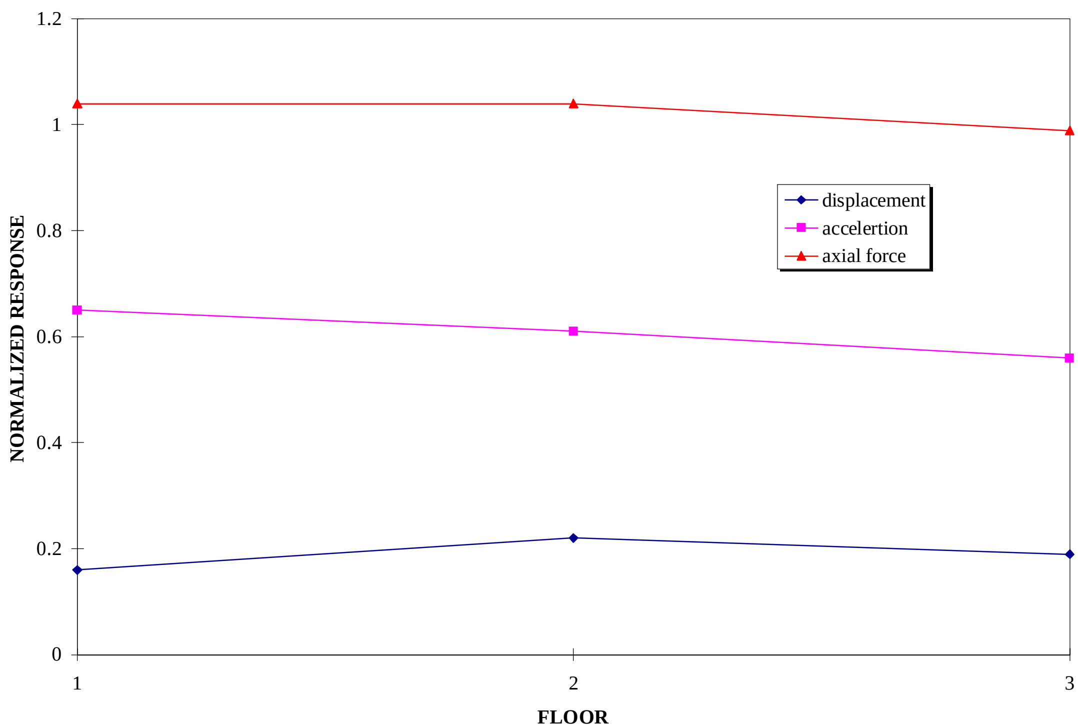

Figure 6.14 Normalized responses obtained for the 16 ft square slabs building using the lumped mass model.

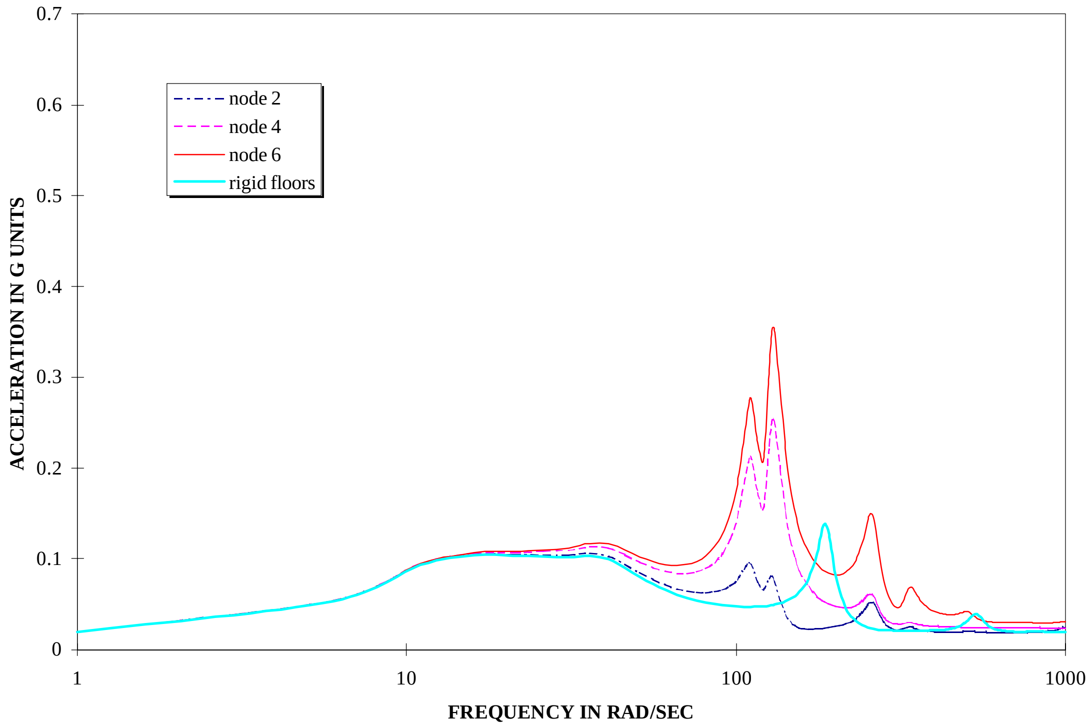

Figure 6.15 Comparison of floor spectra for the first floor of the 16 ft square slabs building calculated at different locations of the flexible floor model and the rigid floor model.

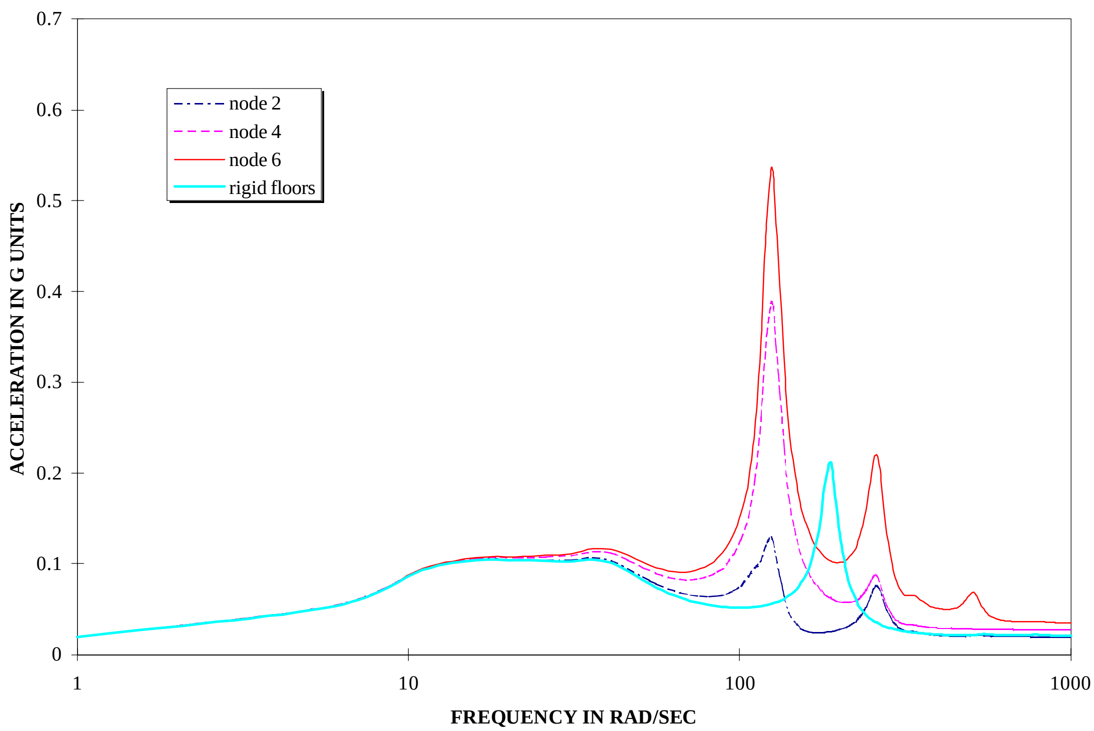

Figure 6.16 Comparison of floor spectra for the second floor of the 16 ft square slabs building calculated at different locations of the flexible floor model and the rigid floor model.

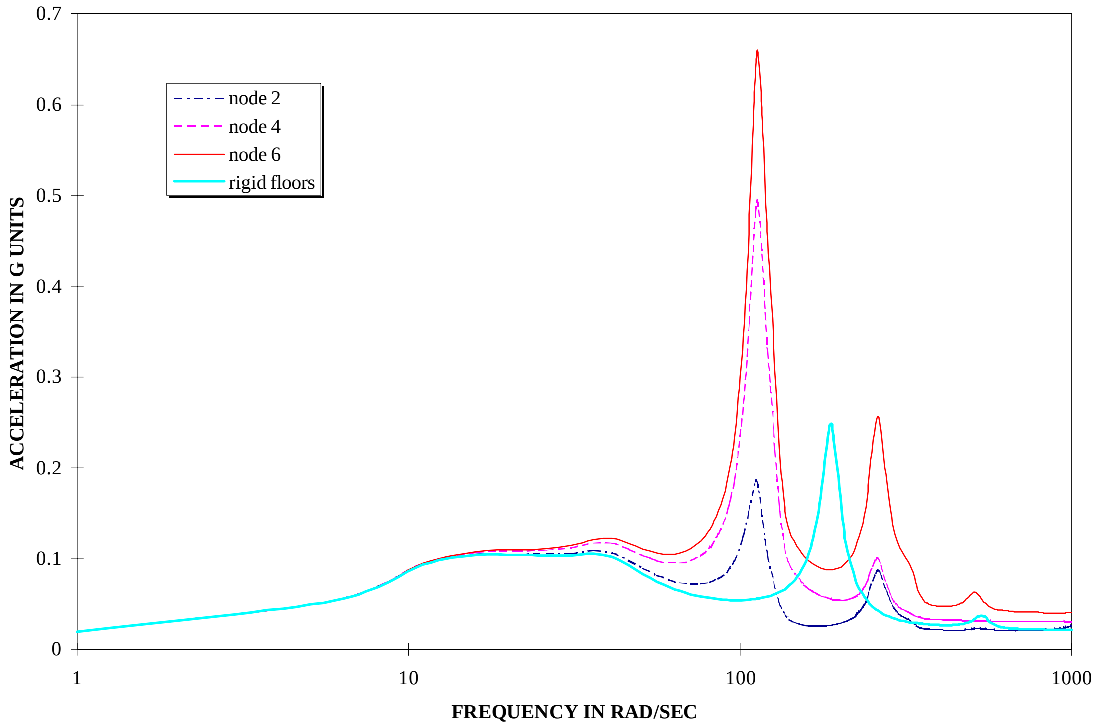

Figure 6.17 Comparison of floor spectra for the third floor of the 16 ft square slabs building calculated at different locations of the flexible floor model and the rigid floor model.

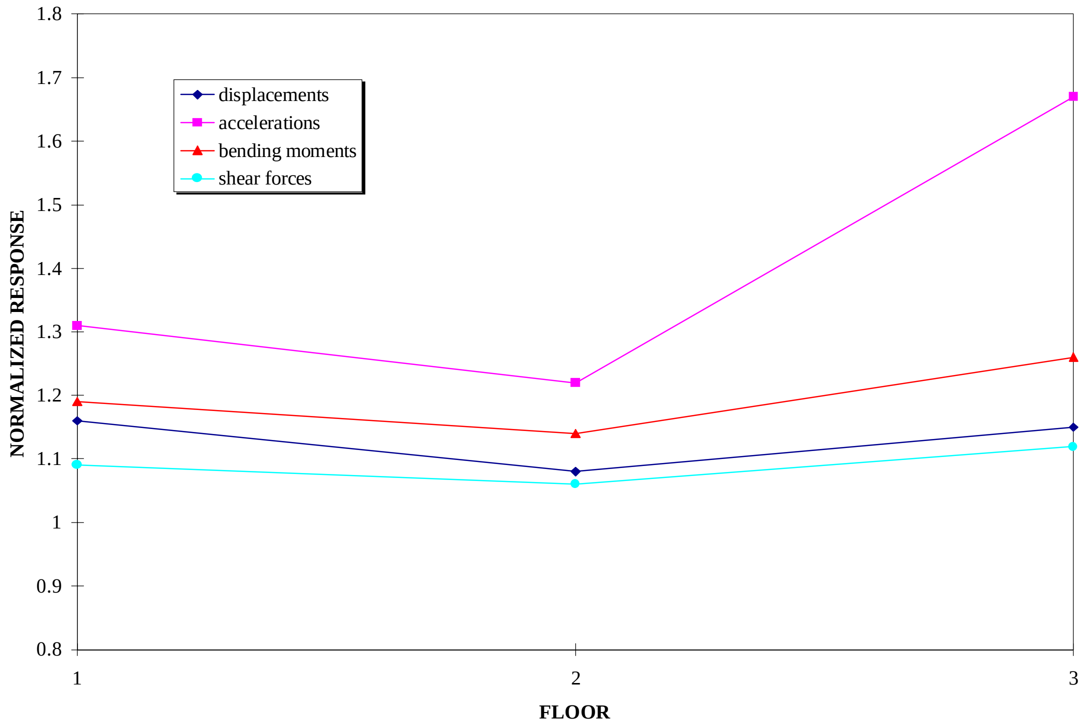

Figure 6.18 Normalized responses obtained with the cascade approach.

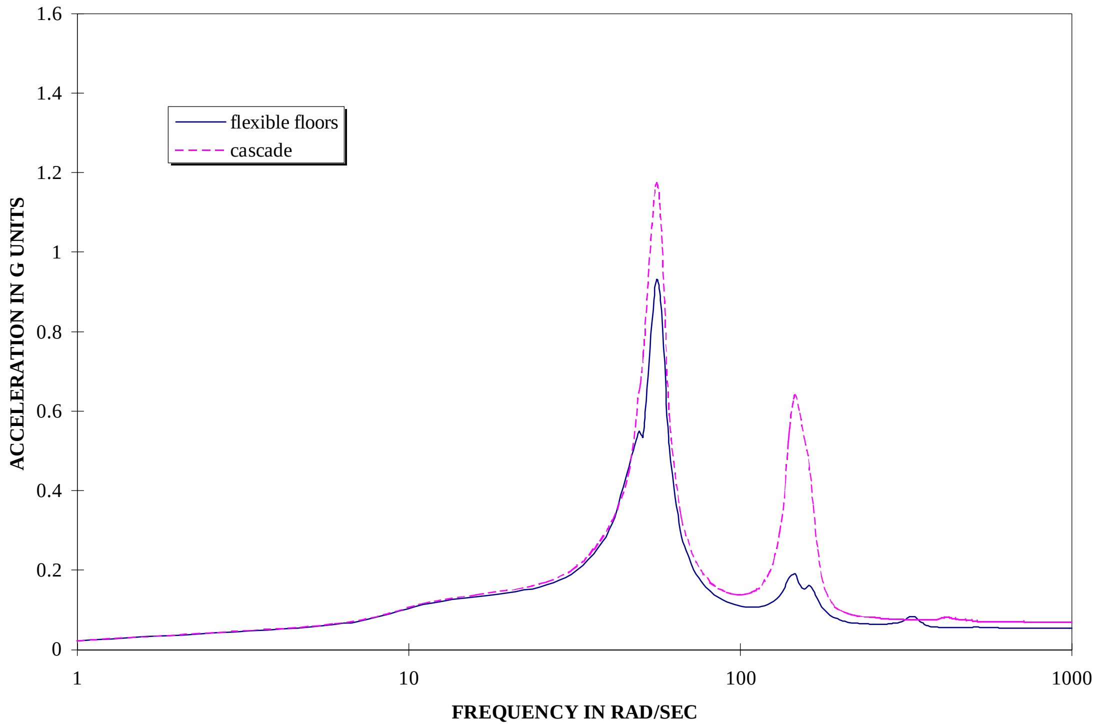

Figure 6.19 Comparison of floor spectra for the center of the first floor calculated with the flexible floor model and the cascade approach.

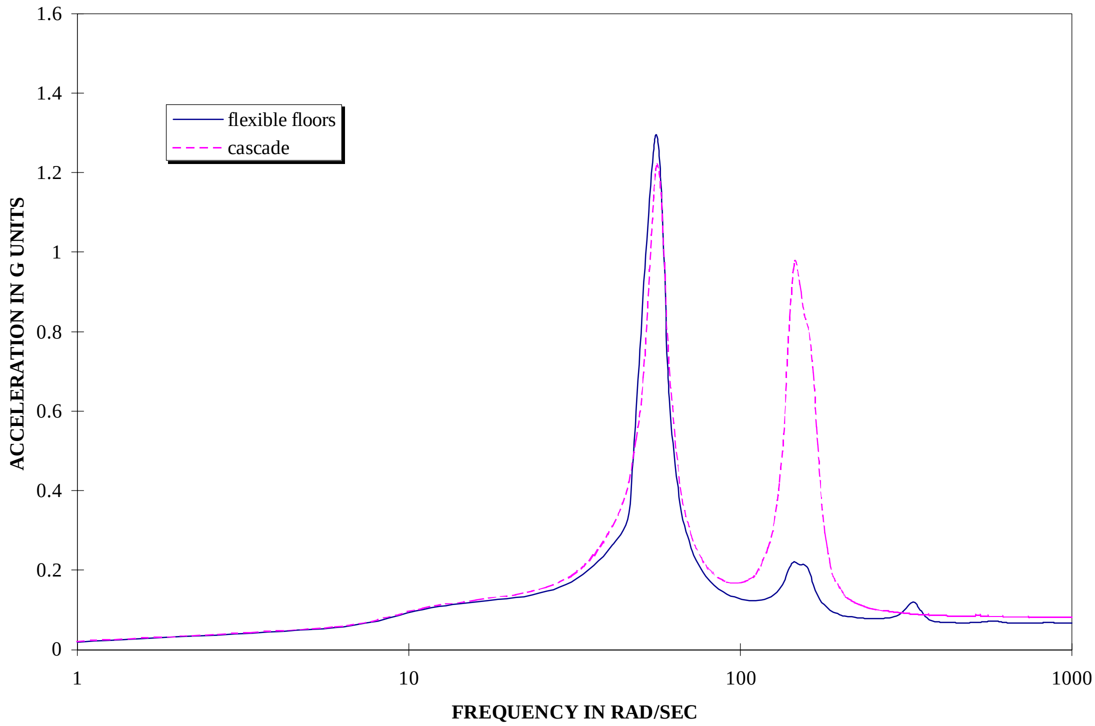

Figure 6.20 Comparison of floor spectra for the center of the second floor calculated with the flexible floor model and the cascade approach.

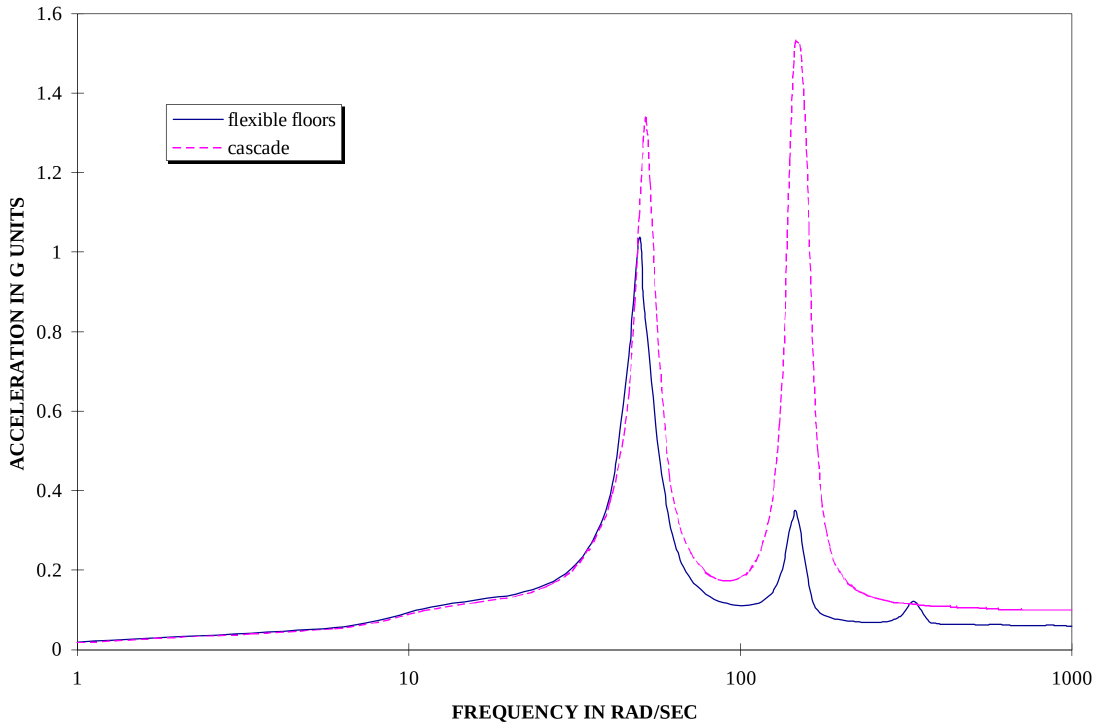

Figure 6.21 Comparison of floor spectra for the center of the third floor calculated with the flexible floor model and the cascade approach.

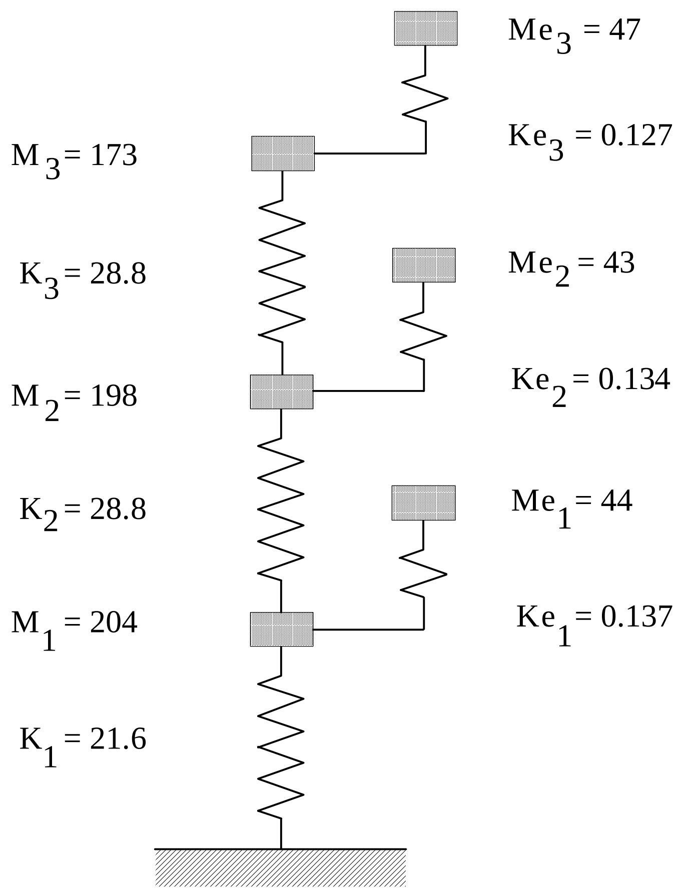

Figure 6.22 Modified lumped mass model of the structure in Figure 6.1. (Stiffness K in kips/in, and mass M in kips-s^2/ in)

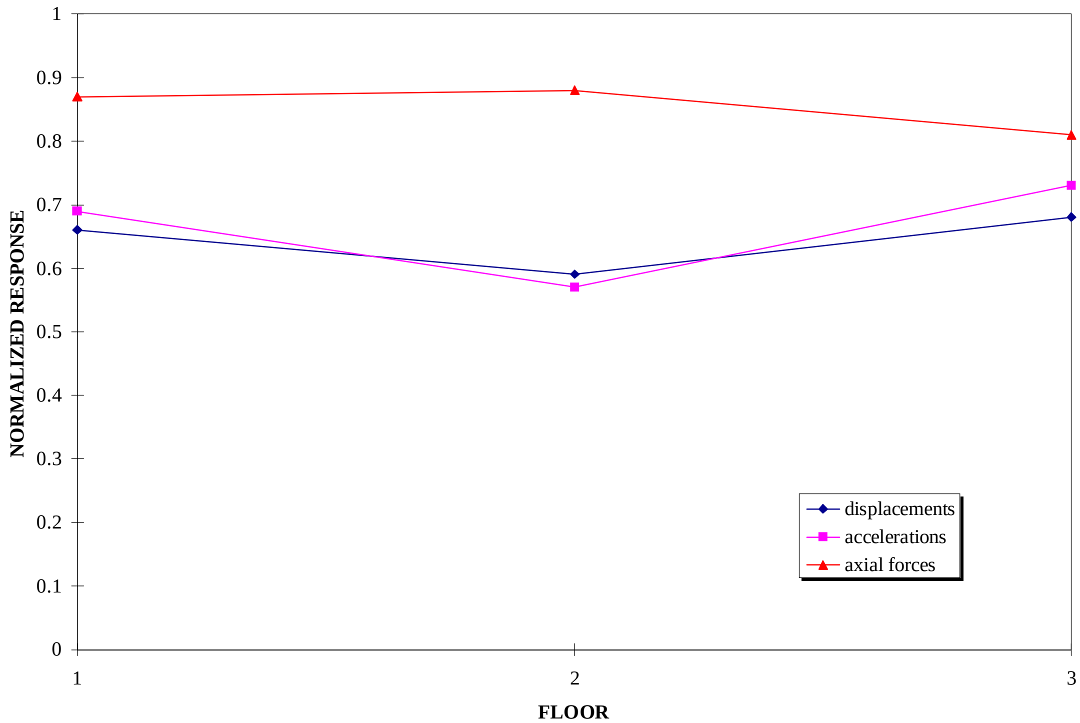

Figure 6.23 Normalized responses obtained from the modified lumped mass model.

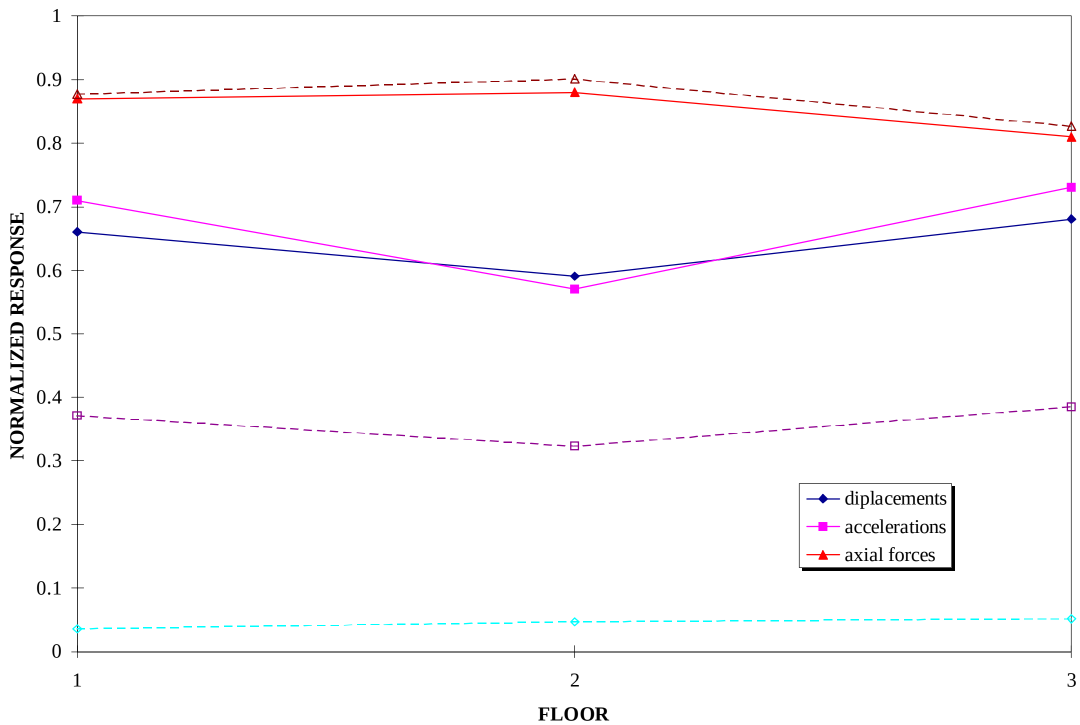

Figure 6.24 Comparison of the normalized responses obtained from the modified and the conventional lumped mass model.

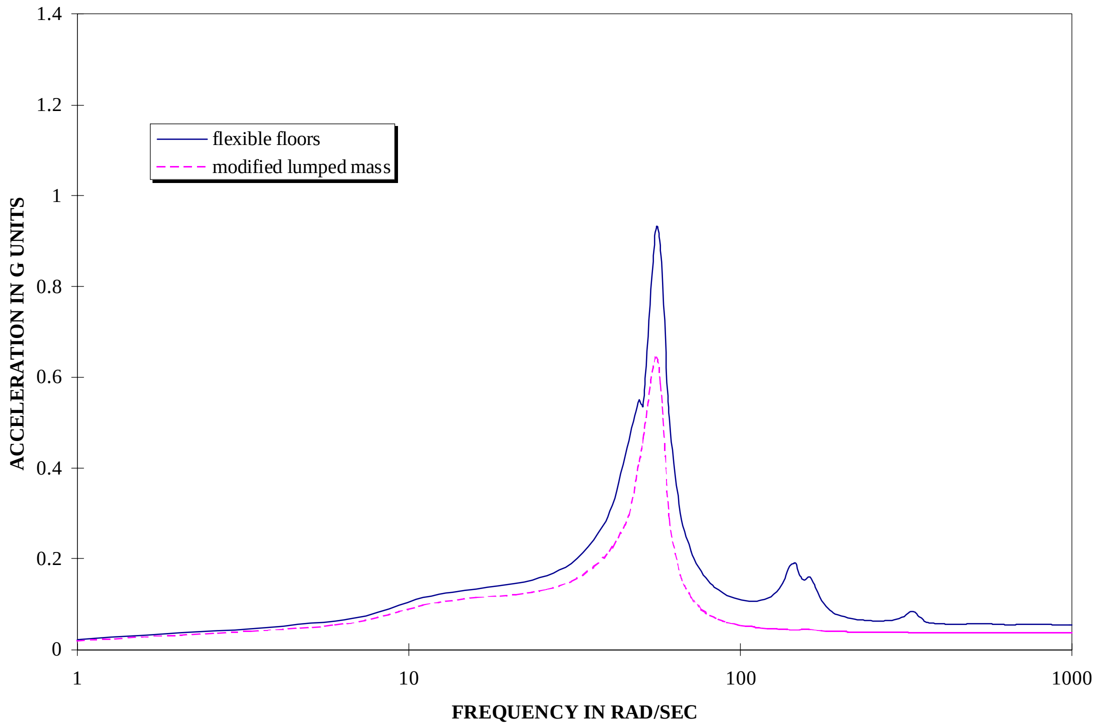

Figure 6.25 Comparison of floor spectra for the center of the first floor calculated with the flexible floor model and the modified lumped mass model.

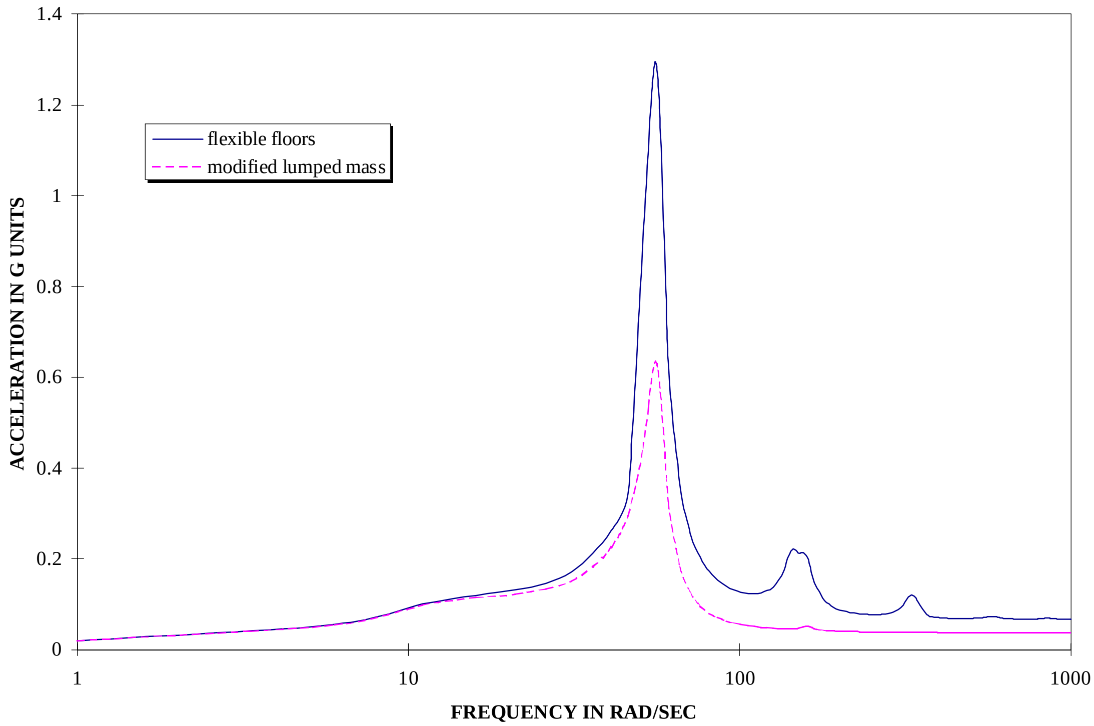

Figure 6.26 Comparison of floor spectra for the center of the second floor calculated with the flexible floor model and the modified lumped mass model.

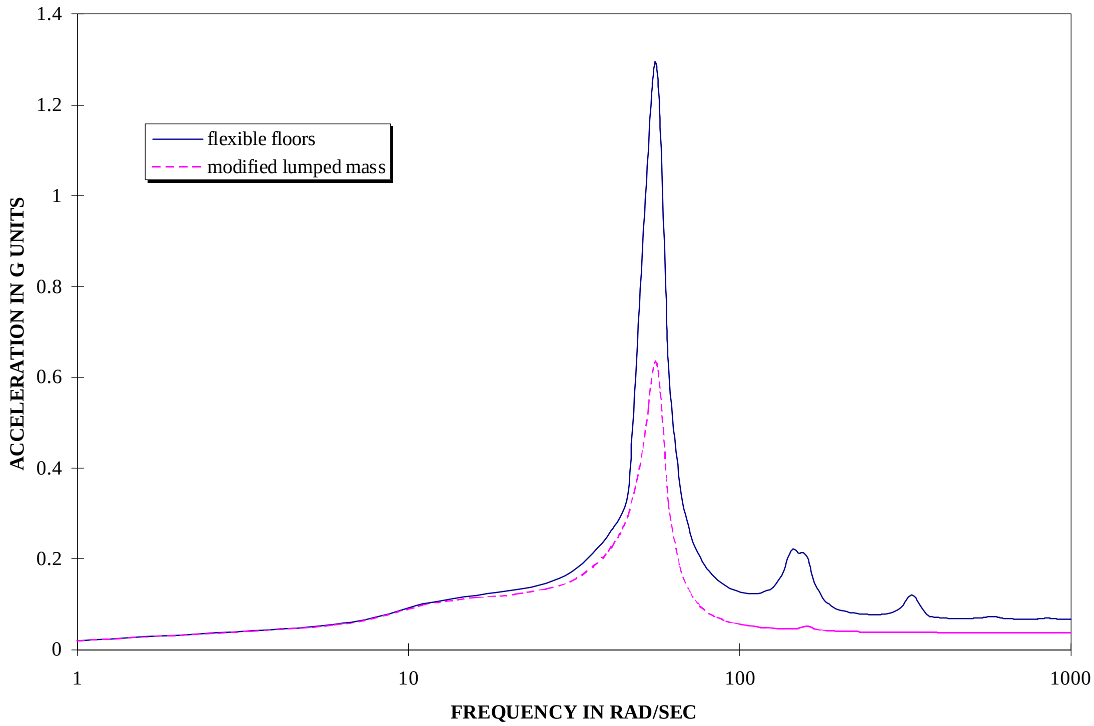

Figure 6.27 Comparison of floor spectra for the center of the third floor calculated with the flexible floor model and the modified lumped mass model.

CHAPTER VII

SUMMARY AND CONCLUSIONS

The flexibility of the floor slabs, especially for the in-plane motion, is often ignored in the seismic analysis of structures. For the out-of-plane motion, some simplified procedures are used to include floor flexibility especially in the analysis of secondary systems. These simplified procedures can, however, lead to over and underestimation of the responses for vertical seismic motions. To include the flexibility effects more accurately, a detailed finite element model of the structure can be constructed. This procedure is, however, computationally involved and often not practical. This study has been directed toward the development of accurate and efficient approaches to include the effect of the out-of-plane flexibility of floor slabs in the analytical model of a structure in a rational way so that seismic response for vertical motions can be accurately calculated. Since modal properties are commonly required for seismic analysis of linearly behaving structures, these new approaches have focused on accurate calculation of these properties with reduced computational effort.

In Chapter 3, a dynamic condensation approach is developed to calculate accurate complex valued eigenproperties for nonclassically damped structures. The basic idea of the approach is to reduce the size of the eigenvalue problem associated with the equations of motion of the structure before it is solved. To accomplish this goal, the degrees of freedom of the structure are divided into kept and reduced coordinates, and they are related through a condensation matrix that is used to form a condensed eigenvalue problem. The first few modes of the structure are obtained by solving iteratively the resulting condensed eigenvalue problem. The eigenproperties calculated at each iteration step are utilized to update the condensation matrix for the following iteration step. The process of updating the condensation matrix is repeated until the eigenvalues satisfy a required convergence criteria. If desired, the rest of the eigenproperties can be obtained by solving a complementary eigenvalue problem associated with the higher modes. The iteration process can be carried out not only with the lower modes but also with the higher modes. Once the eigenproperties of the structure are known, the seismic response can be calculated.

The formulation to use the condensation approach developed in Chapter 3 with two substructuring procedures is presented in Chapter 4. In the first substructuring technique, referred to as the Condensed Substructure Superposition Approach which was initially formulated in Chapter 2, the condensation process takes place at the substructure level. In other words, the initial condensation matrix relating the boundary and interior degrees of freedom of each substructure is used to condensed out the interior degrees of freedom. A reduced size eigenvalue problem associated with the boundary degrees of freedom of the combined structure is obtained by assembling the contribution of each substructure. The solution of this condensed eigenvalue problem provides the eigenproperties associated with the lower modes. Each substructure condensation matrix is then updated and an improved eigenvalue problem is obtained. The process continues until a desired convergence criteria for the eigenvalues is achieved. As opposed to the formulation presented in the previous chapter, here the global matrices of the combined structure or any of its submatrices are not required in the iteration process.

In the second substructuring technique considered in Chapter 4, a combination of the mode synthesis approach and the dynamic condensation approach of Chapter 3 is used to obtain the eigenproperties of the combined structural system. In this case, the equations of motion of the combined structure are obtained in terms of the eigenproperties of the substructures. This is done by transforming the physical coordinates of the substructure into a set of generalized coordinates through a matrix of component modes. The eigenproperties of the substructures or component modes are obtained with free interface boundary conditions for one of the substructure and fixed for the other. The dynamic condensation approach is then used to solve the eigenvalue problem associated with these transformed equations of motion.

The dynamic condensation approach developed in this work, as well as all its variations, can also be applied to classically damped structures. It is demonstrated in Chapter 5 that the expressions obtained for nonclassically damped structures are directly applicable to classically damped structures if the state space submatrices are replaced appropriately as in Eqs. (5.7a) and (5.7b). Thus, the dynamic condensation for classically damped structures can be considered as a special case of the nonclassically damped structures.

Various numerical results are presented throughout the dissertation to show the effectiveness of the proposed approaches. In general, almost exact eigenproperties are obtained with a few iteration steps. However, the results also indicate that the selection of coordinates to be kept in the reduced eigenvalue problem affects the convergence rate of the iterative process. The proper choice of the coordinates is important in the condensation process since different choices will generate different initial estimate of the condensation matrix. Although the iteration process reduces significantly the errors in the eigenproperties regardless the coordinates selected, it will need more iteration steps to satisfied a given convergence criteria. Nevertheless, it was found that the combination of the mode synthesis and the condensation process leads to a faster convergence, if the system matrices are reordered according to the magnitude of the eigenvalues of the constituent substructures.

The proposed approach provided accurate eigenproperties of the structure for the calculation of seismic response of flexible floor structures carried out in Chapter 6. Numerical results obtained for a three-story building demonstrate this. The accuracy of the different response quantities of the floor slabs, the axial forces in the columns, and acceleration floor response spectra obtained with the eigenproperties computed with the dynamic condensation approach was excellent. Thus, the use of the dynamic condensation approach is advocated for including the effect of floor flexibility and dynamic interaction for accurate analytical modeling and seismic analysis of structures.

The influence of the out-of-plane flexibility of the floor in the response of primary and secondary systems subjected to vertical ground excitation is also investigated. The results clearly show that the inclusion of the floor flexibility in the analytical model increases the design response significantly, especially when computing acceleration floor response spectra. Therefore, unless the floor slabs have vertical natural frequencies greater than the so-called rigid range value of 33 Hz [55], the floor flexibility cannot be neglected.

Two popular approaches -- the cascade approach and the modified lumped mass approach -- used in the current practice to consider the floor flexibility effects in the analytical model of the structure have been evaluated. The comparison of the numerical results obtained by the cascade approach with the results obtained by the finite element model shows that the cascade approach overestimate the seismic responses. On the other hand, the use of the modified lumped mass method, underestimate the responses. Both approaches can leads to significant errors, especially when computing accelerations and floor response spectra required for the design of secondary systems.

REFERENCES

1. Ahmadi G. and Abdel S., “Stability of Elastic Frames Subjected to Earthquake Excitations", Earthquake Engineering and Structural Dynamics, Vol. 14, pp. 455-474, 1986.

2. Anderson R. G., Irons B. M. and Zienkiewicz O. C., “Vibration and Stability of Plates Using Finite Elements", International Journal of Solids and Structures, Vol. 4, pp.1031-1055, 1968.

3. Anderson L. R. and Hallauer W. L., “A Method of Order Reduction for Structural Dynamics Based on Riccati Iteration", AIAA Journal, Vol. 19, No. 6, pp. 796-800, 1980.

4. Appa K., Smith G. C. C. and Hughes J. T., “Rational Reduction of Large-Scale Eigenvalue Problems", AIAA Journal, Vol. 10, pp. 964-965, 1972.

5. Barr A. D. S. and McWhannell D. C., "Parametric Instability in Structures Under Support Motion", Journal of Sound and Vibration, Vol. 14, No. 4, pp. 491-509, 1971.

6. Blair M. A., Camino T. S. and Dickens J. M., "An iterative approach to a reduced mass matrix", Proceedings of the 9th International Modal Analysis Conference, Florence, Italy, Vol. I, pp. 621-626, 1991.

7. Bouhaddi N. and Fillod R., "Substructures using a linearized dynamic condensation method", Computers & Structures, Vol. 45, No. 4, pp. 679-683, 1992.

8. Bouhaddi N. and Fillod R., "A method of selecting master DOF in dynamic substructuring using the Guyan condensation method", Computers & Structures, Vol. 45, No. 5/6, pp. 941-946, 1992.

9. Bouhaddi N. and Fillod R., "Substructuring by a two level dynamic condensation method", Computers & Structures, Vol. 60, No. 3, pp. 403-409, 1996.

10. Button M. R., Kelly T. E. and Jones L. R., “The Influence of Diaphragm Flexibility on the Seismic Response of Buildings", 8th World Conference on Earthquake Engineering, San Francisco, California, 1984.

11. Chen S. H. and Pan H. H., “Guyan Reduction", Communications in Applied Numerical Methods, Vol. 4, pp. 549-556, 1988.

12. Cheng F. Y. and Oster K. B., “Ultimate Instability of Earthquake Structures", Journal of the Structural Division, ASCE, Vol. 102, No. ST5, pp. 961-972, 1976.

13. Chin S. L., White M. P. and Dzialo F. J., “Response of Structures with Flexible Floor Systems Subject to Vertical Ground Motion", 1st IMAC, Orlando, Florida, 1982.

14. Craig R. R., *Structural Dynamics, An Introduction to Computer Methods*, John Wiley & Sons, New York, 1981.

15. Craig R. R. and Chung Y. T., “Generalized Substructure Coupling Procedure for Damped Systems", AIAA Journal, Vol. 20, No. 3, pp. 442-444, 1982.

16. Despeyroux J., “The El Asnam Earthquake of 10 October 1980: Characteristics of the Main Shock and Lessons to be Drawn for Earthquake Engineering", Engineering Structures, Vol. 4, pp. 139-146, July 1982.

17. Downs B., “Accurate Reduction of Stiffness and Mass Matrices for Vibration Analysis and a Rationale for Selecting Master Degrees of Freedom", Journal of Applied Mechanics, ASME, Vol. 102, 1980.

18. Dyka C. T., Ingel R. P. and Flippen L. D., "A new approach to dynamic condensation for FEM", Computers & Structures, Vol. 61, No. 4, pp. 763-773, 1996.

19. Flax A. H., Comment on “Reduction of Structural Frequency Equations", AIAA Journal, Vol. 13, No. 5, pp. 701-702, 1975.

20. Flippen L. D., "A theory of condensation model reduction", Computers and Mathematical Applications, Vol. 27 No. 2, pp. 9-40, 1994.

21. Foutch D. A., “The Effects of Vertical Earthquake Motions on the Response of Highway Bridges", Proceedings of the 3rd Conference on Dynamics Response of Structures, Engineering Mechanics Division, ASCE, Los Angeles, California, 1986.

22. Fox G. L., “A Method for Estimating the Error Induced by the Guyan Reduction", Shock and Vibration Bulletin, Vol. 51, pp. 19-24, 1981.

23. Friswell M. I., Garvey S. D. and Penny E. T., "Model Reduction Using Dynamic and Iterated IRS Techniques", Journal of Sound and Vibrations, 186(2), pp. 311-323, 1995.

24. Geradin M., “Error Bounds for Eigenvalue Analysis by Elimination of Variables", Journal of Sound and Vibration, Vol. 19, pp.111-132, 1971.

25. Goldberg J. H. and Herness E. D., “Vibration of Multistory Buildings Considering Floor and Wall Deformations", Bulletin of the Seismological Society of America, Vol. 55, No. 1, pp. 181-200, February 1965.

26. Guyan R. J., “Reduction of Stiffness and Mass Matrices", AIAA Journal, Vol. 3, No. 2, pp. 380, 1965.

27. Hanson R. D. and Degenkolb H. C., “The Venezuela Earthquake, July 29,1967", American Iron and Steel Institute, New York, 1969.

28. Henshell R. D. and Ong J. H., “Automatic Masters for Eigenvalue Economization", Earthquake Engineering and Structural Dynamics, Vol. 3, pp. 375-383, 1975.

29. Irons B. M., “Structural Eigenvalue Problems: Elimination of Unwanted Variables", AIAA Journal, Vol. 3, No. 5, pp. 961-962, 1965.

30. Iyengar R. N. and Shinozuka M., “Effect of Self-Weight and Vertical Acceleration on the Behavior of Tall Structures During Earthquake", Earthquake Engineering and Structural Dynamics, Vol. 1, pp. 69-78, 1972.

31. Jain S. K. and Jennings P. C., “Analytical Models for Low-Rise Buildings with Flexible Floor Diaphragms", Earthquake Engineering and Structural Dynamics, Vol. 13, pp. 225-241, 1985.

32. Johnson C.P., Craig R. R. and Yargicoglus A., “Quadratic Reduction for the Eigenproblem", International Journal for Numerical Methods in Engineering, Vol. 15, pp. 911-923, 1980.

33. Kammer D. C., “Test-Analysis- Model Development Using an Exact Modal Reduction", Journal of Modal Analysis, Vol. 2, No. 4, pp. 174-179, 1987.

34. Karadogan H. F., “Earthquake Analysis of 3D Structures with Flexible Floors", 7th World Conference on Earthquake Engineering, Istanbul, Turkey, 1980.

35. Kidder R. L., “Reduction of Structural Frequency Equations", AIAA Journal, Vol. 11, No. 6, pp. 892, 1973.

36. Kim K. O., "Hybrid dynamic condensation for eigenproblems", Computers & Structures, Vol. 56, pp. 105-112, 1995.

37. Kunnath Sashi K., Panahshahi Nader and Reinhorn Andrei M., "Seismic Response of Rc Buildings with Inelastic Floor Diaphragms", Journal of Structural Engineering, Vol. 117, No. 4, pp. 1218-1237, 1991.

38. La Framboise W., Warapius K., Kassawara R. P. and Costello S. D., "Vertical Seismic Analysis of Buildings and Floor Systems in the Nuclear Power Industry", 7th SMiRT Conference, Chicago, Illinois, Paper K5/4, 1983.

39. Lee J. P. and Chen C., "Vertical Responses of Nuclear Power Plant Structures Subject to Seismic Ground Motions", 3rd SMiRT Conference, London, United Kingdom, Paper K5/3, 1975.

40. Leung Y.-T., "An Accurate Method of Dynamic Condensation in Structural Analysis", International Journal for Numerical Methods in Engineering, Vol. 12, pp. 1705-1715, 1978.

41. Leung Y.-T., "An Accurate Method of Dynamic Substructuring with Simplified Computation", International Journal for Numerical Methods in Engineering, Vol. 14, pp. 1241-1256, 1979.

42. Leung Y.-T., "A Simple Dynamic Substructure Method", Earthquake Engineering and Structural Dynamics, Vol. 16, pp. 827-837, 1988.

43. Lin Y. K. and Shih T. Y., "Vertical Seismic Load Effect on Building Response", Journal of the Engineering Mechanics Division, ASCE, Vol. 107, No. EM2, pp. 331-343, April 1982.

44. Matta K. W., "Selection of Degrees of Freedom for Dynamic Analysis", Journal of Pressure Vessel Technology, Vol. 109, pp. 65-69, 1987.

45. Miller C. A., "Dynamic Reduction of Structural Models", Journal of Structural Engineering, ASCE, Vol. 106, No. ST10, pp. 2097-2108, 1980.

46. Nakashima M., Huang T. and Lu L. W., "Effect of Diaphragm Flexibility on Seismic Response of Building Structures", 8th World Conference on Earthquake Engineering, San Francisco, California, 1984.

47. O'Callahan J., "A procedure for an Improved Reduced System (IRS) model", Seventh International Modal Analysis Conference, Las Vegas, Nevada, Vol. I, pp. 17-21, 1989.

48. Ojalvo I. V. and Newman M., “Vibration Modes of Large Structures by an Automatic Matrix-Reduction Method", AIAA Journal, Vol. 8, No. 7, pp. 1234-1239, 1970.

49. Onen Y. H. and Tomac M. S., “Dynamic Analysis of Complete Building Structures", 7th European Conference on Earthquake Engineering, Athens, Greece, 1982.

50. Ong J. H., “Improved Automatic Masters for Eigenvalue Economization", Finite Elements and Design, Vol. 3, pp. 149-160, 1987.

51. Paz, M., “Practical Reduction of Structural Eigenproblems", Journal of Structural Engineering, ASCE, Vol. 109, No. 11, pp. 2591-2599, 1983.

52. Paz, M., “Dynamic Condensation", AIAA Journal, Vol. 22, No. 5, pp. 724-727, 1984.

53. Paz, M., “Modified Dynamic Condensation Method", Journal of Structural Engineering, ASCE, Vol. 115, No. 1, pp. 234- 238, 1989.

54. Penny J. E. T., Friswell M. I. and Garvey S. D., "Automatic choice of measurement locations for dynamics testing", AIAA Journal, Vol. 32, No. 2, pp. 407-414, 1994.

55. Perumalswami P. R. and Dala S., “Modeling of Slabs in Seismic Analysis of Nuclear Power Plant Buildings", Nuclear Engineering and Design, Vol. 47, pp. 135-143, 1978.

56. Pittelko H. P., “Vertical Forces in the Alaska Earthquake", Civil Engineering, ASCE, Vol. 35, No. 1, pp. 56-58, 1965.

57. Popplewell N., Bertels A. W. M. and Arya B., “A Critical Appraisal of the Elimination Technique", Journal of Sound and Vibration, Vol. 31, pp. 213-233, 1973.

58. Ramsden J. N. and Stoker J. R., “Mass Condensation: A Semi-Automatic Method for Reducing the Size of Vibration Problems", International Journal for Numerical Methods in Engineering, Vol. 1, pp. 333-349, 1969.

59. Razzaque A., "The Irons-Guyan reduction method with iterations", Proceedings of the 10th International Modal Analysis Conference, San Diego, California, Vol. I, pp. 137-145, 1992.

60. Reddy V. R. and Sharan A. M., “The Static and Dynamic Analyses of Machine Tools using Dynamic Matrix Reduction Technique", 4th International Modal Analysis Conference, Los Angeles CA, Vol. II, pp. 1104-1109, 1986.

61. Rothe K. and Voss H., "Improving condensation methods for eigenvalue problems via Rayleigh functionals", Computer Methods in Applied Mechanics and Engineering, Vol. 111, pp. 169-183, 1994.

62. Rouch K. E. and Kao J. S., “Dynamic Reduction in Rotor Dynamics by the Finite Element Method", Journal of Mechanical Design, Vol. 102, pp. 360-368, 1980. Sauer G., "Iterative improvement of eigensolutions from reduced matrices", Communications in Applied Numerical Methods, Vol. 5, pp. 329-335, 1989.

63. Sauer G., "Iterative improvement of eigensolutions from reduced matrices", Communications in Applied Numerical Methods, Vol.5, pp. 329-335, 1989.

64. Shah V. N. and Raymund M., “Analytical Selection of Masters for reduced Eigenvalue Problem", International Journal for Numerical Methods in Engineering, Vol. 18, pp. 89-98, 1982.

65. Shiau J. J., “Simplified Analysis of Vertical Vibrations", Journal of the Energy Division, ASCE, Vol. 105, No. EY2, pp. 251-264, August 1979.

66. Singh M. P. and Chu S. L., “Stochastic Considerations in Seismic Analysis of Structures", Earthquake Engineering and Structural Dynamics, Vol. 4, pp. 295-307, 1976.

67. Singh M. P. and Maldonado G. O., “An Improved Response Spectrum Method for Calculating Seismic Design Response. Part I: Classically Damped Structures", Earthquake Engineering and Structural Dynamics, Vol. 20, pp. 621-635, 1991.

68. Sotiropoulos G. H., “Dynamic Reduction Algorithms for the Structural Eigenproblem", Acta Mecanica, Vol. 50, pp. 231-248, 1984.

69. Suarez L. E. and Singh M. P., “Dynamic Condensation with Synthesis of Substructures Eigenproperties", Report No. VPI E-88-37, Virginia Polytechnic Institute & State University, Blacksburg, Virginia, 1988.

70. Syrmakezis C. A. and Chronopoulos M. P., “Diaphragm Action of Floor Systems of R. C. Buildings Under Earthquake Action", 8th European Conference on Earthquake Engineering, Lisbon, Portugal, 1986.

71. Thomas D. L., “Errors in Natural Frequency Calculations Using Eigenvalue Economization", International Journal for Numerical Methods in Engineering, Vol. 18, pp. 1521-1527, 1982.

72. Torkamani M. A.M. and Huang J. T., “Consideration of Floor Flexibility in Dynamic Analysis of High-Rise Buildings", 3rd U. S. National Conference on Earthquake Engineering, Charleston, South Carolina, 1986.

73. Unemori A. L., Roesset J. M. and Becker J. M., “Effect of Inplane Floor Slab Flexibility on the Response of Crosswall Buildings Systems", Reinforced Concrete Structures Subjected to Wind and Earthquake Forces, ACI publication SP 63, pp. 113-134, 1980.

74. Vysloukh V. A., Kandidov V. P. and Chesnokov S. S., “Reduction of Degrees of Freedom in Solving Dynamic Problems by the Finite Element Method", International Journal for numerical Methods in Engineering, Vol. 7, pp. 185-194, 1973.

75. Wittrick W. H. and Williams F. W., “A General Algorithm for Computing Natural Frequencies of Elastic Structures", Quarterly Journal of Mechanics and Applied Mathematics, Vol. 24, pp. 263-284, 1971.

76. Wolff F. H., Molnar A. J. and Gribik J. A., “Study of Guyan Reduction of Two Degree of Freedom Systems", Shock and Vibration Bulletin, Vol. 51, pp. 11-18, 1981.

77. Wyllie L. R. and Poland C. D., “A Documented Vertical Acceleration Failure", 2nd U.S.National Conference on Earthquake Engineering, Stanford, California, 1979.

78. Zingone G. and Muscolino G., “Dynamic Stability of Plane Elastic Frames", Journal of Sound and Vibration, Vol. 85, No. 3, pp. 397-406, 1982.

APPENDIX A

SEISMIC DESIGN RESPONSE

This appendix provides equations used for the calculation of various response quantities for the cascade approach presented in Chapter 6 for seismic motions defined by spectral density functions. The basic development of these formulas for response calculation is presented in References 66 and 67. They are provided here for the sake of completeness and for ready reference.

A.1) Response mean square value :

Mode Displacement Approach :

$$E\,[R^2(t)] = \sum_{j=1}^{N} \gamma_j^2\, \rho_j^2\, \frac{I_{1j}}{\omega_j^2} + 2 \sum_{j=1}^{N-1} \sum_{k=j+1}^{N} \gamma_j\, \gamma_k\, \rho_j\, \rho_k \left(\frac{A_1\, I_{1j} + r^2\, B_1\, I_{2j}}{\omega_j^2} + \frac{C_1\, I_{1k} + D_1\, I_{2k}}{\omega_k^2} \right) \qquad \text{(A.1)}$$

where :

N = number of modes

ω_j = jth natural frequency

β_j = jth modal damping ratio

γ_j = jth modal participation factor

ρ_j = value of the response quantity for the jth mode r = ω_j / ω_k

$I_{1j} = \int_{-\infty}^{+\infty} \omega_j^2 \; \Phi_a(\omega) \; |H_j(\omega)|^2 \; d\omega$

$I_{2j} = \int_{-\infty}^{+\infty} \omega^2 \; \Phi_a(\omega) \; |H_j(\omega)|^2 \; d\omega$

$\Phi_a(\omega)$ = absolute acceleration Power Spectral Density Function

$|H_j(\omega)|^2 = |H_j|^2$ = frequency response function = $\dfrac{1}{(\omega_j^2 - \omega^2)^2 + 4\,\beta_j^2\,\omega_j^2\,\omega^2}$

A.2) Absolute acceleration mean square value :

Modified Mode Displacement Approach :

$$E[\ddot{X}_u^2(t)] = C^2 I_0 + C\sum_{j=1}^{N} \gamma_j\,\phi_j(u)\,\omega_j^2\,\left\{2\,(I_{1j} - I_{2j}) + 8\,\beta_j^2\,I_{2j}\right\} + \sum_{j=1}^{N} \gamma_j^2\,\phi_j^2(u)\,\omega_j^2\,\left(I_{1j} + 4\,\beta_j^2\,I_{2j}\right)$$
$$+ 2\sum_{j=1}^{N-1}\sum_{k=j+1}^{N} \gamma_j\,\gamma_k\,\phi_j(u)\,\phi_k(u)\,\omega_k^2\left(\frac{A_2\,I_{1j}}{r^2} + B_2\,I_{2j} + C_2\,I_{1k} + D_2\,I_{2k}\right) \qquad (A.2)$$

where :

$\phi_j(u)$ = jth modal displacement of coordinates u

$C = 1 - \sum_{j=1}^{j_r} \gamma_j\,\phi_j$

$I_0 = \int_{-\infty}^{+\infty} \Phi_g(\omega)\; d\omega$

$\Phi_g(\omega)$ = Kanai-Tajimi Power Spectral Density Function

$= S_0 \sum_g S_g\,(\omega_g^4 + 4\,\beta_g^2\,\omega_g^2\,\omega^2)\,|H_g|^2$

ω_g = dominant ground frequency

β_g = dominant ground damping factor

$|H_g|^2$ = ground frequency response function

A.3) Oscillator mean square absolute acceleration :

$$E\left[\ddot{X}_o^2(t)\right] = \omega_o^2 \left(I_{1o} + 4\,\beta_o^2\, I_{2o} \right) \tag{A.3}$$

where :

ω_o = oscillator's natural frequency

β_o = oscillator's modal damping ratio

A.4) Partial fraction coefficients A_i, B_i, C_i and D_i :

Constants A_i, B_i, C_i and D_i are obtained from the solution of the following simultaneous equations :

$$[M_{jk}] \left\{ K \right\} = \left\{ P \right\} \tag{A.4}$$

$$\begin{bmatrix} 1 & 0 & r^4 & 0 \\ 2\,(2\,\beta_k^2 - 1) & 1 & 2r^2\,(2\,\beta_j^2 - 1) & r^4 \\ 1 & 2\,(2\,\beta_k^2 - 1) & 1 & 2r^2\,(2\,\beta_j^2 - 1) \\ 0 & 1 & 0 & 1 \end{bmatrix} \begin{Bmatrix} A \\ B \\ C \\ D \end{Bmatrix}_i = \begin{Bmatrix} P_1 \\ P_2 \\ P_3 \\ P_4 \end{Bmatrix}_i$$

For response mean square values :

$$\left\{ P \right\}_1 = \begin{Bmatrix} r^2 \\ -\left(r^2 - 4\,\beta_j\,\beta_k\, r + 1 \right) \\ 1 \\ 0 \end{Bmatrix} \tag{A.5}$$

For the absolute acceleration mean square values :

$$\left\{ \mathrm{P} \right\}_2 = \left\{ \begin{array}{c} \mathrm{r}^4 \\ \mathrm{r}^2 \left[4 \left(\beta_j^2 + \mathrm{r}^2 \beta_k^2 \right) - \mathrm{r}^2 - 1 \right] \\ \mathrm{r}^2 \left[16 \beta_j^2 \beta_k^2 - 4 \left(\beta_j^2 + \beta_k^2 \right) + 1 \right] \\ 4 \beta_j \beta_k \mathrm{r} \end{array} \right\} \tag{A.6}$$

A.5) Power Spectral Density Functions :

A.5.1) Cascade approach :

Power Spectral Density Function of the absolute acceleration of point u on the structure, Figures A.1 and A.2 :

$$\Phi_u(\omega) = \sum_{j=1}^{M} \gamma_j^2 \, \phi_j^2(u) \, \omega_j^2 \, \left\{ \omega_j^2 + 4 \beta_j^2 \omega^2 \right\} \, |\mathrm{H}_j|^2 \, \Phi_g(\omega) \tag{A.7}$$

$$+ 2 \sum_{j=1}^{M-1} \sum_{k=j+1}^{M} k_{jk} \left\{ \left(\frac{\omega_j^2 \ \mathrm{A}_{2jk}}{\mathrm{r}_{jk}^2} + \omega^2 \ \mathrm{B}_{2jk} \right) |\mathrm{H}_j|^2 + \left(\omega_k^2 \ \mathrm{C}_{2jk} + \omega^2 \ \mathrm{D}_{2jk} \right) |\mathrm{H}_k|^2 \right\} \Phi_g(\omega)$$

where :

$$k_{jk} = \gamma_j \, \gamma_k \, \phi_j(u) \, \phi_k(u) \, \omega_k^2 \tag{A.7a}$$

M = number of vibration modes

$\mathrm{r}_{jk} = \omega_j / \omega_k$

A_{2jk}, B_{2jk}, C_{2jk} and D_{2jk} are obtained from the solution of equation (A.4) and $\{\mathrm{P}_i\}$ is given in (A.6).

A.5.2) Double cascade approach :

Power Spectral Density Function of the absolute acceleration of point p on the floor slab, Figures A.3 :

$$\Phi_p(\omega) = \sum_{l=1}^{N} \gamma_l^2\ \phi_l^2\ (p)\ \omega_l^2\ \ \{\ \omega_l^2 + 4\ \beta_l^2\ \omega^2\ \}\ \ |\mathrm{H}_l|^{\,2}\ \ \Phi_u(\omega) \tag{A.8}$$

$$+\ 2\sum_{l=1}^{N-1}\ \sum_{m=l+1}^{N} k_{lm}\left\{\left(\frac{\omega_l^2\ \mathrm{A}_{2lm}}{\mathrm{r}_{lm}^2} + \omega^2\ \mathrm{B}_{2lm}\right)|\mathrm{H}_l|^{\,2} + (\omega_m^2\ \mathrm{C}_{2lm} + \omega^2\ \mathrm{D}_{2lm})|\mathrm{H}_m|^{\,2}\right\}\Phi_u(\omega)$$

where :

N = number of vibration modes of flexible floor slab

$$k_{lm} = \gamma_l\ \gamma_m\ \phi_l\ (u)\ \phi_m\ (u)\ \omega_l^2 \tag{A.8a}$$

$$\mathrm{r}_{lm}\ =\ \omega_l\ /\ \omega_m \tag{A.8b}$$

A_{2lm}, B_{2lm}, C_{2lm} and D_{2lm} are obtained from the solution of equation (A.4) and $\{\mathrm{P}_i\}$ is given in (A.6).

$\Phi_p(\omega)$ can be express as :

$$= \sum_{l=1}^{N}\sum_{j=1}^{M} K_{lj}\left\{\left(\frac{\omega_l^2\ \mathrm{A}_{3lj}}{\mathrm{r}_{lj}^2} + \omega^2\ \mathrm{B}_{3lj}\right)|\mathrm{H}_l|^{\,2} + \left(\ \omega_j^2\ \mathrm{C}_{3lj} + \omega^2\ \mathrm{D}_{3lj}\ \right)|\mathrm{H}_j|^{\,2}\right\}\Phi_g(\omega)$$

$$+\ 2\sum_{l=1}^{N}\ \sum_{j=1}^{M-1}\ \sum_{k=j+1}^{M} K_{ljk}\left\{\left(\ \omega_l^2\left(\frac{\mathrm{A}_{4lj}}{\mathrm{r}_{lj}^2} + \frac{\mathrm{A}_{5lk}}{\mathrm{r}_{lk}^2}\right) + \omega^2(\ \mathrm{B}_{4lj} + \mathrm{B}_{5lk}\ )\right)|\mathrm{H}_l|^{\,2}\right.$$

$$\left. +\ \left(\ \omega_j^2\ \mathrm{C}_{4lj} + \omega^2\ \mathrm{D}_{4lj}\ \right)|\mathrm{H}_j|^{\,2} + \left(\ \omega_k^2\ \mathrm{C}_{5lk} + \omega^2\ \mathrm{D}_{5lk}\ \right)|\mathrm{H}_k|^{\,2}\right\}\Phi_g(\omega)$$

$$+\ 2\sum_{l=1}^{N-1}\ \sum_{m=l+1}^{N}\ \sum_{j=1}^{M} K_{lmj}\left\{\left(\frac{\omega_l^2\ \mathrm{A}_{6lj}}{\mathrm{r}_{lj}^2} + \omega^2\ \mathrm{B}_{6lj}\right)|\mathrm{H}_l|^{\,2} + \left(\frac{\omega_m^2\ \mathrm{A}_{7mj}}{\mathrm{r}_{mj}^2} + \omega^2\ \mathrm{B}_{7mj}\right)|\mathrm{H}_m|^{\,2}\right.$$

$$\left. +\ \left(\ \omega_j^2\ (\ \mathrm{C}_{6lj} + \mathrm{C}_{7mj}\ ) + \omega^2(\ \mathrm{D}_{6lj} + \mathrm{D}_{7mj}\ )\right)|\mathrm{H}_j|^{\,2}\right\}\Phi_g(\omega)$$

$$+ 4\sum_{l=1}^{N-1} \sum_{m=l+1}^{N} \sum_{j=1}^{M-1} \sum_{k=j+1}^{M} K_{lmjk}\Bigg\{ \Bigg(\omega_l^2 \Bigg(\frac{A_{8lj}}{r_{lj}^2} + \frac{A_{9lk}}{r_{lk}^2} \Bigg) + \omega^2 (B_{8lj} + B_{9lk}) \Bigg) |H_l|^2$$

$$+ \Bigg(\omega_m^2 \Bigg(\frac{A_{10mj}}{r_{mj}^2} + \frac{A_{11mk}}{r_{mk}^2} \Bigg) + \omega^2 (B_{10mj} + B_{11mk}) \Bigg) |H_m|^2$$

$$+ \big(\omega_j^2 (C_{8lj} + C_{10mj}) + \omega^2 (D_{8lj} + D_{10mj}) \big) |H_j|^2$$

$$+ (\omega_k^2 (C_{9lk} + C_{11mk}) + \omega^2 (D_{9lk} + D_{11mk})) |H_k|^2 \Big\} \Phi_g(\omega) \qquad \text{(A.9)}$$

where :

$$K_{lj} = \gamma_l^2 \ \phi_l^2(p) \ \omega_l^2 \ \gamma_j^2 \ \phi_j^2(u) \ \omega_j^2 \qquad \text{(A.9a)}$$

$$K_{ljk} = \gamma_l^2 \ \phi_l^2(p) \ \omega_l^2 \ \gamma_j \ \phi_j(u) \ \gamma_k \ \phi_k(u) \ \omega_k^2 \qquad \text{(A.9b)}$$

$$K_{lmj} = \gamma_l \ \phi_l(p) \ \gamma_m \ \phi_m(p) \ \omega_m^2 \ \gamma_j^2 \ \phi_j^2(u) \ \omega_j^2 \qquad \text{(A.9c)}$$

$$K_{lmjk} = \gamma_l \ \phi_l(p) \ \gamma_m \ \phi_m(p) \ \omega_m^2 \ \gamma_j \ \phi_j(u) \ \gamma_k \ \phi_k(u) \ \omega_k^2 \qquad \text{(A.9d)}$$

A_{ixy}, B_{ixy}, C_{ixy} and D_{ixy} are obtained from the solution of equation (A.4) and $\{P_i\}$ is given by :

$$\omega_j^2 \ P_{3lj} = \{ r_{lj}^2 , \ 4 (\beta_j^2 + \beta_l^2 \ r_{lj}^2) , \ 16 \ \beta_l^2 \ \beta_j^2 , \ 0 \} \qquad \text{(A.10a)}$$

$$\omega_j^2 \ P_{4lj} = \left\{ \frac{r_{lj}^2 \ A_{1jk}}{r_{jk}^2} , \ \frac{4 \ \beta_l^2 \ r_{lj}^2 \ A_{1jk}}{r_{jk}^2} + B_{1jk} , \ 4 \ \beta_l^2 \ B_{1jk} , \ 0 \right\} \qquad \text{(A.10b)}$$

$$\omega_k^2 \ P_{5lk} = \{ r_{lk}^2 \ C_{1jk} , \ 4 \ \beta_l^2 \ r_{lk}^2 \ C_{1jk} + D_{1jk} , \ 4 \ \beta_l^2 \ D_{1jk} , \ 0 \} \qquad \text{(A.10c)}$$

$$\omega_j^2 \ P_{6lj} = \left\{ \frac{r_{lj}^2 \ A_{2lm}}{r_{lm}^2} , \ \frac{4 \ \beta_j^2 \ A_{2lm}}{r_{lm}^2} + r_{lj}^2 \ B_{2lm} , \ 4 \ \beta_j^2 \ B_{2lm} , \ 0 \right\} \qquad \text{(A.10d)}$$

$$\omega_j^2\ P_{7mj} = \left\{\ r_{mj}^2\ C_{2lm}\ ,\ 4\ \beta_j^2\ C_{2lm} + r_{mj}^2\ D_{2lm}\ ,\ 4\ \beta_j^2\ D_{2lm}\ ,\ 0\ \right\} \tag{A.10e}$$

$$\omega_j^2\ P_{8lj} = \left\{\ \frac{r_{lj}^2\ A_{2lm}\ A_{1jk}}{r_{lm}^2\ \ r_{jk}^2}\ ,\ \frac{A_{2lm}\ B_{1jk}}{r_{lm}^2} + \frac{r_{lj}^2\ B_{2lm}\ A_{1jk}}{r_{jk}^2}\ ,\ B_{2lm}\ B_{1jk}\ ,\ 0\ \right\} \tag{A.10f}$$

$$\omega_k^2\ P_{9lk} = \left\{\ \frac{r_{lk}^2\ A_{2lm}\ C_{1jk}}{r_{lm}^2}\ ,\ \frac{A_{2lm}\ D_{1jk}}{r_{lm}^2} + r_{lk}^2\ B_{2lm}\ C_{1jk}\ ,\ B_{2lm}\ D_{1jk}\ ,\ 0\ \right\} \tag{A.10g}$$

$$\omega_j^2\ W_{10mj} = \left\{\ \frac{r_{mj}^2\ C_{2lm}\ A_{1jk}}{r_{jk}^2}\ ,\ C_{2lm}\ B_{1jk} + \frac{r_{mj}^2\ D_{2lm}\ A_{1jk}}{r_{jk}^2}\ ,\ D_{2lm}\ B_{1jk}\ ,\ 0\ \right\} \tag{A.10h}$$

$$\omega_k^2\ W_{11mk} = \{\ r_{mk}^2\ C_{2lm}\ C_{1jk}\ ,\ C_{2lm}\ D_{1jk} + r_{mk}^2\ D_{2lm}\ C_{1jk}\ ,\ D_{2lm}\ D_{1jk}\ ,\ 0\ \} \tag{A.10i}$$

where :

$$r_{xy} = \omega_x\ /\ \omega_y \tag{A.10j}$$

A.6) Frequency Integrals I_{1i} and I_{2i} :

A.6.1) Vertical ground excitation, $\Phi_a(\omega) = \Phi_g(\omega)$:

1) Mean Square Pseudo Velocity Ground Spectra

$$I_{1i}\ (\ \omega_i\ ,\ \beta_i\ )\ =\ \omega_i^2 \int_{-\infty}^{+\infty}\ \Phi_g(\omega)\ \ |H_i\ (\omega)|^{\,2}\ \ d\omega\ =\ \omega_i^2\ \ R_{1i} \tag{A.11}$$

2) Mean Square Relative Velocity Ground Spectra

$$I_{2i}\ (\ \omega_i\ ,\ \beta_i\ )\ =\ \int_{-\infty}^{+\infty}\ \omega^2\ \ \Phi_g(\omega)\ \ |H_i\ (\omega)|^{\,2}\ \ d\omega\ =\ R_{2i} \tag{A.12}$$

A.6.2) Cascade approach, $\Phi_a(\omega) = \Phi_u(\omega)$:

1) Mean Square Auto Pseudo Velocity Floor Spectra

$$\mathrm{I}_{1i}\,(\omega_i\,,\,\beta_i\,) \;=\; \omega_i^2 \int_{-\infty}^{+\infty} \Phi_u\,(\omega)\;\; |\mathrm{H}_i\,(\omega)|^{\,2}\;\; d\omega$$

$$=\;\omega_i^2\;\left\{\;\sum_{j=1}^{M}\gamma_j^2\;\phi_j^2\;(u)\;\omega_j^2\left(\;\omega_j^2\;\;\hat{\mathrm{I}}_{1j}+4\;\beta_j^2\;\;\hat{\mathrm{I}}_{2j}\;\right)\right.$$

$$\left.+\;\;2\sum_{j=1}^{M-1}\;\;\sum_{k=j+1}^{M}k_{jk}\;\left(\;\frac{\omega_j^2\;\mathrm{A}_1\;\hat{\mathrm{I}}_{1j}}{\mathrm{r}^2}+\mathrm{B}_1\;\hat{\mathrm{I}}_{2j}+\omega_k^2\;\mathrm{C}_1\;\hat{\mathrm{I}}_{1k}+\mathrm{D}_1\;\hat{\mathrm{I}}_{2k}\;\right)\;\right\} \qquad \text{(A.13)}$$

2) Mean Square Auto Velocity Floor Spectra

$$\mathrm{I}_{2i}\,(\omega_i\,,\,\beta_i\,) \;=\; \int_{-\infty}^{+\infty}\;\omega^2\;\;\Phi_u\,(\omega)\;\;|\mathrm{H}_i\,(\omega)|^{\,2}\;\;d\omega$$

$$=\sum_{j=1}^{M}\gamma_j^2\;\phi_j^2\;(u)\;\omega_j^2\;\;\left\{\;\omega_j^2\;\;\hat{\mathrm{I}}_{2j}+4\;\beta_j^2\;\;\hat{\mathrm{I}}_{3j}\;\right\} \qquad \text{(A.14)}$$

$$+\;\;2\sum_{j=1}^{M-1}\;\;\sum_{k=j+1}^{M}\gamma_j\;\gamma_k\;\phi_j\;(u)\;\phi_k\;(u)\;\omega_k^2\;\;\left\{\;\frac{\omega_j^2\;\mathrm{A}_1\;\hat{\mathrm{I}}_{2j}}{\mathrm{r}^2}+\mathrm{B}_1\;\hat{\mathrm{I}}_{3j}+\mathrm{C}_1\;\omega_k^2\;\hat{\mathrm{I}}_{2k}+\mathrm{D}_1\;\hat{\mathrm{I}}_{3k}\;\right\}$$

where

$$\hat{\mathrm{I}}_{nr}\;(\omega_i,\,\beta_i)\;=\int_{-\infty}^{+\infty}\;\omega^{2(n-1)}\;\;\Phi_g(\omega)\;\;|\mathrm{H}_r(\omega)|^{\,2}\;\;|\mathrm{H}_i(\omega)|^{\,2}\;\;d\omega \qquad \text{(A.15)}$$

A.6.3) Double cascade approach, $\Phi_a\,(\omega) = \Phi_p\,(\omega)$:

1) Mean Square Auto Pseudo Velocity Floor Spectra

$$\mathrm{I}_{1o}\;=\;\omega_o^2\int_{-\infty}^{+\infty}\Phi_p\,(\omega)\;\;|\mathrm{H}_o\,(\omega)|^{\,2}\;\;d\omega$$

$$=\;\omega_o^2\;\sum_{l=1}^{N}\;\sum_{j=1}^{M}K_{lj}\;\left\{\;\left(\;\mathrm{A}_{3jl}\,\hat{\mathrm{I}}_{1j}+\mathrm{B}_{3jl}\,\hat{\mathrm{I}}_{2j}\right)\;+\;\left(\;\mathrm{C}_{3jl}\,\hat{\mathrm{I}}_{1l}+\mathrm{D}_{3jl}\,\hat{\mathrm{I}}_{2l}\;\right)\;\right\}$$

$$+ \; 2\,\omega_o^2 \sum_{l=1}^{N} \sum_{j=1}^{M-1} \sum_{k=j+1}^{M} K_{ljk} \; \Big\{ \; A_{4jl}\,\hat{I}_{1j} \; + \; B_{4jl}\,\hat{I}_{2j} \; + \; A_{5kl}\,\hat{I}_{1k} \; + \; B_{5kl}\,\hat{I}_{2k}$$

$$+ \; (\,C_{4jl} + C_{5kl}\,)\,\hat{I}_{1l} \; + \; (\,D_{4jl} + D_{5kl}\,)\,\hat{I}_{2l} \; \Big\}$$

$$+ \; 2\,\omega_o^2 \sum_{l=1}^{N-1} \sum_{m=l+1}^{N} \sum_{j=1}^{M} K_{lmj} \; \Big\{ \; (\,A_{6jl} + A_{7jm}\,)\,\hat{I}_{1j} \; + \; (\,B_{6jl} + B_{7jm}\,)\,\hat{I}_{2j}$$

$$+ \; C_{6jl}\,\hat{I}_{1j} \; + \; D_{6jl}\,\hat{I}_{2l} \; + \; C_{7jm}\,\hat{I}_{1m} \; + \; D_{7jm}\,\hat{I}_{2m} \; \Big\}$$

$$+ \; 4\,\omega_o^2 \sum_{l=1}^{N-1} \sum_{m=l+1}^{N} \sum_{j=1}^{M-1} \sum_{k=j+1}^{M} K_{lmjk} \; \Big\{ \; (\,A_{8jl} + A_{9jm}\,)\,\hat{I}_{1j} \; + \; (\,B_{8jl} + B_{9jm}\,)\,\hat{I}_{2j}$$

$$+ \; (\,A_{10kl} + A_{11km}\,)\,\hat{I}_{1k} \; + \; (\,B_{10kl} + B_{11km}\,)\,\hat{I}_{2k}$$

$$+ \; (\,C_{8jl} + C_{10kl}\,)\,\hat{I}_{1l} \; + \; (\,D_{8jl} + D_{10kl}\,)\,\hat{I}_{2l}$$

$$+ \; (\,C_{9jm} + C_{11km}\,)\,\hat{I}_{1m} \; + \; (\,D_{9jm} + D_{11km}\,)\,\hat{I}_{2m} \; \Big\} \qquad \text{(A.16)}$$

2) Mean Square Auto Velocity Floor Spectra

$$I_{2o} = \int_{-\infty}^{+\infty} \omega^2 \;\; \Phi_p(\omega) \;\; |H_o(\omega)|^2 \;\; d\omega$$

$$= \sum_{l=1}^{N} \sum_{j=1}^{M} K_{lj} \; \Big\{ \; \Big(A_{3jl}\,\hat{I}_{2j} + B_{3jl}\,\hat{I}_{3j} \Big) \; + \; \Big(C_{3jl}\,\hat{I}_{2l} + D_{3jl}\,\hat{I}_{3l} \Big) \; \Big\}$$

$$+ \; 2 \sum_{l=1}^{N} \sum_{j=1}^{M-1} \sum_{k=j+1}^{M} K_{ljk} \; \Big\{ \; A_{4jl}\,\hat{I}_{2j} \; + \; B_{4jl}\,\hat{I}_{3j} \; + \; A_{5kl}\,\hat{I}_{2k} \; + \; B_{5kl}\,\hat{I}_{3k}$$

$$+ \; (\,C_{4jl} + C_{5kl}\,)\,\hat{I}_{2l} \; + \; (\,D_{4jl} + D_{5kl}\,)\,\hat{I}_{3l} \; \Big\}$$

$$+ \; 2 \sum_{l=1}^{N-1} \sum_{m=l+1}^{N} \sum_{j=1}^{M} K_{lmj} \; \Big\{ \; (\,A_{6jl} + A_{7jm}\,)\,\hat{I}_{2j} \; + \; (\,B_{6jl} + B_{7jm}\,)\,\hat{I}_{3j}$$

$$+\ C_{6jl}\,\hat{I}_{2j} + D_{6jl}\,\hat{I}_{3l} + C_{7jm}\,\hat{I}_{2m} + D_{7jm}\,\hat{I}_{3m} \Big\}$$

$$+\ 4 \sum_{l=1}^{N-1} \sum_{m=l+1}^{N} \sum_{j=1}^{M-1} \sum_{k=j+1}^{M} K_{lmjk} \Big\{ (A_{8jl} + A_{9jm})\,\hat{I}_{2j} + (B_{8jl} + B_{9jm})\,\hat{I}_{3j}$$

$$+ (A_{10kl} + A_{11km})\,\hat{I}_{2k} + (B_{10kl} + B_{11km})\,\hat{I}_{3k}$$

$$+ (C_{8jl} + C_{10kl})\,\hat{I}_{2l} + (D_{8jl} + D_{10kl})\,\hat{I}_{3l}$$

$$+ (C_{9jm} + C_{11km})\,\hat{I}_{2m} + (D_{9jm} + D_{11km})\,\hat{I}_{3m} \Big\} \qquad \text{(A.17)}$$

A.7) Closed-form solution of frequency integrals R_{ni} :

$$R_{ni}(\omega_i, \beta_i) = \int_{-\infty}^{+\infty} \omega^{2(n-1)}\, \Phi_g(\omega)\, |H_i(\omega)|^2 \, d\omega$$

$$= -\pi\ S_0 \left(\sum_{g=1}^{N_g} S_g \frac{b_0\, d_1 + b_1\, d_2 + b_2\, d_3 + b_3\, d_4}{a_1\, d_1 + a_3\, d_2} \right) \qquad \text{(A.18)}$$

where :

$$a_0 = 1 \qquad \text{(A.19a)}$$

$$a_1 = -2\,(\beta_g\,\omega_g + \beta_i\,\omega_i) \qquad \text{(A.19b)}$$

$$a_2 = -(\omega_g^2 + \omega_i^2 + 4\,\beta_g\,\omega_g\,\beta_i\,\omega_i) \qquad \text{(A.19c)}$$

$$a_3 = 2\,\omega_g\,\omega_i\,(\beta_g\,\omega_i + \beta_i\,\omega_g) \qquad \text{(A.19d)}$$

$$a_4 = \omega_g^2\,\omega_i^2 \qquad \text{(A.19e)}$$

$$d_1 = a_4\,(a_2\,a_3 - a_1\,a_4) \qquad \text{(A.20a)}$$

$$d_2 = -a_0\,a_3\,a_4 \qquad \text{(A.20b)}$$

$$d_3 = a_0\ a_1\ a_4 \tag{A.20c}$$

$$d_4 = -\ a_0\ (\ a_0\ a_3 - a_1\ a_2\ ) \tag{A.20d}$$

For $n = 1$

$$b_0 = b_1 = 0 \tag{A.21a}$$

$$b_2 = 4\ \beta_g^2\ \omega_g^2 \tag{A.21b}$$

$$b_3 = \omega_g^4 \tag{A.21c}$$

For $n = 2$

$$b_0 = b_3 = 0 \tag{A.22a}$$

$$b_1 = 4\ \beta_g^2\ \omega_g^2 \tag{A.22b}$$

$$b_2 = \omega_g^4 \tag{A.22c}$$

A.8) Closed-form solution of frequency integrals $\hat{I}_{nr}$:

$$\hat{I}_{nr}\ (\omega_i,\ \beta_i)\ = \int_{-\infty}^{+\infty}\ \omega^{2(n-1)}\ \ \Phi_g(\omega)\ \ |H_r(\omega)|^{\ 2}\ \ |H_i(\omega)|^{\ 2}\ \ d\omega$$

$$= -\ \pi\ S_0\ \left(\ \sum_{g=1}^{N_g}\ S_g\ \ \frac{b_0\ d_1 + b_1\ d_2 + b_2\ d_3 + b_3\ d_4 + b_4\ d_5 + b_5\ d_6}{a_1\ d_1 + a_3\ d_2 + a_5\ d_3}\ \right) \tag{A.23}$$

where :

$$a_0 = 1 \tag{A.24a}$$

$$a_1 = -\ 2\ (\ \beta_g\ \omega_g + \beta_r\ \omega_r + \beta_i\ \omega_i\ )$$

$$a_2 = -\ (\ \omega_g^2 + \omega_r^2 + \omega_i^2\ ) - 4\ (\ \beta_g\ \omega_g\ \beta_r\ \omega_r + \beta_g\ \omega_g\ \beta_i\ \omega_i + \beta_r\ \omega_r\ \beta_i\ \omega_i\ ) \tag{A.24b}$$

$$a_3 = 2\ \omega_g\ \omega_r\ (\ \beta_g\ \omega_r + \beta_r\ \omega_g\ ) + 2\ \omega_g\ \omega_i\ (\ \beta_g\ \omega_i + \beta_i\ \omega_g\ ) \tag{A.24c}$$

$$+ 2\,\omega_r\,\omega_i\,(\,\beta_r\,\omega_i + \beta_i\,\omega_r\,) + 8\,\beta_g\,\omega_g\,\beta_r\,\omega_r\,\beta_i\,\omega_i \tag{A.24d}$$

$$\mathrm{a}_4 = 4\,\omega_g\,\omega_r\,\omega_i\,(\,\beta_r\,\beta_i\,\omega_g + \beta_g\,\beta_i\,\omega_r + \beta_g\,\beta_r\,\omega_i\,) + \omega_g^2\,\omega_r^2 + \omega_g^2\,\omega_i^2$$

$$+ \omega_r^2\,\omega_i^2 \tag{A.24e}$$

$$\mathrm{a}_5 = -\,2\,\omega_g\,\omega_r\,\omega_i\,(\,\beta_i\,\omega_g\,\omega_r + \beta_r\,\omega_g\,\omega_i + \beta_g\,\omega_r\,\omega_i\,) \tag{A.24f}$$

$$\mathrm{a}_6 = -\,\omega_g^2\,\omega_r^2\,\omega_i^2 \tag{A.24g}$$

$$\mathrm{d}_1 = \mathrm{a}_5\,\mathrm{a}_6\,\{\,\mathrm{a}_2\,(\,\mathrm{a}_3\,\mathrm{a}_4 - \mathrm{a}_2\,\mathrm{a}_5\,) + \mathrm{a}_4\,(\,\mathrm{a}_0\,\mathrm{a}_5 - \mathrm{a}_1\,\mathrm{a}_4\,) + \mathrm{a}_6\,(\,\mathrm{a}_1\,\mathrm{a}_2 - \mathrm{a}_0\,\mathrm{a}_3\,)\,\}$$

$$+ \mathrm{a}_6^2\,\{\,\mathrm{a}_1\,(\,\mathrm{a}_3\,\mathrm{a}_4 - \mathrm{a}_1\,\mathrm{a}_6\,) + \mathrm{a}_2\,(\,\mathrm{a}_1\,\mathrm{a}_5 - \mathrm{a}_3^2\,)\,\} \tag{A.25a}$$

$$\mathrm{d}_2 = \mathrm{a}_0\,\mathrm{a}_6\,\{\,\mathrm{a}_3\,(\,\mathrm{a}_3\,\mathrm{a}_6 - \mathrm{a}_4\,\mathrm{a}_5\,) + \mathrm{a}_5\,(\,\mathrm{a}_2\,\mathrm{a}_5 - \mathrm{a}_1\,\mathrm{a}_6\,)\,\} \tag{A.25b}$$

$$\mathrm{d}_3 = \mathrm{a}_0\,\mathrm{a}_6\,\{\,\mathrm{a}_1\,(\,\mathrm{a}_4\,\mathrm{a}_5 - \mathrm{a}_3\,\mathrm{a}_6\,) - \mathrm{a}_0\,\mathrm{a}_5^2\,\} \tag{A.25c}$$

$$\mathrm{d}_4 = \mathrm{a}_0\,\mathrm{a}_6\,\{\,\mathrm{a}_0\,\mathrm{a}_3\,\mathrm{a}_5 + \mathrm{a}_1\,(\,\mathrm{a}_1\,\mathrm{a}_6 - \mathrm{a}_2\,\mathrm{a}_5\,)\,\} \tag{A.25d}$$

$$\mathrm{d}_5 = \mathrm{a}_0\,\mathrm{a}_6\,\{\,\mathrm{a}_0\,(\,\mathrm{a}_1\,\mathrm{a}_5 - \mathrm{a}_3^2\,) + \mathrm{a}_1\,(\,\mathrm{a}_2\,\mathrm{a}_3 - \mathrm{a}_1\,\mathrm{a}_4\,)\,\} \tag{A.25e}$$

$$\mathrm{d}_6 = \mathrm{a}_0\,\mathrm{a}_1\,\{\,\mathrm{a}_2\,(\,\mathrm{a}_2\,\mathrm{a}_5 - \mathrm{a}_3\,\mathrm{a}_4\,) + \mathrm{a}_4\,(\,\mathrm{a}_1\,\mathrm{a}_4 - \mathrm{a}_0\,\mathrm{a}_5\,) + \mathrm{a}_6\,(\,\mathrm{a}_0\,\mathrm{a}_3 - \mathrm{a}_1\,\mathrm{a}_2\,)\,\}$$

$$+ \mathrm{a}_0^2\,\{\,\mathrm{a}_3\,(\,\mathrm{a}_3\,\mathrm{a}_4 - \mathrm{a}_2\,\mathrm{a}_5\,) + \mathrm{a}_5\,(\,\mathrm{a}_0\,\mathrm{a}_5 - \mathrm{a}_1\,\mathrm{a}_4\,)\,\} \tag{A.25f}$$

For $n = 1$

$$\mathrm{b}_0 = \mathrm{b}_1 = \mathrm{b}_2 = \mathrm{b}_3 = 0 \tag{A.26a}$$

$$\mathrm{b}_4 = 4\,\beta_g^2\,\omega_g^2 \tag{A.26b}$$

$$\mathrm{b}_5 = \omega_g^4 \tag{A.26c}$$

For $n = 2$

$$\mathrm{b}_0 = \mathrm{b}_1 = \mathrm{b}_2 = \mathrm{b}_5 = 0 \tag{A.27a}$$

$$\mathrm{b}_3 = 4\,\beta_g^2\,\omega_g^2 \tag{A.27b}$$

$$\mathrm{b}_4 = \omega_g^4 \tag{A.27c}$$

For n = 3

$$b_0 = b_1 = b_4 = b_5 = 0 \tag{A.28a}$$

$$b_2 = 4\,\beta_g^2\,\omega_g^2 \tag{A.28b}$$

$$b_3 = \omega_g^4 \tag{A.28c}$$

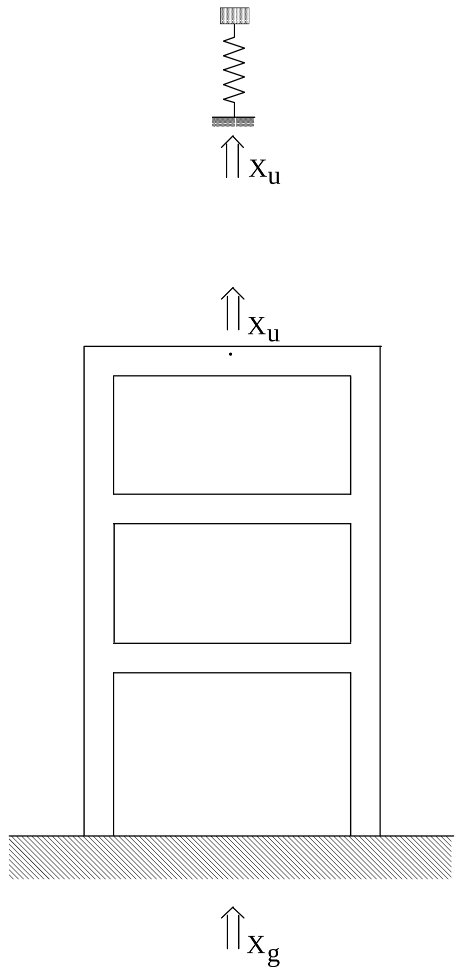

Figure A.1 Cascade analysis of an oscillator on the third floor slab subjected to vertical seismic excitations.

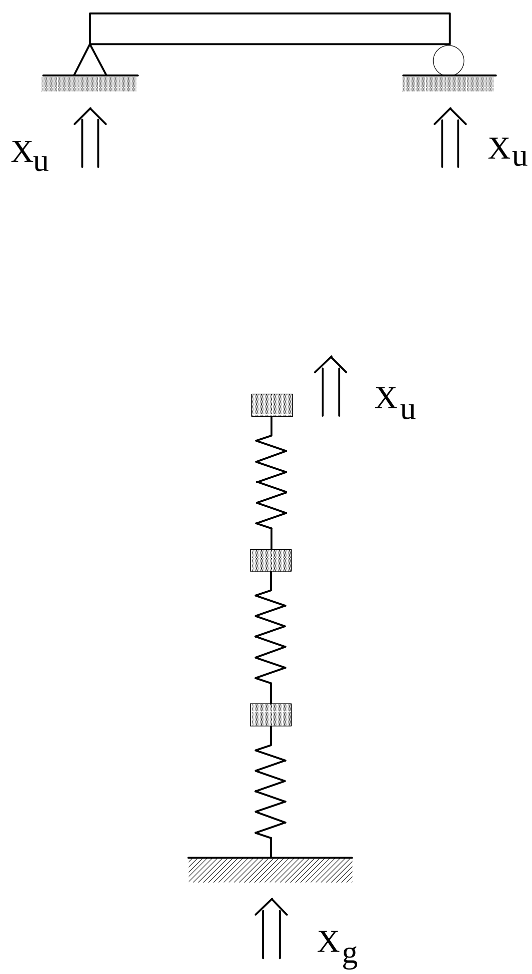

Figure A.2 Cascade analysis of the third floor slab subjected to vertical seismic excitations.

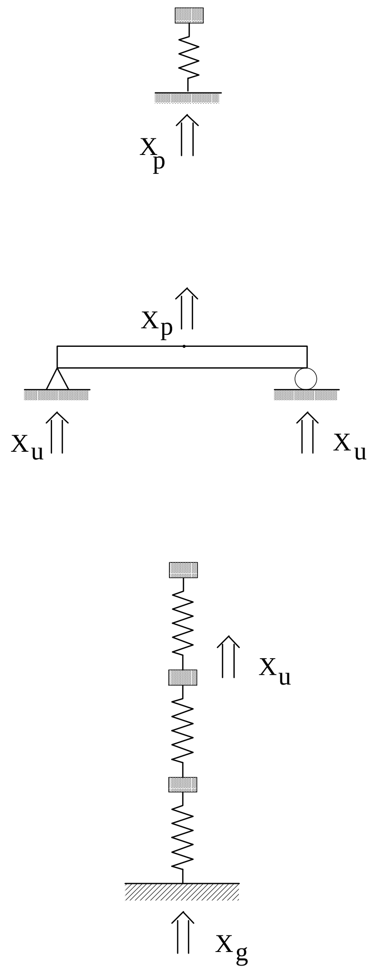

Figure A.3 Double cascade analysis of an oscillator on the second floor slab subjected to vertical seismic excitations.

APPENDIX B

NOMENCLATURE

$\underset{\sim}{r}$ = excitation influence vector

$\underset{\sim}{x}$ = vector of structural degrees of freedom

$\underset{\sim}{y}$ = state vector of structural degrees of freedom

$\underset{\sim}{z}$ = vector of transformed structural degrees of freedom

$\underset{\sim}{\Gamma}$ = participation factors

$[A]$ = mass state matrix

$[B]$ = stiffness state matrix

$[C]$ = damping matrix

$[G]$ = Guyan condensation matrix

$[I]$ = unity matrix

$[K]$ = stiffness matrix

$[M]$ = mass matrix

$[R]$ = condensation matrix

$[S]$ = transformation matrix

$[U]$ = modal transformation matrix

$[\Delta]$ = diagonal damping matrix

$[\Lambda]$ = real eigenvalue matrix

$[\Phi]$ = real eigenvector matrix

$[\phi]$ = substructure real eigenvector matrix

$[\Omega]$ = complex eigenvalue matrix

$[\Psi]$ = complex eigenvector matrix

$[\psi]$ = substructure complex eigenvector matrix

$[\wedge]$ = matrix associated with the condensation process with lower modes

$[-]$ = matrix associated with the condensation process with higher modes

$[\;^*]$ = transformed matrix

$[\quad]^{-1}$ = inverse matrix

$[\quad]^{T}$ = transpose of a matrix

Subscripts

b = boundary degrees of freedom

i = interior degrees of freedom

k = kept coordinates when iterating with lower modes

r = kept coordinates when iterating with higher modes

M = Guyan condensation matrix in terms of mass submatrices

K = Guyan condensation matrix in terms of stiffness submatrices

α = substructure α

β = substructure β

Superscripts

(0) = initial iteration step

(l) = iteration step

α = substructure α

β = substructure β

VITA

Mario Alfredo Rivera Borrero was born on July 4, 1956 in San Juan, Puerto Rico. He attended the University of Puerto Rico-Mayagüez Campus where he received a B.S. degree in Civil Engineering on May, 1979. Upon graduation, he was hired by a consulting firm as a structural engineer. In January, 1981 he was hired by the Department of General Engineering at the University of Puerto Rico to work as an instructor and to continue his graduate studies. In July, 1983 he received a M.S. degree from the University of Puerto Rico-Mayagüez Campus. In September, 1984 he began graduate studies in the Engineering Science and Mechanics Department at Virginia Polytechnic Institute and State University. In December, 1989 he returned to his tenure track position at the University of Puerto Rico. He obtained his Ph.D. in Engineering Mechanics on April, 1997.